# CONDITIONAL MOMENT CLOSURE FOR LES OF COMPRESSIBLE TURBULENT REACTIVE FLOWS

PIETRO PAOLO CIOTTOLI


DIMA - Mechanical and Aerospace Engineering Department
Sapienza University
Rome, IT

Advisor: Prof. M. Valorani

Dec 2013

# ABSTRACT

While the Conditional Moment Closure (CMC) method has been developed with reference to low Mach number flows, the formulations considered in this thesis work avoid taking any simplification on the acoustics, so as to pursue a fully compressible formulation. Two coupling strategies for a LES formulation of fully compressible reactive flows adopting the CMC method are presented.

Similarly to standard CMC approaches, both strategies rely on recasting the full Navier-Stokes system into two sub-systems, the first filtered and solved by means of LES in the physical space, the other conditionally filtered and solved in the CMC space.

The two approaches differ by the way the two sub-systems are coupled. In the first coupling strategy, referred to as "Vector Field Update" (VFU), the CMC interacts with the LES sub-system by actually modifying the density and sensible energy LES fields. In the second coupling strategy, referred to as "Energy Source Update" (ESU), the source term in the LES energy equation is computed on the basis of the species source terms obtained by the time integration of the CMC system. This way, the CMC interaction with the LES sub-system relies on the modification of the LES energy source term, while any LES state variable is directly modified.

The numerical implementation of the LES/CMC equations for both coupling strategies has been carried out and explained in detail. The LES flow solver relies on central two-to-six order discretization of the convective terms of the Navier-Stokes equations cast in fully split form, leading to a locally conservative formulation which guarantees discrete conservation of the total kinetic (mechanical) energy. This approach allows a stable and accurate spatial discretization of the convective terms without the addition of numerical dissipation.

The conditionally filtered CMC subsystem is discretized on a Cartesian mesh in the CMC space, and the time advance is based on a further splitting in time between an explicit treatment of the convective operator and an implicit treatment (using BDF, as in CVODE) of the fully coupled reactive-diffusive operators.
The predictive capabilities of a zero-dimensional version of the CMC code are presented. The solution sensitivity to scalar dissipations is tested varying its strength and shape. An a-priori prediction of the SANDIA-D flame has been performed, and the comparison with experimental results is presented. The VFU and ESU CMC-LES coupling strategies are compared by means of 2D test case, and the differences are discussed. The scalability performance, and the preliminary results of a 3D version of the code are presented.

# PUBLICATIONS

Some ideas and figures have appeared previously in the following publications:

P.P. Ciottoli, M. Valorani, M. Bernardini,S. Pirozzoli, "Methane/Air Turbulent Coaxial Jet Flame with Large Eddy Simulation and Conditional Moment Closure", European Fluid Mechanics Conference 9, University of Rome "Tor Vergata", 9-13 Sep 2012.

P.P. Ciottoli, M. Bernardini, S. Pirozzoli, M. Valorani, "A Conditional Moment Closure Formulation for Large Eddy Simulation of Compressible Non-Premixed Turbulent Reactive Flows", XXXV Meeting of the Italian Section of the Combustion Institute, 10-12 October 2012.

P.P. Ciottoli, M. Bernardini, S. Pirozzoli, M. Valorani, "A Conditional Moment Closure Formulation for Large Eddy Simulation of Compressible Non-Premixed Turbulent Reactive Flows", SIAM Numerical Combustion, San Antonio, TX, 11 Apr 2013.

P.P. Ciottoli, M. Bernardini, S. Pirozzoli, M. Valorani, "Two-way coupling strategies for Conditional Moment Closure and Large Eddy Simulation in compressible reacting flows", XXXVI Meeting of the Italian Section of the Combustion Institute, 13-15 June 2013.

*The combustion of fossil fuels*
*remains a key technology for the foreseeable future.*
*It is therefore important that we understand*
*the mechanisms of combustion and, in particular,*
*the role of turbulence within this process.*

— Norbert Peters [1]


## ACKNOWLEDGEMENTS

I would like to express my heartfelt gratitude to my advisor Professor M. Valorani[1] for the continuous support during my work, his guidance, support, and patience. I am also very grateful to Professor S. Pirozzoli[2] for providing me the numerical tools at the core of the LES library and his scientific advice. I want to express my warmest thanks to Dr. M. Bernardini[3] for sharing his valuable experience with me, for his support, insight, and friendship.

I could not close these acknowledgements without expressing my debt of gratitude to Prof. E. Mastorakos[4], who was instrumental to kick-off this work by introducing me to the Conditional Moment Closure method. Without his initial guidance, and a preliminary version of his zero-dimensional CMC code, I would not probably even started my Ph.D. work.


1 Full Professor, Sapienza University of Rome, IT
2 Associate Professor, Sapienza University of Rome, IT
3 Research fellow, Sapienza University of Rome, IT
4 Full Professor, Cambridge University, UK

# CONTENTS

# ACRONYMS

| | |
|---|---|
| LES | Large Eddy Simulation |
| RANS | Reynolds Averaged Navier Stokes Equations |
| CMC | Conditional Moment Closure |
| VFU | Vector Field Update |
| ESU | Energy Source Update |
| PDF | Probability Density Function |
| FDF | Filtered Density Function |

# 1

# INTRODUCTION

The accurate prediction of reacting turbulent flows is of important economic consequence in many engineering fields. There is a great interest in predicting efficiency, heat transfer, and pollutant formation in internal combustion engines and aerospace engines combustion chambers. These are typically characterized by partially premixed or non-premixed turbulent flames, also called turbulent diffusive flames. These kind of turbulent flames are ruled by a large number of physical phenomena coupled each other. Combustion in the gas phase requires first reactive species to reach, by molecular diffusion, the flame front. A non-premixed flame is unable to impose its own dynamics on the flow field because it is not a combustion wave endowed with its own speed of propagation. Hence a non-premixed flame is highly sensitive to turbulence and a sufficiently strong turbulent fluctuation can provoke a local quenching. Moreover in such kind of flames, reactants have to be ignited by a an external energy deposition (such as a spark or a torch) and later always reignited by burnt hot gases for combustion to continue, this constituting a process called flame stabilization, which is a central combustion chamber and ignitors design requirement. However, despite its potential usefulness, the predictability of flame stabilization by numerical simulations is still an unsolved challenge.

A validated tool of numerical analysis can favorably impact on the lowering of the development costs of new combustion chambers by allowing "virtual" testing of new designs, concepts, and operating conditions, in lieu of standard experimental testing in the lab. The main requirement of a tool of numerical analysis should be the ability to describe combustive phenomena such as flame instabilities, local

anchoring, local quenching, and thermo-acoustic instabilities. An accurate prediction of these phenomena is crucial for an in-depth comprehension of the qualitative behavior of ignition transients and combustion instabilities, as well as for an accurate quantitative prediction of pollutants, and of the thermo-acoustic behavior of a combustion chamber under different operating regimes.

## 1.1 THE ISP-1 LEGACY

Methane as a fuel propellant in liquid rocket engines trust chambers is currently considered for the evolution of space propulsion systems and upper stage engines. It is within this framework that the author of this thesis participated, as Ph.D student, to an EC FP-7, 3-year, project named " In-Space Propulsion 1" (ISP-1), which was partly devoted to an exploratory study on the use of methane in in-space engines. In Italy, ASI (Italian Space Agency) is sponsoring a long term program, HyProb, led by CIRA and AVIO Group aimed at developing the technologies for LCH4/Lox propulsion, to which the author of this thesis is participating. One goal in ISP-1 was the validation of numerical simulations to predict the ignition transient in a combustion chamber (DLR/M3 test facility) having a squared cross-section of dimensions: 60mm x 60mm x 140mm, with a single coaxial injector, and ignition triggered by a laser-pulse [2].

A 2D axisymmetric Unsteady Reynolds Averaged Navies-Stokes (URANS) computation of the combustion chamber was performed, the kinetic model adopted was generated in-house by starting from GRI Mech 3.0, removing the nitrogen kinetics so to treat nitrogen as a simple inert diluent, and finally by retaining only the reactions and species important in the prediction of the hot kernel initiation and flame propagation. Still, this smaller mechanism consisted of 15 species and 57 reactions, which made the reactive flow simula-

tion quite demanding both in terms of physics and computational demand .

The validation in ISP-1 showed that an Unsteady Reynolds Averaged Navies-Stokes (URANS) model is able to identify qualitatively a number of important features. More specifically, an axisymmetric URANS can qualitatively reproduce at least two significant transient phenomena (i) the development of a large recirculation region surrounding the jet emanating from the co-axial injector, and (ii) the occurrence of a strong blast wave triggered by the laser pulse. A three-dimensional LES calculation using a relatively simple model for the kinetics (an extended Jones and Lindstedt mechanism) was also carried out in ISP-1 by P. Grenar (ONERA). LES predictions showed that the improved fidelity of fluid-dynamics was not able to compensate for the poor kinetic modeling to the extent that the accuracy of the 3D LES and the axisymmetric URANS models was comparable. In short, the quantitative accuracy of both 3D LES and axisymmetric URANS was not satisfactory, with the main source of errors being associated to the lack of a proper turbulent combustion modeling in the 2D URANS model, and of the kinetic modeling and turbulent closure in the 3D LES model.

## 1.2 AIM OF THE WORK

It was eventually decided to develop an in-house, Large Eddy Simulation, compressible, reactive flow model, able to account for a kinetic modeling of moderate complexity through a proper closure model for the turbulent fluctuations. The Large Eddy Simulation (LES) model, where the filtered large anisotropic scales are resolved, while the smaller and isotropic scales are simply modeled, represents a good compromise between URANS and DNS. Many turbulent reacting flows of interest involve significant transient effects which cannot be modeled using conventional Reynolds averaging approaches, LES

can provide more accurate predictions of the flow and mixing fields than conventional RANS-based methods, in particular for the complex geometries of many engineering applications. The chosen closure model for the chemical source term is the Conditional Moment Closure (CMC) because of its intrinsic capability to include unsteady effects also far away from the "flamelet regime".

## 1.3 AN INTRODUCTION TO THE CONDITIONAL MOMENT CLOSURE

In the LES context, the CMC method models the spatially filtered values of the chemical source terms. The chemical source term is a strongly non linear function of temperature, pressure and composition. Because of that, the filtered value of the chemical source term can not be written as function of the filtered values of pressure, temperature and species mass fractions.
The theoretical basis of the CMC relies on the assumption, experimentally verified, that in non-premixed flames the chemical source term fluctuations are strongly dependent on the degree of mixing of fuel and oxidizer [3]. This mixing degree is well represented by a properly defined conserved scalar, the mixture fraction. Once defined the mixture fraction, it has been demonstrated that the conditionally filtered chemical source term can be written as a function of the conditionally filtered values of pressure, temperature and species mass fraction.
This said, the model is based on the following idea: a chemically frozen field is solved on an LES mesh in order to obtain the field values of a conserved scalar representing the reacting mixture stream, i.e. the mixture fraction. The evolution equations of the conditionally filtered species are solved on a computational domain which has the mixture fraction as additional dimension. The filtered values of the species mass fractions are then obtained from the conditionally filtered values by means of a presumed shape pdf.

The coupling between the two systems is given by a source term in the chemically frozen field energy equation, that is the energy released by the chemical reactions. The additional dimension required in the CMC space could be computationally expensive. Nevertheless in some classes of problems, such as a jet flame, the CMC space could be two-dimensional instead of four-dimensional. For example, this is possible when the radial direction and the mixture fraction space are strongly related each other. Moreover, the weak space dependence of the conditionally filtered values and the CMC requirement of having good statistics on the conditional quantities, prescribe to adopt a CMC mesh resolutions coarser than the LES, this implying a lower computational cost. The saving in the CMC space resolution might be reinvested in a more detailed description of the chemical kinetics.

## 1.4 THESIS OUTLINE

A major goal of this work has been to asses the predictive capabilities of the Conditional Moment Closure for partially premixed and non premixed flames. Part of the work has been the development of a brand-new suite of numerical toolkits for turbulent reactive flows analysis based a Conditional Moment Closure extension to the Large Eddy Simulation of compressible reacting flows. The document is organized as follows.

In Chapter 2, a short review on the state of the art of the passive scalar-based approaches is presented, with a special attention to the LES and RANS formulation of the CMC method.

In Chapter 3, the Navier-Stokes equations for a reacting flow are presented and a review of turbulent diffusive flame modeling is given. The numerical issues arising from the space and time discretization requirements of the previously introduced balance equations is illustrated, and the Large Eddy Simulation approach is introduced. The consequent need of both a fluid-dynamic and a chemical closure mod-

els is explained. The flamelet equations derivations as example to introduce the basic idea of the passive scalar approach; then the choice the Conditional Moment Closure has been motivated.
In Chapter 4 the Conditional Moment Closure equations formulation has been presented.
In Chapter 5, two coupling strategies for the Conditional Moment Closure combustion sub-grid model to Large Eddy Simulation are presented. While the CMC method has been developed with reference to the low Mach number approximation, where the energy equation is conditionally filtered and solved in the CMC space, in the present approach, we avoid making any simplification on the acoustics, so as to pursue a fully compressible formulation. Hence the set of reactive compressible Navier-Stokes equations is rearranged in two sub-sets, one filtered and solved in the physical LES space, the other conditionally filtered and solved in the CMC space. Mass and momentum conservation law equations are included in the LES sub-set, while the rate equations describing the species evolution are part of the CMC sub-set. The energy equation requires a special treatment: on one hand, it must be kept tightly coupled with the momentum equation in the LES context so as to describe wave propagation; on the other hand, it must remain coupled in the CMC context with the species rate equations to account for the thermal expansion, which is crucial for the description of the non linear coupling between temperature and reaction rates. We present two different formulations to obtain a two-way coupling between the two sub-sets. In both formulations, the LES sub-set provides the unconditional values of the velocity, pressure, and mixture fraction fields; these are conditionally filtered and used to compute the coefficients required to close the CMC equations. Moreover, the mean molecular weight and the specific heat of the mixture required by the thermal and caloric equations of state in the LES sub-system, are updated with the species mass fractions informations resulting from the CMC sub-system evolution. The energy rise due to chemical reactions, described by the CMC equations

under the assumption of constant pressure, affects the LES sub-set as well. The two approaches differ in the way this issue is handled. In the first approach, referred to as "Vector Field Update" (VFU), the sensible energy equation is split into two contributions: (i) the heat release rate due to chemical reactions, which is conditionally filtered and solved in the CMC space, and (ii) the transport, convective and diffusive, of sensible energy in a fully compressible frozen mixture, which is filtered and solved in the physical space. Hence the CMC interacts with the LES sub-system, directly modifying the density and sensible energy LES fields. In the second approach, here referred to a "Energy Source Update" (ESU), the energy equation is entirely retained in the LES system, and its energy source term is computed on the basis of the species source term known from the CMC system. This way, the CMC interaction with the LES subsystem relies on the modification of the LES energy source term, while any LES variable is directly modified.

In Chapter 6, the numerical implementation of the LES/CMC equations for both the two CMC coupling strategies is explained in detail. The LES flow solver relies on central two-to-six order discretization of the convective terms of the Navier-Stokes equations cast in fully split form [13]. As shown by Pirozzoli [14], this arrangement, leading to a locally conservative formulation, guarantees discrete conservation of the total kinetic (mechanical) energy if the frozen mixture. This approach allows a stable and accurate spatial discretization of the convective terms without the addition of numerical dissipation. The conditionally filtered CMC subsystem is discretized on a Cartesian mesh in the CMC space and the time advanced is based on a further splitting in time between an explicit treatment of the convective operator and an implicit treatment (using BDF, as in CVODE) of the coupled reactive-diffusive operators.

In Chapter 7 the predictive capabilities of a zero-dimensional version of the CMC code are presented. The solution sensitivity to scalar dissipations is tested varying its strength and shape. An a-priori pre-

diction of the SANDIA -D flame [4] has been performed and the comparison with experimental results is presented. The VFU and ESU CMC-LES coupling strategies are compared by means of a 2D test-case, and their differences are discussed. The preliminary results of a 3D version of the code are presented and the numerical solution of various reactive mixing layer computations are shown. Moreover, both weak and strong scalability tests have been performed on the 3D version of the code and the results are reported in detail.

# 2

# STATE OF THE ART

Turbulent jet diffusion flames have been studied at length. The turbulence-chemistry interactions have been modeled by the chemical equilibrium assumption, laminar flamelet modeling [5], probability density function modeling [6], and Conditional Moment Closure (Klimenko, [7] and Bilger [8, 3]).
The ignition transients of a turbulent non-premixed flame are characterized by a large range of time and space scales. This makes the assumption of full chemical equilibrium not accurate, since it relies on the hypothesis of infinitely fast chemistry, and neglects the influence of fluid motions on chemical processes, this excluding the possibility of describing important combustion phenomena, such as the flame temperature dependence on local strain, local quenching, and reignition.

## 2.1 PASSIVE SCALAR METHODS

The steady laminar flamelet models (LFM) [5], relying on the hypothesis of having a local balance between fluid mechanics and chemistry, takes into account the effect of the fluid dynamics on the flame in term of maximum temperature and products formation, but is not able to predict the flame behavior outside the steady flamelet regime [9], that is when the chemical and fluid-dynamic effects are unbalanced and strongly unsteady, such as local quenching and reignition. The dynamic version of the flamelet models [10] is capable to take into account the local unbalances and unsteady effects, while the Lagrangian flamelet formulation [11] is able to take into account the

convective effects and to describe very fundamental phenomena like lifted flames. Anyway, these variants require the temporal evolution of the flamelet equations and are more computationally expensive than the steady laminar flamelet, since the lookup table approach is impossible and the number of flamelet equations to integrate in time rises with the number of species involved. Moreover the flamelet approach has been developed in the context of laminar flames and then recast to cope with turbulent flows, while the statistic nature of turbulence is taken into account by introducing a presumed-shape probability density function.

Probability density function (PDF) calculations of flows allow to relax all hypotheses concerning the shape of pdfs, since a pdf transport equation is directly solved. Anyway the PDF approach [12, 13] with detailed chemical mechanisms is extremely expensive [14] and have inherent problems in the modeling of molecular diffusion terms. The conditional source estimation (CSE) method for closing the chemical source terms in the filtered governing equations of motion has been proposed by Bushe [15, 16, 17]. Both CSE and CMC rely on the same main hypothesis about the species source term, whose conditionally filtered value is written as function of the conditionally filtered values of the reactive scalars. However, while in the CMC approach the entire set of the reactive scalars evolution equations is conditionally filtered and evolved in the CMC space, in the CSE approach the set of the reactive scalars evolution equations is evolved in the physical space; the unconditionally filtered source terms are obtained from the conditionally filtered ones by means of a convolution operation and a presumed shape pdf. However, the conditionally filtered values of the reactive scalars, required to compute the conditionally filtered source terms, are computed by inverting the integral relation that links the unconditional and the conditional values, this involving several computational difficulties. A Conditional Source-term Estimation (CSE) model has been used to close the mean reaction rates for a turbulent premixed flame with different presumed probability density function

(PDF) models were studied by Jin, et al. in 2008 [17]. The conditional means of reactive scalars were evaluated with CSE and compared to DNS showing promising results.

## 2.2 CMC FOR RANS

Conditional Moment Closure was firstly applied in the **RANS** context, allowing to investigate turbulence chemistry interactions with large chemical mechanisms at a reasonable computational cost. The LFM and a RANS/CMC model have been compared to direct numerical simulations by V. Nilsen et.al in 1994 [18]. The results and their analyses showed that, although SLFM is a substantial improvement over equilibrium modeling, the conditional moment closure leads to excellent data predictions provided the average scalar dissipation rate conditioned on the mixture fraction is properly modeled.
By comparison with DNS results, Mastorakos and Bilger, in 1998 [19], inquired the differences between the first- and second-order CMC closure for autoignition times and structures of a turbulent non-premixed flow with one-step chemistry, finding important qualitative differences between the two closures only for high values of strain. The weak cross stream dependence of the conditional averages has been established by Swaminathan, et al., in 1998 [20], using measurements made using the Raman/Rayleigh/LIF technique on the counter rotating recirculation region in the wake of a bluff-body stabilized flame. It was demonstrated that the conditional averages have a very weak dependence on the cross-stream position in recirculation regions. From the conditional moment closure view point, this weak dependence allows to simplify the CMC equations by integrating them across the flow. This simplification, known as shear flow approximation, is very important since it may compensate for the increased dimensionality of the CMC domain. In 2000, Kim et. al

[21] employed the CMC closure for the RANS numerical prediction of a turbulent non-premixed flame of methanol stabilized on a bluff body, showing good agreement for the conditional averages of the temperature and major species concentrations, while some discrepancy for OH, CO, and H2, possibly due to an inaccurate prediction of the conditional scalar dissipation rate. Anyway, the results of the CMC model are in better agreement with conditional measurements than those of the LFM method.

A good agreement was found by Roomina in 2001 [22] from the comparison of laser diagnostic measurements for the velocity and mixing fields and temperature and species mass fractions and RANS-CMC predictions for a turbulent jet diffusion flame of a Methane/Air mixture.

Fairweather and Wooley in 2003 [23] used a cross-stream average CMC formulation to model turbulent non-premixed flames of Hydrogen and Hydrogen/Helium mixtures. Various Reynolds stress tensor closure models and kinetic schemes, employing 5, 24, and 62 reaction steps, have been employed and compared. The superiority of Reynolds stress turbulence model over the eddy viscosity-based approach, as well as a weak dependence on the kinetic scheme has been shown. Moreover, good agreement between the CMC results and some previously obtained PDF transport results was obtained. Results, however, exhibited errors in the NO prediction.

Devaud and Bray in 2003 applied the CMC method to a lifted turbulent flame [24]. By comparison with published experimental data, they found out that the first order, radially averaged CMC, is able to accurately predict the lift-off height of a lifted flame. The computational results agreed well with the experimental results even though turbulence and combustion were decoupled, so the effect of turbulence upon combustion were included but the thermal effects on the turbulent flow field were not accounted for.

Two-dimensional CMC coupled with commercial CFD has been applied to study n-heptane spray autoignition under diesel engine con-

ditions by Wright, et al. in 2005 [25] with the aim of quantifying the sensitivity of the predictions to the operator splitting errors in various numerical configurations.

A conditional moment closure (CMC) model was applied, by Kim, et al. in 2005, to predict a co-flow jet flame structures and NO formation in the moderate and intense low oxygen dilution combustion mode. A new PDF was proposed to describe a three stream mixing system in term of a single mixture fraction. Although the differential diffusion effects appeared to be non-premixed, the predictions of temperature, CO, OH, and NO mass fractions were in good agreement with measurements, showing that the CMC model is an attractive choice for this kind of problems.

In 2005 Kim, et al. [26] simulated H2/Air lifted jet flames by means of a two-dimensional CMC formulation coupled with a commercial CFD software. The capability of reproducing the flame behavior varying the inlet jet velocity, including the hysteresis behavior of lifted flames, was shown to be consistent with experimental observation. Moreover the alternative approach of employing a cross-stream averaged CMC, was justified since the radial components of spatial convection and diffusion were always small.

Simulations of turbulent CH4-air counterflow flames were presented by Kim, et al.[27], obtained in terms of zero and two-dimensional first-order Conditional Moment Closure (CMC) and a CFD software to study the flame structure and extinction limits, capturing the trend of increasing extinction velocity with air dilution of the fuel stream.

A three-dimensional, elliptic, CMC modeling of a low-swirl stabilized non-premixed flame of methane was performed by Fairweather and Woolley in 2007 [28] with encouraging results in both a qualitative and a quantitative sense. Both experiments and numerics (CMC and a CFD code ) were employed by Markides, et al. in 2007 [29] to investigate the autoignition of a gaseous n-heptane plume in heated turbulent. The first-order, spatially averaged CMC model reproduced

well the experimental trends.

The accuracy of the gradient diffusion model for the conditional turbulent flux term in the CMC equation has beed assessed by Richardson, et al. [30] in 2007. The comparison with DNS showed that the usual gradient diffusion approximation for the conditional turbulent flux seems to be adequate for high turbulence intensity relative to the laminar burning velocity of a stoichiometric mixture, but the strong counter-gradient transport found at weak turbulence cannot be described with the simple gradient model.
A first-order, three-dimensional, moving-grid CMC method coupled with a commercial CFD code was successfully employed to simulate combustion in a direct-injection diesel engine in 2008 by Paola, et al. [31]. A CMC domain reduction of the three-dimensional problem to two- and zero- dimensions was explored in terms of accuracy and computational time, showing that integral method can be effective to predict combustion in diesel engines at a reduced computational cost.
Recently, in 2013, Bolla, et al [32], pursued the first application of a semi-empirical soot model in the framework of multidimensional CMC for spray combustion, simulating an n-heptane autoigniting spray in a constant-volume vessel under diesel engine conditions. The results suggested that CMC is a promising framework for soot modeling under diesel engine conditions.

## 2.3 CMC FOR LES

Recently, the CMC equation has been formulated for **LES**. Kim and Pitsch [33] in 2005 proposed a CMC approach for the LES combustion sub-grid modeling issue. The conditionally filtered equations were derived and a priori tests, performed by means of DNS, showed that the

resolved large-scale fluctuations of the reactive scales have a favorable impact on accuracy of the CMC, in particular for the sub-filter flux in mixture fraction.

Consistently with the LES formulation, in 2005 Navarro-Martinez derived the transport equations for the conditionally filtered species [34]. The LES extension of the CMC model has been validated by comparison with measurements of a piloted, turbulent Methane/Air jet diffusion flame (Sandia-D). In 2007 Navarro-Martinez and Kronenburg [35] applied the LES/CMC formulation with detailed chemistry to a bluff-body stabilized flame, showing improvements on the RANS/CMC and LES/LFM formulations. Moreover, prediction of endothermic regions close to the neck of the recirculation zone demonstrated the potential of LES-CMC to predict unsteady finite rate effect.

In 2009 Navarro-Martinez and Kronenburg [36] included a detailed mechanism of 44 species and 256 reactions in an LES/CMC solver to represent the chemistry of a lifted diffusion flame produced by a partially premixed jet issuing into a vitiated co-flow. The inflow turbulence influence on the lift-off height could be captured with success, and ignition trends were reproduced satisfactorily.

In 2009 Floyd, et al. [37] carried out thorough phenomenological analysis of DNS data from a planar jet and of experimental data from a turbulent opposed jet. They found that, in the LES context, the top-hat distribution provides an excellent alternative to the now much more common $\beta$ function, both in terms of ease of implementation and physical interpretation.

Navarro-Martinez and Rigopoulos in 2011 [38] incorporated a soot model into an LES/CMC framework. The results of calculations were compared with experimental data for atmospheric methane flames demonstrating that the model, in conjunction with a representation of differential diffusion effects, is capable of predicting soot formation at a fundamental level.

In 2009, Triantafallydis [39] investigated the feasibility of the use of CMC/LES for ignition problems by modeling the forced ignition of

a bluff-body stabilized non-premixed methane flame. The particular three-dimensional formulation of the CMC equation there employed was able to reproduce the pattern of flame expansion and overall flame appearance accurately. Moreover, the sensitivity of the flame behavior on the spark intensity and position agreed with the experimental evidence.

In 2009, Triantafyllidis and Mastorakos [40] performed an LES/CMC simulation of a bluff-body stabilized burner to assess the influence of the different options for transferring information from the LES to the CMC grid, showing that special care is required for mixture fraction variance modeling. Moreover the Amplitude Mapping Closure model feasibility for the scalar dissipation in the LES context was demonstrated.

The sensitivity of CFD mesh resolution, CMC mesh resolution, inlet boundary conditions, and conditional scalar dissipation rate modeling, was treated by Stankovic, et al. [41] in 2010 by means of an LES/CMC simulated nitrogen-diluted hydrogen jet, igniting in a turbulent co-flowing hot air stream. The trends in the experimental observations were well reproduced, the auto-ignition location dependence on turbulence and mixing was underlined, finding that stronger turbulence promotes ignition.

A coupling between a high order accurate fully compressible upwind LES method with the CMC combustion has been proposed by Thornber, et al. in 2011 [42], providing a very useful framework for future CMC application. The new method was validated against DNS data for a lean premixed methane slot burner.

A three dimensional LES/CMC approach has been applied to the Sandia piloted jet diffusion flames (type D and F) by Garmory, et al., in 2011 [43]. The results where in very good agreement with the experiments, and the local transient extinction and re-ignition events were observed in flame F as well.

Accurate prediction of localized extinctions and reignitions in locations consistent with Delft III piloted turbulent non-premixed flame

experiment where found by Ayache, et al,. in 2013 [44] by means of an LES/CMC formulation and the GRI 3.0 chemical mechanism. Simulations of an n-heptane spray autoigniting under conditions relevant to a diesel engine are performed using two-dimensional, first-order conditional moment closure (CMC) with full treatment of spray terms in the mixture fraction variance and CMC equations by Borghesi, et al., in 2011 [45].

By performing various numerical predictions of the Sandia piloted jet Flames D and F while varying some CMC parameters, the influence of the grid size on the scalar dissipation prediction was inquired by Garmory, et al., in 2013 [46], this highlighting the capabilities of the LES/CMC approach to capture flames very close to extinction.

A hydrogen jet, diluted with nitrogen, issued into a turbulent co-flowing hot air stream was reproduced by means of the LES/CMC method by Stankovic in 2013 [47]. In the experiments, varying the co-flow temperature, different auto-ignition regimes, including low Damkohler number situations, were obtained; all regimes were recovered in the simulations.

# 3

# PASSIVE SCALAR APPROACH FOR TURBULENT DIFFUSIVE FLAMES

The Navier-Stokes equations for a reacting flow are here presented and a brief introduction to the mathematical modeling of turbulent diffusive flames is given. The numerical issues arising from the space and time discretization of the differential equations governing the problem are illustrated, and the Large Eddy Simulation approach is introduced. The consequent need of both a fluid-dynamic and a chemical closure models is explained. The basic idea of the passive scale approach is explained using the flamelet equations derivations as example. The choice of adopting the Conditional Moment Closure is motivated.

## 3.1 BALANCE EQUATIONS

The fully compressible reactive Navier-Stokes equations augmented by the transport equation of a passive scalar $\xi$, according to the Einstein summation convention, reads:

$$\frac{\partial \rho}{\partial t} + \frac{\partial \rho u_j}{\partial x_j} = 0, \tag{1}$$

$$\frac{\partial \rho u_j}{\partial t} + \frac{\partial \rho u_i u_j}{\partial x_j} + \frac{\partial p}{\partial x_j} - \frac{\partial \tau_{ij}}{\partial x_j} = 0, \tag{2}$$

$$\frac{\partial E}{\partial t} + \frac{\partial (E+p) u_j}{\partial x_j} - \frac{\partial \tau_{ij} u_j}{\partial x_i} + \frac{\partial}{\partial x_j}\left[\lambda \frac{\partial T}{\partial x_j}\right] + \sum_{\alpha=1}^{N} [\rho \dot{\omega}_\alpha \Delta h_{0_\alpha}] = 0, \tag{3}$$

$$\rho \frac{\partial Y_\alpha}{\partial t} + \frac{\partial (\rho u_j Y_\alpha)}{\partial x_j} = -\frac{\partial J_j^\alpha}{\partial x_j} + \dot{\omega}_\alpha \quad \alpha = 1, ..., N, \tag{4}$$

$$\frac{\partial \rho \xi}{\partial t} + \frac{\partial (\rho u_j \xi)}{\partial x_j} + \frac{\partial}{\partial x_j}\left( D_\xi \frac{\partial \xi}{\partial x_j} \right) = 0. \tag{5}$$

Where $\rho$, $p$, $T$, and are the density, pressure, temperature, and specific sensible energy the mixture respectively; while $u_j$ is the $j$-th component of the velocity vector. The thermal and caloric equations of state for mixtures of ideal gases are also provided:

$$p = \rho \overline{R}_{mix} T \qquad \overline{R}_{mix} = \sum_{\alpha=1}^{N} R_\alpha Y_\alpha, \tag{6}$$

$$E = \rho e = \rho \left[ \frac{1}{2} u_j u_j + \sum_{\alpha=1}^{N} Y_\alpha \left( \int_{T_0}^{T} \hat{C}_{v_\alpha} T \right) \right] = \rho \left[ e_{kin} + e_{sens} \right], \tag{7}$$

The caloric equation in Eq. (7) defines the mixture total absolute internal energy $E$ as summation of the sensible energy $\rho e$ and the kinetic energy $\rho u_i u_j$ of the mixture. The state vector of this system is $\mathbf{w} = \{\rho, \mathbf{u}, E, T, p, \xi, Y_\alpha\}$, with $\alpha = 1, ..., N$, where $Y_\alpha$ is the mass fractions of the $\alpha$-th species. Here the subscript $mix$ stands for the mixture value, $\overline{R}_{mix}$ is the gas constant of the gas mixture, $\hat{C}_{v_\alpha}$ is the specific heat of the $\alpha$-th species. The energy release due to reactions is described by the term $\sum_{\alpha=1}^{N} [\rho \dot{w}_\alpha \Delta h_{0_\alpha}]$, where $\Delta h_{0_\alpha}$ is the formation enthalpy of the $\alpha$-th species. The passive scalar $\xi$ is not strictly needed to close the problem. Anyway $\xi$ can be defined so as to be 1 where the fluid is pure fuel and 0 where the fluid is pure oxidizer, this making $\xi$ and its gradients an index of the mixing degree of the mixture. Hence, even if its evolution is not essential for the closure of the set of governing equations, the knowledge of the evolution of the passive scalar field $\xi$, as well as the choice of its diffusive coefficient $D_\xi$, will be required in the next sections. The fluids are assumed to be Newtonian and the viscous stress tensor is:

$$\tau_{ij} := \mu \left( \frac{\partial u_i}{\partial x_j} + \frac{\partial u_j}{\partial x_i} \right) - \frac{2}{3} \mu \delta_{i,j} \frac{\partial u_k}{\partial x_k}. \tag{8}$$

The species diffusive flux $J_j^\alpha$ can be approximated by a Fickian model as follows:

$$J_j^\alpha := -\rho D_\alpha \frac{\partial Y_\alpha}{\partial x_j}, \tag{9}$$

where the $D_\alpha$ is the diffusive coefficient of the $\alpha$-th species.
The term $\dot{\omega}_\alpha$ is the chemical source term of the $\alpha$-th species. For an irreversible reaction including $l$ reactions of the kind:

$$\sum_\alpha \nu'_{\alpha,l} M_\alpha \rightleftharpoons \sum_\alpha \nu''_{\alpha,l} M_\alpha, \qquad l = 1, L \tag{10}$$

where $M_\alpha$ is the chemical symbol, and $\nu_{\alpha,l}$ is the stoichiometric coefficient of the $l$-th reaction, for the $\alpha$-th species. The variation of the the number of moles of the $\alpha^{th}$ species $N_\alpha$, due to the L reactions, can be written as:

$$\sum_l^L \frac{dN_\alpha}{dt} = \sum_l^L (\nu''_{\alpha,l} - \nu'_{\alpha,l}) \frac{dq_l}{dt} = \sum_l^L \nu_{\alpha,l} \frac{dq_l}{dt} = \dot{w}_\alpha, \tag{11}$$

$$\dot{\omega}_\alpha = \dot{w}_\alpha \frac{W_\alpha}{\rho}, \tag{12}$$

which $W_\alpha$ being the molecular weight of the $\alpha$-th species; $q_l$ is the progress variable of the $l$-th reaction, and its time variation, for each reaction, is given by the difference of the forward and reverse rates:

$$\frac{dq_l}{dt} = k_{f,l} \prod_\alpha^L [X_\alpha]^{\nu'_{al,l}} - k_{b,l} \prod_\alpha^L [X_\alpha]^{\nu''_{al,l}} \tag{13}$$

where $[X_\alpha]$ is the molar concentration of the $\alpha$-th species, while $k_{f,l}$ and $k_{b,l}$ are the forward and backward constants of the $l$-th reaction. The constants $k_{f,l}$ and $k_{b,l}$ depend on temperature and are generally assumed to follow the Arrhenius law :

$$k_{f,l}(T) = A_l T^{\beta_l} e^{-E_{a,l}/(\mathcal{R}T)} \tag{14}$$

where $\mathcal{R}$ is the universal gas constant, while $A_k$, $\beta_k$ and $E_{a,k}$ are the pre-exponential factor, the temperature exponent and the activation energy of the $l$-th reaction, respectively.

### 3.1.1 *Non-dimensional numbers*

For the following discussion the definition of a few non-dimensional numbers could be useful. The Schmidt number for the species $\alpha$ is defined as:

$$Sc_\alpha = \frac{\mu}{\rho D_\alpha}, \tag{15}$$

and represents the ratio of kinematic viscosity and molecular diffusion. The Prandtl number is defined as:

$$Pr = \frac{\mu C_p}{\lambda} = \frac{\nu}{\alpha}, \qquad \text{with:} \qquad \alpha = \frac{\lambda}{\rho C_p}; \qquad \nu = \frac{\mu}{\rho}; \tag{16}$$

representing the ratio between the molecular kinematic viscosity $\nu$ and the thermal diffusivity $\alpha$. The Lewis number for the $\alpha^{th}$ species $Le_\alpha$ is defined as:

$$Le_\alpha = \frac{\alpha}{D_\alpha} = \frac{k}{\rho C_p D_\alpha} = \frac{Sc_\alpha}{Pr}. \tag{17}$$

It represents the ratio between the thermal diffusivity $\alpha$ and the molecular diffusivity $D$. Once a characteristic fluid-dynamic time $\tau_f$ and a characteristic chemical time $\tau_C$ is defined, the Damkholer number $Da$ is defined as:

$$Da = \frac{\tau_f}{\tau_C} \tag{18}$$

Hence for $Da \simeq 1$, the chemical and fluid-dynamic scales are of the same order of magnitude. Otherwise, when $Da >> 1$, the chemical time scales are much smaller than the fluid-dynamic ones, hence chemical processes are much faster than fluid-dynamic processes, on the opposite, when $Da << 1$ the fluid-dynamic processes are faster than the chemical ones.

## 3.2 TURBULENT NON-PREMIXED FLAMES

The physics of a flame is characterized by a strong coupling between chemistry and fluid motions. This coupling is stronger in presence of turbulence; turbulent energy distribution influences the occurring chemical reactions, while the changes in the temperature and composition due to chemistry strongly affect the turbulent motions of the fluid. Non-premixed flames are affected by various processes, most of them are present in all kinds of turbulent flames, such as flame-generated vorticity, viscous effects, stretching.
Nevertheless, non-premixed flames are characterized by specific processes. First, reacting species have to reach, by molecular diffusion, the flame front reaction (this is the reason why they are called diffusion flames). Because of turbulence the diffusion speed of species can vary strongly across the field. The overall reaction rate is driven by the species diffusion toward the flame front. Hence non-premixed flames do not propagate: they are located where fuel and oxidizer meet. Without a propagation speed a non-premixed flame is unable to impose its own dynamics on the flow field.

Non-premixed flames do not exhibit well defined characteristic scales. A diffusion flame does not feature a propagation speed and the local flame thickness depends on flow conditions. Moreover chemical reaction rates are generally limited by mixing, but a fast mixing, may lead to premixed combustion. Because of this dependence on mixing, non-premixed flames do not exhibit well defined flow independent characteristic scales. Flame scales can be defined unambiguously in flame/vortex interactions only.

A flame thickness $\delta_i$ can be estimated as function of the mixing layer thickness as:

$$\delta_i = \left( \frac{1}{|\nabla \xi|} \right)_{\xi=\xi_{st}} = \sqrt{\frac{2D_{st}}{\chi_{st}}}. \tag{19}$$

Here the subscript $st$ means that the value is calculated at stoichiometric conditions. The variable $\chi_{st} = 2D_{st}|\nabla \xi|^2$ is the scalar dissi-

pation rate and $D_{st}$ is the stoichiometric molecular diffusion rate. A chemical time can then be defined from asymptotic theories as:

$$\tau_c = \frac{1}{\chi_{st} Da}, \tag{20}$$

where $Da$ is the previously defined Damköhler number. Once these two quantities have been defined, a flame velocity can be introduced as:

$$u_f = \frac{\delta_i}{\tau_c}. \tag{21}$$

Two other flow scales are introduced, corresponding to the vortex characteristics at the beginning of the simulation, that is the vortex ideal size $r$ and velocity fluctuations about the mean velocity $u'$. Then one can define two non dimensional numbers: a length scale ratio: $\frac{r}{\delta_i}$, and a velocity ratio: $\frac{u'}{u_f}$.

A Flame/vortex interaction regimes diagram can be identified in a log-log plot based on velocity ($u'\tau_c/\delta_i$) and length ($r_i/\delta_i$) scale ratios. Two characteristic lines appear [9]:

- A constant Damköhler number $Da$, comparing vortex and chemical times:

$$Da = \frac{r/u'}{\tau_c} = \frac{r}{\delta_i}\left(\frac{u'}{\delta_i/\tau_c}\right)^{-1} \tag{22}$$

- A vortex Reynolds number defined as:

$$Re_{vortex} = \frac{u'r}{\nu} = \frac{\tau_d}{\tau_c}\left(\frac{u'}{\delta_i/\tau_c}\right)\left(\frac{r}{\delta_i}\right) \tag{23}$$

  where $\tau_d/\tau_c$ compares diffusion ($\tau_d = \delta_i^2/\nu$) and chemical ($\tau_c$) times.

To better understand the flame behavior in a turbulent velocity field as a function of the Damköhler number, it can be useful to define a reference Damköhler number $Da^{SE}$, as the value of $Da$ corresponding to the extinction of a steady laminar counter-flow flame. Hence, for

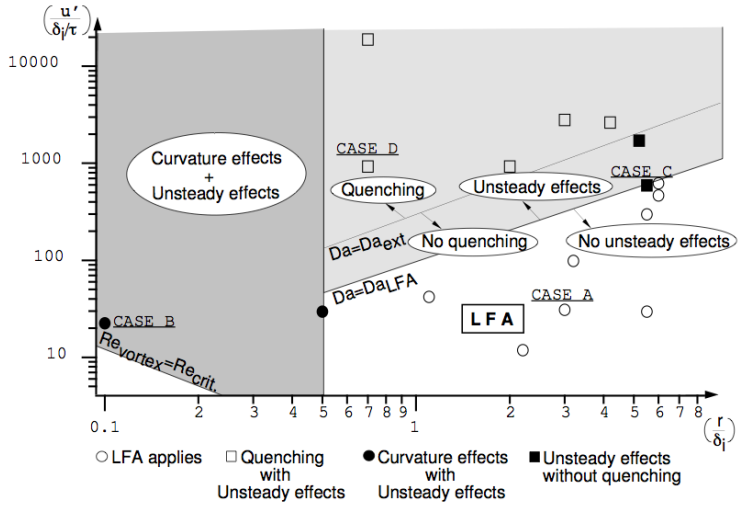


Figure 1: Combustion regimes scheme [9]

$Da$ numbers lower than $Da^{SE}$, the flow time scales are so fast that chemical reactions are inhibited by the strain.

For sufficiently large Damköhler numbers ($Da > Da^{LFA}$), chemistry is sufficiently fast to follow flow changes induced by the vortices. In this situation (case A), the flame front behaves like a laminar flame element relying on the stoichiometric isosurface and having the same strain rate of the flow field. The steady laminar flamelet assumption (LFA) applies, since both maximum temperature and reaction rate are in good agreement with laminar flame theory. The limit of this regime corresponds to $Da^{LFA} = 2Da^{SE}$.

In case B (small length scale ratio), a strong curvature of the flame front is observed and molecular and heat diffusion along tangential direction to the flame front become non negligible.

For case C ($Da^{ext} < Da < Da^{LFA}$) compared to case A, the Damköhler number decreases (or vortex speed $u'$ increases). The chemical time order of magnitude is comparable to the vortex characteristic time and the chemistry is not sufficiently fast to instantaneously "follow" the flow changes as in LFA regime. In this situation unsteady effects become relevant. The temporal evolution of the flame lags the temporal evolution of the flow and, accordingly also lags results from

asymptotic theories.
When the strain rate induced by the vortex on the flame front becomes too strong ($Da < Da^{ext}$), quenching occurs (case D). The quenching Damköhler number was measured from DNS: $Da^{ext} = 0.4Da^{SE}$.

## 3.3 NUMERICAL ISSUES

The numerical solution of the Navier-Stokes system for multi-species, chemically reacting, flows requires a numerical space and time discretization. The numerical discretization should ensure an accurate description of the space and time evolution of the system status. Hence a major physical constraint on the computational discretization of the system is given by its characteristic space and time scales.

### 3.3.1 *Turbulence*

Turbulent non reacting flows are characterized by a highly non regular motion in which larger eddies brake up into smaller ones, so the the kinetic energy of the flow is typically acquired at a large scale, the integral length scale $L_0$, then transferred to smaller eddies whose inertial energy is higher then the viscous forces, passing down the energy from the largest to the smallest without dissipation. The smallest eddies are small enough to have a balance between the inertial forces and the fluid viscosity, leading to the full dissipation of the kinetic energy. Kolmogorov proposed the first statistical theory of this mechanism, called the Richardson energy cascade, putting in relation the integral length scale $L_0$, at which energy is injected into the system, and the smallest space scale, the Kolmogorov scale $l_\eta$, at which the whole energy is dissipated.

Kolmogorov's theory relies on the assumption that while the large scale vortex are anisotropic and unstable, the smaller eddies are mainly isotropic. The smaller scale at which the eddies loose a mean direc-

tionality is estimated to be $l_{IE} = 1/6 l_0$. The motion occurring at scales smaller than $l_{IE}$ is quite universal and non dependent on the larger scale motions. Starting from this assumption, Kolmogorov deduced that the universal behavior of the small scales could be a function of fluid viscosity $\nu$ and energy dissipation $\epsilon$. The only space, velocity and time scales which can be defined in term of $\nu$ and $\epsilon$ are:

$$l_\eta = \left(\frac{\nu^3}{\epsilon}\right)^{\frac{1}{4}}, \tag{24}$$

$$u_\eta = (\epsilon\nu)^{\frac{1}{4}}, \tag{25}$$

$$\tau_\eta = \left(\frac{\nu}{\epsilon}\right)^{\frac{1}{2}}. \tag{26}$$

A second assumption involves having the whole kinetic energy dissipated at scales of the order of the Kolmogorov, that to achieve the balance of inertial and viscous forces. This assumption is supported by the fact that, expressing the local Reynolds number as a function of the previously defined quantities, one obtain that its value is unitary, that is:

$$Re_\eta = \frac{u_\eta l_\eta}{\nu} = 1. \tag{27}$$

Once defined $\nu$,$u_\eta$ and $l_\eta$, the energy dissipation rate $\epsilon$ as well as the characteristic time scale can be written as:

$$\epsilon = \nu \left(\frac{u_\eta}{l_\eta}\right)^2 \qquad ; \qquad \left(\frac{u_\eta}{l_\eta}\right) = \frac{1}{\tau_\eta^2}. \tag{28}$$

One more assumption is about the nature of the energy cascade, that is on the hypothesis of the existence of an inertial sub-range. This consisting of eddies smaller than the integral scale but larger than the Kolmogorov scale $l_{IE} < l < l_\eta$ whose role is to transfer energy from the larger scales to the Kolmogorov scale, without this process involving any dissipation. This last assumption allows to establish a relation between the large scales of motion $L_0$ and $u_0$ and the smallest one $l_\eta$, by means of the following estimate:

$$\epsilon = \nu \left(\frac{u_\eta}{l_\eta}\right)^2 \simeq \frac{u_0^3}{l_0}. \tag{29}$$

By means of Eq. (29), the ratio between the integral and Kolmogorov scales can be deduced as a function of the Reynolds number:

$$\frac{\eta}{l_0} = Re^{-\frac{3}{4}}, \tag{30}$$

$$\frac{u_\eta}{u_0} = Re^{-\frac{3}{4}}, \tag{31}$$

$$\frac{t_\eta}{t_0} = Re^{-\frac{1}{2}}. \tag{32}$$

These relations identify the minimum requirements for a numerical space and time discretization for a given integral length scale $L_0$ and time scale $t_0$. It is important to remark that Eq. (30) refers to only one dimension, for a three-dimensional, single species, problem $n_{\mathbf{x}} > Re^{\frac{9}{4}}$ points in space and $n_t > (Re^{\frac{1}{2}})$ time steps are required.

### 3.3.2 *Chemistry*

The computational effort required to directly solve the full system in Eqns (1)-(5) is much higher than the one needed to solve the finest fluid-dynamic motions of the corresponding non-reacting field at the Kolmogorov scales. This is mainly because of two major causes: the state vector dimension is increased and the time and space scales are much smaller than the Kolmogorov ones. The first is because every species mass fraction $Y_\alpha(\mathbf{x}, t)$ is an unknown variable which needs its evolution equation to be numerically discretized and integrated. The latter is because of the intrinsic nature of the chemical source term, whose characteristic time and space scales are usually smaller than the smallest fluid-dynamic ones. As an example one can chose the simplest case of one-step unimolecular irreversible reaction for the species $A$:

$$\frac{d[A]}{dt} = k_f(T)[A] \quad \rightarrow \quad [A](t) = e^{k_f t} \tag{33}$$

The time evolution of the concentration of the species [A] has a characteristics time scale $\tau = 1/k_f$. A detailed chemical mechanism

involves many species and reversible reactions, the reaction constant are temperature dependent, hence they vary in the field and can locally reach very high values since $k \propto T^{\beta} e^{-E_a/T}$ with very large values of $E_a$. Hence the space and time scales spectrum is usually broader than the fluid mechanic one.

### 3.3.3 *A model is required*

Although the turbulence constraints on a direct numerical simulation (DNS) are less severe than the chemistry ones, they are sufficient to make DNS approach unfeasible for studies of practical interest (i.e. a real engine combustion chamber).
The study of the averaged values of the field, obtained by the evolution of the Reynolds averaged Navier Stokes Equation (RANS), is much more computationally affordable. Anyway, by construction, RANS provide good information only on the averaged fields of motion. This making the description of transient phenomena inaccurate in most of the cases.
The Large Eddy Simulation (LES) approach is a good compromise between DNS and RANS. The LES approach relies on the assumption that a scale of motion $l_{IE}$ below which the eddies are mainly isotropic exists and is larger than the Kolmogorov one. Hence the motion whose length scale is $l$, with $\eta > l_{IE} > l > l_{filt}$, is directly simulated, while those effects on the fluid dynamics due to motions with smaller space frequency are properly modelled by means of the so called sub-grid models. In the LES approach the state vector of the system (1)-(5) $\mathbf{w}$, describing a chemically reacting flow, is decoupled into a spatially filtered value $\widetilde{\mathbf{w}}$ and its spatial sub-grid oscillations $\mathbf{w}'$ as follows:

$$\mathbf{w} = \widetilde{\mathbf{w}} + \mathbf{w}'. \tag{34}$$

Next Eq. (59) it is substituted in the original system (1)-(5) which is then wholly filtered, leading to a new system describing the time

evolution of the filters field. This brings to two major problems, one concerning the fluid dynamics, the other concerning chemistry, which make the LES system unclosed.

The first arises when the non-linear convective term is filtered, since:

$$\nabla \cdot \widetilde{u_i u_i} = \nabla \cdot \widetilde{(u_i + u_i')(u_i + u_i')} = \nabla \cdot (\widetilde{u}_i \widetilde{u}_i) + \nabla \cdot (\widetilde{u_i' u_i'}). \quad (35)$$

The term $\nabla \cdot (\widetilde{u_i' u_i'})$ is function of the sub-grid motions, and thus it is unclosed. This closure usually achieved by modelling the unclosed term as a function of the motions at larger scales. The second issue is the result of the filtering procedure on the chemical source terms $\widetilde{\dot{\omega}_\alpha}$. These filtered source terms can not be easily expressed as mere functions of $\widetilde{T}$ and $\widetilde{Y_\alpha}$, since the source term is a strongly non-linear function of temperature and species mass fractions. This can be showed with a simple irreversible reaction between fuel $F$ and oxidizer $O$ which gives products $P$. The source term depends on fuel concentration $[F] = Y_f \rho / W_\alpha$, oxidizer concentration $[O] = Y_O \rho / W_\alpha$ and temperature only. Defining a constant $A = \frac{A_O}{W_O}$, the activation temperature $T_a = \frac{E_a}{R}$ in Eq. (12) can be written as:

$$\dot{\omega}_F = A \rho^2 T^b Y_F Y_O e^{-T_a/T}. \quad (36)$$

This can be readily decomposed into a filtered value and a spatial fluctuation:

$$\dot{\omega}_F = \widetilde{\dot{\omega}_F} + \omega_F' = A \rho^2 (\widetilde{T} + T')^b (\widetilde{Y_F} + Y_F')(\widetilde{Y_O} + Y_O') e^{-T_a/(\widetilde{T}+T')}. \quad (37)$$

If the temperature oscillations are small, that is if $T'/\widetilde{T} << 1$, we have:

$$\widetilde{\dot{\omega}_F} = A \rho^2 (\widetilde{T})^b (\widetilde{Y_F}\widetilde{Y_O} + \widetilde{Y_F' Y_O'}) e^{-T_a/\widetilde{T}}. \quad (38)$$

Because of the exponential term, the chemical source term is highly dependent on temperature oscillations $T'$. Expanding the exponential

terms in a Taylor series as proposed by Poinsot and Veynante [9], we have:

$$e^{-T_a/T} = e^{-T_a/\widetilde{T}} \left(1 + \sum_{n=1}^{+\infty} P_n \frac{T'^n}{\widetilde{T}}\right) \tag{39}$$

$$T^b = \widetilde{T}^b \left(1 + \sum_{n=1}^{+\infty} Q_n \frac{T'^n}{\widetilde{T}}\right) \tag{40}$$

$$P_n = \sum_{k=1}^{n} (-1)^{n-k} \frac{(n-1)!}{(n-k)![(k-1)!]^2 k} \left(\frac{T_a}{\widetilde{T}}\right)^k$$

$$Q_n = \frac{b(b+1)..(b+n-1)}{n!}. \tag{41}$$

Hence the chemical source term of a one-step irreversible reaction can be rewritten as follows:

$$\begin{aligned} \widetilde{\dot{\omega}}_\alpha = A\rho^2 T^b \widetilde{Y}_F \widetilde{Y}_O e^{-T_a/\widetilde{T}} & \\ \cdot [1 + \frac{\widetilde{Y'_F Y'_O}}{\widetilde{Y}_F \widetilde{Y}_F} + (P_1 + Q_1) \frac{\widetilde{Y'_F Y'_O}}{\widetilde{Y}_F \widetilde{T}} + & \\ (P_2 + Q_2 + P_1 Q_1) \left(\frac{\widetilde{Y'_F T'}^2}{\widetilde{Y}_F \widetilde{T}^2} + \frac{\widetilde{Y'_O T'}^2}{\widetilde{Y}_F \widetilde{T}^2}\right) + ...]. & \end{aligned} \tag{42}$$

The first think to stress is that the Taylor series in Eq.(39) converge only of $T'/\widetilde{T} << 1$. Moreover, the source chemical source term expansion in Eq. (42) contains unclosed terms, such as $\widetilde{Y'_F Y'_O}^n$, which need to be modelled. Finally, it should be stressed that the high complexity of the previous equation is referred to the easiest chemistry mechanism, and is expected to be much higher for the case of realistic chemistry with up to hundreds of species and thousands reactions.
In few words, has been said before can be summarized as:

$$\widetilde{\dot{\omega}_\alpha(Y_\alpha, T)} \neq \dot{\omega}_\alpha(\widetilde{Y_\alpha}, \widetilde{T}). \tag{43}$$

The aim of turbulent combustion sub-grid models is to solve this problem. The conditional moment closure, in particular, by-passes

the problem of modelling $\widetilde{\dot{\omega}_\alpha}$ starting from the assumption that a conserved scalar field $\xi$ exists, such that:

$$\widetilde{\dot{\omega}_\alpha|\eta} \simeq \dot{\omega}_\alpha(\widetilde{Y_\alpha|\eta}, \widetilde{T|\eta}). \tag{44}$$

Where $\eta$ is the sample space variable of the scalar $\xi(\mathbf{x}, t)$, and $\widetilde{\phi|\eta}$, stands for the conditionally filtered value of the variable $\phi(\mathbf{x}, t)$ to $\eta = \xi(\mathbf{x}, t)$. As for the unconditional filtering process, the departure from the conditionally filtered value can be defined as $\phi'' = \phi - \widetilde{\phi|\eta}$. The relation in Eq. (44) is valid only if $T''/\widetilde{T} << 1$ and $\widetilde{Y_F'' Y_O''} \simeq 0$. and this is true if the passive scalar $\xi(\mathbf{x}, t)$ is well representative of the mixing degree of the flow field embedding in its evolution the spatial oscillation of temperature and mass fractions.

## 3.4 A PASSIVE SCALAR EXAMPLE

An example of the existence of passive scalar $\widetilde{\xi}$, such that Eq. (44) is verified, can be found by studying a laminar non-premixed flame, where the degree of mixing can be represented by a proper passive scalar value, the mixture fraction.

This statement can be easily verified in the case of a laminar non-premixed flame with a single-step chemical reaction, which involves only fuel (F), oxidizer (O) and products (P).

$$\nu_F F + \nu_O O \rightleftharpoons \nu_P P. \tag{45}$$

Under the assumptions of having constant thermodynamic pressure (low Mach numbers), equal and independent of temperature heat capacities: $C_{P,\alpha} = C_P$, equal diffusivities and unity Lewis number: $D_\alpha = D$, $Le_\alpha = Le = 1$, Fick's law for species molecular diffusion, the species conservation equations can be written as:

$$\frac{\partial \rho Y_F}{\partial t} + \frac{\partial \rho u_i Y_F}{\partial x_i} = \frac{\partial}{\partial x_i}\left(\rho D \frac{\partial Y_F}{\partial x_i}\right) + \dot{\omega}_F, \tag{46}$$

$$\frac{\partial \rho Y_O}{\partial t} + \frac{\partial \rho u_i Y_O}{\partial x_i} = \frac{\partial}{\partial x_i}\left(\rho D \frac{\partial Y_O}{\partial x_i}\right) + \dot{\omega}_O, \tag{47}$$

$$\frac{\partial \rho T}{\partial t} + \frac{\partial \rho u_i T}{\partial x_i} = \frac{\partial}{\partial x_i}\left(\frac{k}{C_P}\frac{\partial T}{\partial x_i}\right) + \dot{\omega}_T. \tag{48}$$

Once defined the reaction rate $Q$, and the mass stoichiometric reaction rate $s = \nu_O W_O / \nu_F W_F$, in a single-step reaction, the chemical source terms can be written as function of the fuel source term $\dot{\omega}_F$ as follows:

$$\dot{\omega}_F = \nu_F W_F Q, \tag{49}$$

$$\dot{\omega}_O = s\dot{\omega}_F, \tag{50}$$

$$\dot{\omega}_T = -\frac{Q}{C_P}\dot{\omega}_F. \tag{51}$$

So combining the equations (46)-(48), three quantities can be defined: $Z_1 = sY_F - Y_O$, $Z_2 = \frac{C_p T}{Q} + Y_F$, $Z_3 = s\frac{C_p T}{Q} + Y_F + Y_O$. These three quantities are solution of the same homogeneous equation:

$$\frac{\partial \rho Z}{\partial t} + \frac{\partial \rho u_i Z}{\partial x_i} = \frac{\partial}{\partial x_i}\left(\frac{k}{C_P}\frac{\partial Z}{\partial x_i}\right) \tag{52}$$

The previous equation is quite similar to the equations (46)-(48), without a source term. Moreover the new variables can be normalized as follows:

$$z_i = \frac{Z_i - Z_i^O}{Z_i^F - Z_i^O}, \quad i = 1, 2, 3 \tag{53}$$

where $Z_i^O$ and $Z_i^F$ are the values of $Z_i$ in the oxidizer and fuel stream respectively. The new variables $z_i$ are still solution of a convection diffusion equation of the form of Eq. (52), and have the same boundary conditions, that is: $z_i = 0$ in the fuel stream, and $z_i = 1$ in the fuel stream. Hence, all these equations have the same solutions. Defining

$Y_F^0$ as the fuel mass fraction in the fuel stream and $Y_O^0$ as the oxidizer mass fraction in the oxidizer stream, we have:

$$z = \frac{sY_F - Y_O + Y_O^0}{sY_F^0 + Y_O^0} = \frac{\frac{C_P}{Q}(T - T_O^0) + Y_F}{\frac{C_P}{Q}(T_F^0 - T_O^0) + Y_f} = \frac{\frac{sC_P}{Q}(T - T_O^0) + Y_O - Y_O^0}{\frac{sC_P}{Q}(T^0 - T_O^0) + Y_O - Y_O^0}, \tag{54}$$

once introduced the equivalence ratio $\phi = s\frac{Y_F^0}{Y_O^0}$, the mixture fraction can be written as [8] :

$$z = \frac{1}{1+\phi}\left(\phi\frac{Y_F}{Y_F^0} + \frac{Y_O}{Y_O^0} + 1\right). \tag{55}$$

This scalar is solution of a a transport equation of the kind of Eq(5). This simple case shows that the mixture fraction is one of the possible choices of passive scalar, since it is capable to give a full description of the flame behavior, once the initial conditions are known. It should be remarked that the the knowledge of the $z$ field provides the entire knowledge of the variable combinations $z_1$,$z_3$ and $z_3$, but not of the variables $T$, $Y_F$ and $Y_O$.

#### 3.4.0.1 *The flamelet equation*

The previously defined mixture fraction is an index of the degree of mixing of fuel and oxidizer. For instance, the $z = z_{st}$ iso-surface represents the points in space where fuel and oxidizer are in stoichiometric proportions. Hence a new frame of reference can be defined as $(z, y_2, y_3, t)$ where the mixture fraction $z$ is one of the axis, while $y_2$ and $y_3$ are in a plane tangential to the iso-mixture fraction surfaces, $(x, y, z, t) \rightarrow (z, y_2, y_3, t)$.

Since the whole chemical flame dynamics is a function of $z$, it can be assumed that all the space gradients in the $y_2$ and $y_3$ are null or negligible. From a mathematical point of view, this results in a convenient change of variables, with a dimensionality reduction from three spatial direction to only one, the mixture fraction $z$. From a

physical point of view, this implies that the flame dynamics is normal to the flame front, which means that the flame structure is locally thin compared to the flow scales, and one-dimensional.

This would imply the dependence of $Y_\alpha$ and $T_\alpha$ on time and mixture fraction, that is: $T(x,y,z,t) \rightarrow T(z,t)$ and $Y_\alpha(x,y,z,t) \rightarrow Y_\alpha(z,t)$. The species evolution equations (4) can be written in the new frame of reference under the flamelet hypothesis $\partial/\partial y_2 \simeq \partial/\partial y_3 \simeq 0$ and, by taking into account the continuity equation (1) and the mixture fraction equation (52), leads to the following *flamelet equation* [5] :

$$\rho\frac{\partial Y_\alpha}{\partial t} = \dot{\omega}_\alpha - \rho D\left(\frac{\partial z}{\partial x_i}\frac{\partial z}{\partial x_i}\right)\frac{\partial^2 Y_\alpha}{\partial z^2} = \dot{\omega}_\alpha - \frac{1}{2}\rho\chi\frac{\partial^2 Y_\alpha}{\partial z^2}. \tag{56}$$

In the the same way one obtains the temperature equation:

$$\rho\frac{\partial T}{\partial t} = \dot{\omega}_T - \frac{1}{2}\rho\chi\frac{\partial^2 T}{\partial z^2}. \tag{57}$$

Here the scalar dissipation $\chi = 2\rho D\left(\frac{\partial z}{\partial x_i}\frac{\partial z}{\partial x_i}\right)$ as been introduced. The influence of the fluid-dynamic flow field on the combustion processes is totally represented in $\chi$; it has the dimension of the inverse of a time, and gives an estimate of the mixing layer thickness through the relation $\delta_{mix} = \sqrt{D/\chi}$.

In the case of finite rate chemical kinetics, the full set of Eqns. (56) and (57) need to be solved, perhaps in a numerical way, in order to obtain a solution in the mixture fraction space. This solution will strongly depend on the scalar dissipation $\chi$, which embeds the fluid dynamic influence on the flame behavior.

The time dependence of the problem can be eliminated by introducing the *steady flamelet* assumption, that is the assumption of having a steady behavior of the flamelet in the mixture fraction space, even if the flow field is not at the steady state. This would imply that the species mass fractions and temperature are function of the mixture

fraction only: $T = T(z)$ and $Y_\alpha = Y_\alpha(z)$. Under this further hypothesis the Eqns.(56) and (57) become:

$$\dot{\omega}_\alpha = -\frac{1}{2}\rho\chi\frac{\partial^2 Y_\alpha}{\partial z^2} \qquad \dot{\omega}_T = -\frac{1}{2}\rho\chi\frac{\partial^2 T}{\partial z^2}. \tag{58}$$

It should be noted that a set of solution of the Eq. (58), parametrized to several values of the scalar dissipation $\chi$, can be computed off-line to generate a look-up table. Then the knowledge of the mixture fraction and scalar dissipation fields in the physical space, $z(\mathbf{x}, t)$ and $\chi(\mathbf{x}, t)$, would be sufficient to extract from the look-up table the corresponding values of species mass fractions and temperature $Y_\alpha(z(\mathbf{x}, t))$ and $T(z(\mathbf{x}, t))$.

Under the assumption of infinitely fast chemistry, that is the case of very large or infinite Damkholer number, the chemical reactions are much faster than the fluid-dynamics ones, so that chemistry is able to reach equilibrium in a temporal interval which is smaller than the smallest fluid-dynamic time scale. If the equilibrium assumption is introduced, the source terms $\dot{\omega}_\alpha$ and $\dot{\omega}_T$ are null because the equilibrium condition manifest itself in the equations of state, and the equations to be solve are:

$$\chi\frac{\partial^2 Y_\alpha}{\partial z^2} = 0. \tag{59}$$

Equation (59) is satisfied if $\chi = 0$, or $\frac{\partial^2 Y_\alpha}{\partial z^2} = 0$, or if both the previous are verified. In the case of reversible fast chemistry the condition $\chi = 0$ correspond to a locally fully premixed flame, where the mixture fraction is constant in the flow field, and the species reach the chemical equilibrium, so as to satisfy the law of mass action:

$$K(T) = \frac{Y_O^{\nu_O} Y_F^{\nu_F}}{Y_P^{\nu_P}}. \tag{60}$$

In the case of irreversible fast chemistry, fuel and oxidizer can not coexist, hence the condition $\frac{\partial^2 Y_\alpha}{\partial z^2} = 0$ leads to the Burke-Shumann solution, which involve linear profiles of species mass fractions, with a

slope discontinuity at $z = z_{st}$, $Y_O(z) = 0$ for $z > z_{st}$ and $Y_F(z) = 0$ for $z < z_{st}$. This solution, named the Burke-Shumann limit, is representative of a flame that takes place only in an infinitely thin region, the locus where $z = z_{st}$ and a chemical source term that is null everywhere but in the flame front, where it is infinite. A trivial solution of the condition $\frac{\partial^2 Y_\alpha}{\partial z^2} = 0$ is the frozen case, where no reaction occur, the solution is still linear, with constant slope,i.e. $Y_F(z) = z$, $Y_O(z) = 1 - z$, $Y_P(z) = 0$. This corresponds to the case of cold, frozen mixing of fuel and oxidizer.

### 3.4.1 *Splitting the problem in laminar flows*

A common practice in the solution of laminar non-premixed flames models is to split the problem into two different sub-problems coupled one to another, a mixing problem living in the physical space, and a combustion problem, living in the mixture fraction space. In other words the continuity equation, as well as the momentum equation are solved in the physical space $(\mathbf{x}, t)$ together with the conservation equation of the mixture fraction $z = z(\mathbf{x}, t)$ , while the species and temperature evolution equations are solved on the mixture fraction space as $T = T(z, t)$ and $Y_\alpha = Y_\alpha(z, t)$. Once the field of mixture fraction $z(\mathbf{x}, t)$ is known in the physical space, the scalar dissipation field $\chi = 2\rho D \left( \frac{\partial z}{\partial x_i} \frac{\partial z}{\partial x_i} \right)$ is known as well, so that the Eq.(56) and Eq.(57) can be solved, with various degree of accuracy, as discussed above, for the variables $T = T(z, t)$ and $Y_\alpha = Y_\alpha(z, t)$. Since the mixture fraction $z = z(\mathbf{x}, t)$ is a function of space and time in the physical space, the values of $T = T(z(\mathbf{x}, t), t) = T(\mathbf{x}, t)$ and $Y_\alpha = Y_\alpha(z(\mathbf{x}, t), t) = Y_\alpha(\mathbf{x}, t)$ can be retrieved by the look-up table generated by solving the combustion sub-problems.

### 3.4.2 *Splitting the problem in turbulent flows*

The Conditional Moment Closure method will be explained in detail in the next chapter. It can be seen as an extension of the previous method to turbulent flows, for instance in the LES context, where to take advantage of the relation (43), a part of NS system in (1-6) is partially conditionally filtered and solved in terms of conditional moments of the reactive scalars. Similarly to the laminar case, the NS system is recast in two parts, one of which is defined in a space which has the mixture fraction as additional dimension. However, the exact equations for the first moments have terms involving the second moments, these have terms involving the third moments, and so on [7]. The first order Conditional Moment Closure essentially aims at the solution of the evolution equation of the conditionally averaged or filtered values of the reacting scalars. This results in a space transformation that can be viewed in terms of laminar flamelet theories [5] as a more general view of the coordinate transformation, where the new independent conditioning variable is a locally stretched space coordinate.

# 4

# CONDITIONAL MOMENT CLOSURE FOR LES

In this section a Conditional Moment Closure (CMC) method for Large Eddy Simulation (LES) of compressible flows is introduced.

## 4.1 THE LES APPROACH

In LES approaches, the governing equations are spatially filtered so that only the flow scales larger than the filtering length $l_f$ are resolved, while the transport and dissipation at scales smaller than this scale are not and need to be modeled. The basic filtering procedure on a generic field variable $\phi(\mathbf{x}, t)$ relies on a spatial averaging procedure, which originates a filtered field variable $\overline{\phi}(\mathbf{x}, t)$ defined as:

$$\overline{\phi}(\mathbf{x}, t) := \int_V \phi(\mathbf{x}, t) G((\mathbf{x}, t) - (\mathbf{x}', t), \Delta) dV'. \tag{61}$$

The function $G(x - x_0, \Delta)$ is a filtering operator with spatial amplitude $\Delta$; the function $G$ takes the value 1 for $|\mathbf{x} - \mathbf{x}'| < \Delta$ and 0 for $|\mathbf{x} - \mathbf{x}'| > \Delta$. A Favre density-weighted filtered value $\widetilde{\phi}$ of the variable $\phi$ can also be defined as:

$$\overline{\phi}(\mathbf{x}, t) = \overline{\rho}(\mathbf{x}, t)\widetilde{\phi}(\mathbf{x}, t) \qquad \rightarrow \qquad \widetilde{\phi}(\mathbf{x}, t) = \frac{\overline{\phi}(\mathbf{x}, t)}{\overline{\rho}(\mathbf{x}, t)}. \tag{62}$$

The definition in Eq. (62) implies a decomposition of the variable $\phi(\mathbf{x}, t)$ into a filtered value $\widetilde{\phi}(\mathbf{x}, t)$ and its spatial fluctuations $\phi'(\mathbf{x}, t)$, named sub-grid values, which yields:

$$\phi(\mathbf{x}, t) = \widetilde{\phi}(\mathbf{x}, t) + \phi''(\mathbf{x}, t). \tag{63}$$

This decomposition can be applied to the whole state vector $\mathbf{w} = \{\rho, \mathbf{u}, E, T, p, \xi, Y_\alpha\}$, with $\alpha = 1, ..., N$, of Eqns. (64-68). The decomposed field variables can then be substituted into Eqns. (64-68). Given that the commutation error between filtering and space derivative operators is zero if $\Delta$ is not space dependent, the filtering procedure defined in Eq. (62) can be performed on the whole system. The resulting LES system will be the following:

$$\frac{\partial \overline{\rho}}{\partial t} + \frac{\partial \overline{\rho}\widetilde{u}_i}{\partial x_i} = 0, \tag{64}$$

$$\frac{\partial \overline{\rho}\widetilde{u}_i}{\partial t} + \frac{\partial \overline{\rho}\widetilde{u}_i\widetilde{u}_j}{\partial x_j} + \frac{\partial \overline{p}}{\partial x_i} - \frac{\partial \check{\tau}_{ij}}{\partial x_j} = 0, \tag{65}$$

$$\frac{\partial \check{E}}{\partial t} + \frac{\partial (\check{E} + \overline{p})u_j}{\partial x_j} - \frac{\partial \check{\tau}_{ij}\widetilde{u}_j}{\partial x_j} + \frac{\partial}{\partial x_j}\left[\lambda \frac{\partial \widetilde{T}}{\partial x_j}\right] + \sum_{\alpha=1}^{N}[\overline{\rho}\widetilde{\omega}_\alpha \Delta h_{0_\alpha}] = 0, \tag{66}$$

$$\frac{\partial \rho \widetilde{Y}_\alpha}{\partial t} + \frac{\partial \overline{\rho}\widetilde{Y}_\alpha \widetilde{u}_j}{\partial x_j} + \frac{\partial}{\partial x_j}\left(\overline{\rho} D \frac{\partial \widetilde{Y}_\alpha}{\partial x_j}\right) = 0, \tag{67}$$

$$\frac{\partial \widetilde{\xi}}{\partial t} + \frac{\partial (\overline{\rho}\widetilde{u}_j\widetilde{\xi})}{\partial x_j} + \frac{\partial}{\partial x_j}\left(D_\xi \frac{\partial \widetilde{\xi}}{\partial x_j}\right) = 0. \tag{68}$$

Where $\overline{\rho}$ and $\overline{p}$ are the spatially filtered density and pressure; $\widetilde{T}$ and $\widetilde{u}_i$ are the spatially Favre filtered temperature and velocity component in the $i-$th space direction; and $\check{E}$ is the filtered value of the total sensible energy of the mixture. Moreover, $\mu$ and $\lambda$ are the dynamic viscosity and thermal conductivity of the mixture, respectively, and $D_\xi$ stands for the mixture fraction diffusion coefficient. The filtered stress tensor $\check{\tau}_{ij}$ is defined as a function of the filtered values of the filtered velocity $\widetilde{u}_i$:

$$\check{\tau}_{ij} := \mu\left[\left(\frac{\partial \widetilde{u}_i}{\partial x_j} + \frac{\partial \widetilde{u}_j}{\partial x_i}\right) - \frac{2}{3}\delta_{ij}\frac{\partial \widetilde{u}_k}{\partial x}\right]. \tag{69}$$

### 4.1.1 *Transport properties and subgrid modeling*

Accordingly with the Smagorinsky closure model [48] the effects of the unresolved sub-grid scale motion, can be taken into account by means of a correction on the transport coefficients $\nu$, $\lambda$ and $D_\xi$. These can be redefined as the summation of a molecular and a turbulent transport contribution, that is:

$$\nu = \nu_l + \nu_t, \tag{70}$$

$$\lambda = \lambda_l + \lambda_t, \tag{71}$$

$$D = D_{\xi,l} + D_{\xi,t}. \tag{72}$$

The molecular $\nu_l$ viscosity can be modeled in several ways, the less computationally expensive involves assuming an exponential dependence on temperature as in Sutherland's law:

$$\frac{\nu_l}{\nu^*} = \frac{T^* + 113.3}{T + 110.3} \left( \frac{T}{T^*} \right)^{\frac{3}{2}}. \tag{73}$$

The turbulent viscosity $\nu_t$, that takes into account the dissipative effects arising from the sub-grid motion, is modeled as:

$$\nu_t = (C_S \Delta)^2 \|\widetilde{S}\|, \tag{74}$$

$$\widetilde{S} = (2 S_{ij} S_{ij}), \tag{75}$$

$$S_{ij} = \frac{1}{2} \left( \frac{\partial u_j}{\partial x_j} \frac{\partial u_j}{\partial x_j} \right). \tag{76}$$

Here $C_S$ is the Smagorinsky coefficient, and $\Delta$ is the spatial width of the filter in $G(\mathbf{x}, \Delta)$, i.e., the computational cell dimension. So $\nu_t$ is a function of the Frobenius norm of the resolved strain tensor $\|S\| = \sqrt{\frac{1}{2} \frac{\partial \widetilde{u}_i}{\partial x_i} \frac{\partial \widetilde{u}_j}{\partial x_j}}$, and of the filter width $\Delta$.
The thermal diffusion coefficients $\lambda$ and the diffusion coefficient $D$ are

related to the viscosity $\nu$ through the Prandtl and Schmidt numbers, $Pr$ and $Sc$, as done for their turbulent counterparts:

$$\nu = \nu_l + \nu_t, \tag{77}$$

$$\lambda = \frac{\mu_l C_p}{Pr} + \frac{\mu_t C_p}{Pr_t}, \tag{78}$$

$$D_\xi = \frac{\mu_l}{\overline{\rho} Sc} + \frac{\mu_t}{\overline{\rho} Sc_t}. \tag{79}$$

Where $\mu = \nu\overline{\rho}$, while $Pr_t$ and $Sc_t$ are the turbulent Prandtl and Schmidt numbers. Under the assumption of unity Lewis number, we have $Pr = Sc = 0.7$, $Pr_t = Sc_t = 0.4$.

### 4.1.2 *Mixture fraction definition*

The mixture fraction is one of the most important quantities in describing non premixed combustion. It can be defined in several ways, although the most intuitive definition is the one introduced in Sec. (3.4). This definition implies a number of simplifying assumptions, such as equal species diffusivity and single step irreversible chemistry. More generally, the mixture fraction can be defined as that particular scalar bounded between zero and one, which is a solution of (68), plus the boundary condition, which are $\xi = 1$ in pure fuel and $\xi = 0$ in pure oxidizer.

No assumption on the mixture fraction diffusivity is mandatory. Nevertheless, the choices $D_\xi = D_\alpha = D_{mix} = k$, i.e. $Le_\xi = 1$, is often advocated. This is justified in turbulent flows when the species molecular diffusivity $D_\alpha$ can be orders of magnitude smaller than the turbulent diffusivity $D_t$.

In all the passive scalar formulations, the mixture fraction only provides the information about the mixing degree of fuel and oxidizer, hence its filtered value alone is typically unable to offer a satisfactory statistical description of the fluctuating mixing field. Additional statistical moments, such as the mixture fraction variance $\widetilde{\xi''^2}(\mathbf{x}, t)$, need to be cal so considered as described in a following section.

### 4.1.3 *Reaction rate evaluation*

A closure model for the conditional filtered reaction rate $\widetilde{w_\alpha|\eta}$ has to be defined, since we already established that:

$$\widetilde{\dot{\omega}_\alpha(Y_\alpha, T)} \neq \dot{\omega}_\alpha(\widetilde{Y}_\alpha, \widetilde{T}). \tag{80}$$

As already mentioned in 3.3.3, Kilimengo and Bilger [8], [3] showed both numerically and experimentally that:

$$\widetilde{\dot{\omega}_\alpha(Y_\alpha, T)|\eta} \simeq \dot{\omega}_\alpha(\widetilde{Y_\alpha|\eta}, \widetilde{T|\eta}). \tag{81}$$

Where $\eta$ is the sample space variable of the mixture fraction $\xi(\mathbf{x}, \mathbf{t})$, while $\widetilde{\cdot|\eta}$ stands for the conditionally filtering operator. To take advantage of the relation (81), the knowledge of the conditionally filtered values of the reactive scalars $\widetilde{Y_\alpha|\eta}, \widetilde{T|\eta}, \overline{p|\eta}$ is required, while, in the LES context, only their unconditional values $\widetilde{Y}_\alpha, \widetilde{T}, \overline{p}$ are available. To overcome this problem, in the CMC method, the equations for the scalar fields are conditionally filtered and solved in the CMC domain space, whose independent space variables are $\mathbf{x}, \mathbf{t}$, and the mixture fraction $\eta$. In the next section, the exact definitions of what is a conditionally filtered value, as well as the conditionally filtered CMC equations are provided.

## 4.2 CONDITIONAL MOMENT CLOSURE FOR LES

In this section, both the conditional filtering procedure and the CMC equations, describing the evolution of the conditionally filtered values of the scalar fields of the species mass fractions $Y_\alpha$ and temperature $T$ are introduced.

#### 4.2.0.1 *Conditionally filtering the field*

The first step is to define a *fine grained PDF*, $\psi(\eta)$, of the mixture fraction $\xi(\mathbf{x}, t)$ as follows:

$$\psi(\eta) := \delta[\eta - \xi(\mathbf{x}, t)] \tag{82}$$

where $\delta$ stands for the Dirac function, and $\eta$ is the sample space variable of the mixture fraction $\xi(\mathbf{x}, t)$. Once defined a space filter $G(x, \Delta)$ with amplitude $\Delta$ and centered in $\mathbf{x}$ as:

$$G(\mathbf{x}, \Delta) = \begin{cases} 1, & \text{if } \mathbf{x} - \mathbf{x}' < \Delta \\ \\ 0, & \text{if } \mathbf{x} - \mathbf{x}' > \Delta \end{cases}, \tag{83}$$

a *conditional filtering procedure* for the scalar $\Phi$ can be defined as:

$$\widetilde{\Phi|\eta} = \frac{\int_V \rho(\mathbf{x}', t)\Phi\psi(\xi(\mathbf{x}', t) - \eta)G(\mathbf{x} - \mathbf{x}', \Delta)dV'}{\int_V \rho(\mathbf{x}', t)\psi(\xi(\mathbf{x}', t) - \eta)G(\mathbf{x} - \mathbf{x}', \Delta)dV'}, \tag{84}$$

where $V$ is the computational domain and $\widetilde{P}(\eta)$ is the density weighted *filtered probability density function* (FDF) :

$$\widetilde{P}(\eta) = \frac{1}{\overline{\rho}(\mathbf{x}', t)} \int_V \rho\psi(\xi(x', t) - \eta)G(\mathbf{x} - \mathbf{x}', \Delta)dV', \tag{85}$$

where $\overline{\rho}$ if the filtered density. The scalar $\Phi$ represents either a species mass fraction $Y_\alpha$, the temperature $T$, or the enthalpy $h$. It should be stressed that the so defined FDF is a function of the unfiltered values $\xi(\mathbf{x}', t)$ and $\Phi(\mathbf{x}, t)$, which are not available in the context of LES, where only the unconditionally filtered fields, $\widetilde{\xi}(\mathbf{x}, t)$ and $\widetilde{\Phi}(\mathbf{x}, t)$, are known; hence the FDF is unknown. Moreover, the conditionally filtered value $\widetilde{\Phi|\eta}(\eta, \mathbf{x}, t)$ is dependent on space and time and on an additional variable, the mixture fraction sample space variable $\eta$. In the following, a new set of independent variables $(\eta, \mathbf{x}, t)$ is introduced, which includes the conditionally filtered variable and will be referred to as the "CMC space". The unconditional and conditional filtered values are related by:

$$\widetilde{\Phi} = \int \widetilde{\Phi|\eta}\widetilde{P}(\eta)d\eta. \tag{86}$$

In variable density flows, density weighted (Favre) filtering is used. A density weighted filter is given by:

$$\bar{\rho}_\eta \widetilde{\Phi}_\eta = \widetilde{\rho\Phi|\eta}, \tag{87}$$

where the tilde indicates Favre filtering, while the underscript $\eta$ denotes the conditional variable, $\widetilde{\Phi}_\eta \equiv \widetilde{\rho\Phi|\eta}$.

### 4.2.1 *CMC formulation for LES*

The transport equations for the conditionally filtered reactive scalars Eqns. (111,113) are very similar to those derived for RANS formulations [8], although the decomposition method proposed by Bilger does not yield conditionally filtered reactive scalars transport equation consistent with the LES filtering procedure. The approach used by Martinez [34] to derive the LES-CMC equations follows the joint-pdf method proposed by Klimenko [3] and is reported below. The conservation equations of the fine-grained PDF, $\psi \equiv \delta(\xi(\mathbf{x}, y) - \eta)$, and the transport equation of the product of the fine grained pdf with a generic scalar $\Phi(\mathbf{x}, t)\psi$, represent a good starting point for the equation derivation. For a given velocity field $\mathbf{u}$, both the above mentioned equations can be derived as shown in the appendix A.1.3; the resulting two equations, are not mathematical identities, they essentially incorporate the equations that govern the scalar transport in turbulent flows. The evolution equation of the fine grained PDF, $\psi \equiv \delta(\xi(\mathbf{x}, y) - \eta)$, reads:

$$\frac{\partial \rho\psi}{\partial t} + \nabla \cdot (\rho \mathbf{u} \psi) = -\frac{\partial^2}{\partial \eta^2}(\rho N \psi) - \frac{\partial}{\partial \eta} \nabla \cdot (\rho \psi D_\xi \nabla \xi). \tag{88}$$

While for the product $\Phi(\mathbf{x}, t)\psi$ we have:

$$\frac{\partial \rho\Phi\psi}{\partial t} + \nabla\cdot(\rho\mathbf{u}\Phi\psi) = \\ -\frac{\partial^2}{\partial\eta^2}(\rho N\Phi\psi) - \frac{\partial}{\partial\eta}\Phi\nabla(\rho\psi D_\xi\nabla\xi) + \psi\nabla\cdot(\rho D_\phi\nabla\Phi) + \psi W_\Phi. \tag{89}$$

Where $D_\xi$ is the diffusion coefficient of the passive scalar $\xi$, $N \equiv D_\xi(\nabla\xi\cdot\nabla\xi)$ is the scalar dissipation, and $W_\Phi$ is the source term of the generic scalar $\Phi$ in the case $\Phi = Y_i$. Equations (88) and (89) are derived without any assumption on neither diffusivities or acoustic behavior. Anyway Eq. (89) can be simplified under the assumption of unity Lewis number (or equal diffusivity). This assumption is not mandatory for the LES-CMC derivation, anyway it can be reasonably assumed for turbulent flows, where turbulent diffusivity is orders of magnitude higher than molecular diffusivity ($D_t >> D_\alpha$). Hence, assuming $D_\xi = D_\Phi$ in Eqns. (89), yields:

$$\frac{\partial}{\partial t}(\rho\Phi\psi)+\nabla\cdot(\rho\mathbf{u}\Phi\psi) = \psi W_\Phi \\ -\nabla\cdot(\rho D\nabla(\Phi\psi)) + 2\frac{\partial}{\partial\eta}(\psi\rho D\nabla\xi\nabla\Phi) - \frac{\partial^2}{\partial\eta^2}(N\Phi\psi). \tag{90}$$

The $(\Phi\psi)$ dynamics is controlled by the velocity field convection, a molecular diffusion term, a source term, and an unclosed flux term, i.e. $J_\Phi$, defined as:

$$J_\Phi = 2\psi\rho D\nabla\xi\nabla\Phi - \frac{\partial}{\partial\eta}(N\Phi\psi). \tag{91}$$

The flux $J_\Phi$ represents the diffusion in the passive scalar space $\eta$, since the first term is a function of the scalar product of the $\Phi$ gradient and the passive scalar gradient, while the second is a flux in the $\eta$ space. Since our aim is to write the evolution equations for the spatially filtered value of the scalar $\Phi$, Eqns. (267) and Eqns.(90) are multiplied by the spatial filter centered in $\mathbf{x}'$, $G = G(\mathbf{x},\Delta)$ . If $\Delta$ is

constant in space, the filter $G$ commutes with spatial and temporal derivatives, this leading to:

$$\frac{\partial}{\partial t}(\rho\psi G) + \nabla\cdot(\rho\mathbf{u}\psi G) = -\frac{\partial^2}{\partial\eta^2}(\rho N\psi G) - \frac{\partial}{\partial\eta}\nabla(\rho\psi G D\nabla\xi), \quad (92)$$

$$\begin{aligned}\frac{\partial}{\partial t}(\rho\Phi\psi G)+\nabla\cdot(\rho\mathbf{u}\Phi\psi G) &= \psi W_\Phi G \quad (93)\\ &- \nabla\cdot(\rho D\nabla(\Phi\psi G)) + 2\frac{\partial}{\partial\eta}(\psi G\rho D\nabla\xi\nabla\Phi) - \frac{\partial^2}{\partial\eta^2}(N\Phi\psi G).\end{aligned}$$

The equations (92) and (93) can be integrated in the physical space over the whole domain. Given the definition of the FDF in Eq. (86), the FDF transport equation, as well as the conditional scalar transport equations, read respectively:

$$\begin{aligned}&\frac{\partial}{\partial t}\int\rho\psi G dV' + \nabla\cdot\int\rho\mathbf{u}\psi G dV' =\\ &-\frac{\partial^2}{\partial\eta^2}\int\rho N\psi G dV' - \frac{\partial}{\partial\eta}\nabla\cdot\int\rho\psi G D\nabla\xi dV', \quad (94)\end{aligned}$$

$$\begin{aligned}&\frac{\partial}{\partial t}\int\rho\Phi\psi G dV' + \nabla\cdot\int\rho\mathbf{u}\Phi\psi G dV' = \quad (95)\\ &-\frac{\partial^2}{\partial\eta^2}\int\rho N\Phi\psi dV' - \int\nabla\cdot(\rho D\nabla(\Phi\psi G))dV' +\\ &+\int\psi W_\Phi G dV' + 2\frac{\partial}{\partial}\int\psi G\rho D\nabla\xi\nabla\Phi dV'. \quad (96)\end{aligned}$$

Taking into account the definitions of conditional filtered density function, and conditionally filtered scalar value, the last two equations become respectively:

$$\frac{\partial\overline{\rho}_\eta\widetilde{P}(\eta)}{\partial t} + \nabla\cdot\overline{\rho}_\eta\widetilde{\mathbf{u}_\eta}\widetilde{P}(\eta) = -\frac{\partial^2\overline{\rho}_\eta\widetilde{P}(\eta)\widetilde{N}}{\partial\eta^2} - \frac{\partial}{\partial\eta}\nabla\cdot(\overline{\rho}_\eta\widetilde{P}(\eta)\widetilde{D\nabla\xi})_\eta, \quad (97)$$

$$\frac{\partial(\overline{\rho}_\eta\widetilde{\Phi}_\eta\widetilde{P}(\eta))}{\partial t} + (\nabla\cdot\overline{\rho}_\eta(\widetilde{\mathbf{u}\Phi})_\eta\widetilde{P}(\eta)) = \widetilde{W_{\Phi_\eta}}\widetilde{P}(\eta) + \nabla\cdot\mathbf{f}_D + \frac{\partial\widetilde{\mathbf{J}}_\Phi}{\partial\eta}. \quad (98)$$

Where the new notation $(\cdot)_\eta = \widetilde{\cdot|\eta}$ has been introduced. The term $\widetilde{\mathbf{J}}_\Phi$ is the conditionally filtered flux in the conserved scalar space, while $\mathbf{f}_D$ is the molecular flux:

$$\widetilde{\mathbf{J}}_\Phi = 2\overline{\rho}_\eta(\widetilde{D\nabla\xi\nabla\Phi})_\eta - \frac{\partial}{\partial\eta}\left[\overline{\rho}_\eta(\widetilde{N\Phi})_\eta\widetilde{P}(\eta)\right], \tag{99}$$

$$\mathbf{f}_D = \overline{\rho}_\eta\widetilde{P}(\eta)(\widetilde{D\nabla\Phi})_\eta - \frac{\partial}{\partial\eta}\left[\overline{\rho}_\eta\left(\widetilde{D\nabla\xi\Phi}\right)_\eta\widetilde{P}(\eta)\right]. \tag{100}$$

Both the two fluxes are unclosed and need to be modeled. For the conditionally filtered flux in the conserved scalar space $\widetilde{\mathbf{J}}_\Phi$, as for conventional CMC, the flux is assumed to be of Brownian nature. Since this assumption is independent [34] on averaging procedure we would have:

$$\widetilde{\mathbf{J}}_\Phi = A\widetilde{\Phi}_\eta + B\frac{\partial\widetilde{\Phi}_\eta}{\partial\eta} \tag{101}$$

where, analogously to the conventional CMC, the coefficients $A$ and $B$ must preserve the linear properties of turbulent scalar transport and they are therefore independent of $\widetilde{\Phi}_\eta$. So, assuming a linear profile $\Phi^* = a + b\xi$, being the coefficients $a$ and $b$ independent of position, we have $\widetilde{\Phi^*_\eta} = a + b\eta$. Then $\widetilde{\Phi^*_\eta}$ can be replaced in the Eq. (101) and compared to Eq. (99) leading to the following relations:

$$(\widetilde{D\nabla\xi\nabla[a+b\xi]})_\eta = (\widetilde{D\nabla\xi\nabla\xi})_\eta = b\widetilde{N}_\eta \tag{102}$$

$$(\widetilde{N[a+b\xi]})_\eta = \widetilde{N}_\eta[a+b\eta]. \tag{103}$$

We can obtain the following expressions for the coefficients $A$ and $B$:

$$A = \frac{\partial}{\partial\eta}(\overline{\rho}_\eta\widetilde{N}_\eta\widetilde{P}(\eta)) \tag{104}$$

$$B = \overline{\rho}_\eta\widetilde{N}_\eta\widetilde{P}(\eta) \tag{105}$$

The coefficient $A$ and $B$ obtained for $\Phi^*$ are independent on $\widetilde{\Phi}_\eta$, so they are valid for any $\widetilde{\Phi_\eta}$. Once substituted the expression of $\widetilde{\mathbf{J}}_\Phi$, the LES-CMC equation reads:

$$\frac{\partial(\overline{\rho}_\eta \widetilde{\Phi}_\eta \widetilde{P}(\eta))}{\partial t} + (\nabla \cdot \overline{\rho}_\eta (\widetilde{\mathbf{u}\Phi})_\eta \widetilde{P}(\eta)) = \widetilde{W_{\Phi_\eta}} \widetilde{P}(\eta) + \nabla \cdot \mathbf{f}_D + \quad (106)$$
$$+ \overline{\rho}_\eta \widetilde{N}_\eta \widetilde{P}(\eta) \frac{\partial^2 \widetilde{\Phi}_\eta}{\partial \eta^2} - \frac{\partial^2 \overline{\rho}_\eta \widetilde{N}_\eta \widetilde{P}(\eta)}{\partial \eta^2} \widetilde{\Phi}_\eta$$

The presence of the FDF in the previous equation can be eliminated by subtracting from it the FDF transport equation in Eq. (97), leading to:

$$\frac{\partial \widetilde{\Phi}_\eta}{\partial t} + \widetilde{\mathbf{u}_\eta} \nabla \widetilde{\Phi}_\eta = \frac{\widetilde{W_{\Phi_\eta}}}{\overline{\rho}_\eta} + \widetilde{N}_\eta \frac{\partial^2 \widetilde{\Phi}_\eta}{\partial \eta^2} + \mathbf{e_\Phi} + \mathbf{e_D} \quad (107)$$

where $\mathbf{e_D}$ and $\mathbf{e_\Phi}$ are such that:

$$\overline{\rho}_\eta \widetilde{P}(\eta) \mathbf{e_\Phi} \equiv \nabla \cdot [\overline{\rho}_\eta (\widetilde{\mathbf{u}}_\eta \widetilde{\Phi}_\eta - \widetilde{(\mathbf{u}_\eta \Phi)}) \widetilde{P}(\eta)] \quad (108)$$

$$\overline{\rho}_\eta \widetilde{P}(\eta) \mathbf{e_D} \equiv \nabla \cdot \overline{\rho}_\eta \widetilde{P}(\eta) \widetilde{(D \nabla \xi)}_\eta + \quad (109)$$
$$- \frac{\partial}{\partial \eta} \nabla [\overline{\rho}_\eta \widetilde{P}(\eta) \widetilde{(D \nabla \xi \Phi)}_\eta] + \widetilde{\Phi}_\eta \frac{\partial}{\partial \eta} \nabla \cdot [\overline{\rho}_\eta \widetilde{P}(\eta) \widetilde{(D \nabla \xi)}_\eta]$$

The first term $\mathbf{e_\Phi}$ takes into account the degree of spatial correlation of the velocity field $\mathbf{u}$ and the scalar $\Phi$. The second term $\mathbf{e_D}$ takes into account the filtered diffusion of the conditionally filtered scalar and tend to zero for $\mathrm{Re} \to \infty$ and can be neglected. The LES-CMC equation is then obtained for the case of $\Phi = Y_\alpha$ and $\widetilde{\Phi}_\eta = Q_\alpha$:

$$\frac{\partial Q_\alpha}{\partial t} + \widetilde{\mathbf{u}|\eta} \cdot \nabla Q_\alpha = \widetilde{\dot{\omega}_\alpha|\eta} + \widetilde{N|\eta} \frac{\partial^2 Q_\alpha}{\partial \eta^2} + e_y. \quad (110)$$

This equation describes the evolution of the conditionally filtered mass fractions $Q_\alpha = \widetilde{Y_\alpha|\eta}$, which are convected in the physical space, and diffused in the mixture fraction space, with the scalar dissipation acting as a diffusion coefficient, $\widetilde{N|\eta} = D \nabla \widetilde{\xi} \nabla \widetilde{\xi}$, being a function of the physical space only.

#### 4.2.1.1 *Conditionally filtered equations*

The CMC equations describe the evolution of the conditionally filtered values of the reactive scalars $Q_\alpha(\eta, \_, t) := \widetilde{Y_\alpha|\eta}$ in the CMC space. After the primary closure assumption has been applied, the CMC equation can be written as:

$$\frac{\partial Q_\alpha}{\partial t} + \widetilde{u_i|\eta}\frac{\partial Q_\alpha}{\partial x_i} = \widetilde{N|\eta}\frac{\partial^2 Q_\alpha}{\partial \eta^2} + \widetilde{\dot{\omega}_\alpha|\eta} + e_Y \tag{111}$$

The terms $\widetilde{u_i|\eta}$ and $\widetilde{N|\eta}$, where $N = D\frac{\partial \xi}{\partial x_i}\frac{\partial \xi}{\partial x_i}$, are in the order, the conditional filtered velocity and the conditional filtered scalar dissipation rate. These are both unclosed and need to be modeled. The term:

$$e_Y = -\frac{1}{\bar{\rho}\widetilde{P}(\eta)}\frac{\partial}{\partial x_1}[\bar{\rho}\widetilde{P}(\eta)(\widetilde{u_i Y_\alpha|\eta} + \widetilde{u_i|\eta}Q_\alpha)] \tag{112}$$

is the sub-grid scale conditional flux and accounts for the conditional transport in physical space. While $\widetilde{\dot{\omega}_\alpha|\eta}$ is the conditional filtered reaction rate which is known from Eq.(81).

It should be stressed that the previous equations are derived under the assumption of unity Lewis number. Nevertheless a multi diffusive formulation can be derived [38] by following a procedure similar to the one shown it the appendix A.1.3.

Moreover, under the previous assumption, and in the low-Mach number limit, the enthalpy equation can be recast in a very similar form:

$$\frac{\partial Q_h}{\partial t} + \widetilde{u_i|\eta}\frac{\partial Q_h}{\partial x_i} = \widetilde{N|\eta}\frac{\partial^2 Q_h}{\partial \eta^2} - \widetilde{\dot{\omega}_\alpha|\eta} + e_h, \tag{113}$$

where the term $e_h$ and $e_y$ are analogously defined. It can be noted that, defining:

$$\frac{DQ_\alpha}{Dt} = \frac{\partial Q_\alpha}{\partial t} + \widetilde{\mathbf{u}|\eta}\nabla Q_\alpha, \tag{114}$$

and letting $e_y \simeq 0$, which holds for laminar or weakly turbulent flows, the CMC equations take the form:

$$\frac{DQ_\alpha}{Dt} = \widetilde{\dot{\omega}_\alpha|\eta} + \widetilde{N|\eta}\frac{\partial^2 Q_\alpha}{\partial \eta^2}, \tag{115}$$

which is quite similar to the flamelet equation [1], this showing that, along a stream line, in the CMC space $(\mathbf{x}, t, \eta)$, combustion is driven by two contributions: the source term, and the dissipative term. The dissipative term acts in the $\eta$ space only, but its coefficient is strictly a function of the mixing field and fluid diffusivity.

### 4.2.2 *Relating conditional and unconditional values*

In the previously derived CMC equations, some terms are unclosed, such as the scalar dissipation $\widetilde{N|\eta}$, the conditional velocity $\widetilde{\mathbf{v}|\eta}$, and the sub-grid fluxes $e_y$. Following the conditionally filtering definition in Eq. (86), the first issue arises from the fact that the sub grid field of $\xi(\mathbf{x}, t)$ is not directly solved within the LES context. Hence, a conditionally filtered value can not be directly computed on the basis of the definition (84), while it should be modeled on the basis of the corresponding filtered value. Moreover, the CMC equations have to be solved on a meshes coarser than the LES ones, so as to increase the statistical significance of all the conditional quantities. Hence, the modeled conditionally filtered quantities available on the LES mesh, should be properly transferred to the coarser CMC mesh. While the first modeling procedure depends on the nature of the modeled term, and will typically dependent on the fluid dynamic model of closure, the latter can be done as follows [40]:

$$LES \rightarrow CMC: \quad \widetilde{\Phi|\eta}(\eta;\mathbf{x},t)|_{CMC} = \frac{\int_{V_{CMC}} \bar{\rho}\widetilde{\Phi|\eta}\widetilde{P}(\eta;\xi(x,t))dV'}{\int_{V_{CMC}} \bar{\rho}\widetilde{P}(\eta)dV'}, \tag{116}$$

$$CMC \rightarrow LES: \quad \widetilde{\Phi}(x,t) = \int_0^1 \widetilde{\Phi|\eta}|_{CMC}\widetilde{P}(\eta;\xi(x,t))d\eta. \tag{117}$$

As already said, the FDF $\widetilde{P}(\eta)$ is unknown as being a function of the sub-grid value of the mixture fraction $\xi(\mathbf{x},t)$, needs to be modeled.

#### 4.2.2.1 *Presumed shape filtered probability density function*

To solve the CMC equation a Filtered Probability Density function for the mixture fraction, $P(\eta)$, is needed. Although an FDF equation can be obtained analytically from the conservation equation for the velocity field probability distribution, the resulting equation will be unclosed, and a modeling for unclosed terms will be eventually required.

An easier way to get an FDF is to propose a model for it. The most common practice is to model it as a function of the filtered mixture fraction, $\tilde{\xi}$ and the mixture fraction variance $\widetilde{\xi''^2}$. The Beta function is a good candidate for the purpose, because of its ability to capture all the important features of the physics of the problem. If the random variable is the mixture fraction, the beta FDF is given by:

$$\begin{aligned} P(\eta) &= \frac{\eta^{r-1}(1-\eta)^{s-1}}{I_b}, \\ I_b &= \int_0^1 e^{r-1}(1-\eta)^{s-1}d\eta = \frac{\Gamma(r)\Gamma(s)}{\Gamma(r+s)}, \\ r &= \tilde{\xi}\left(\tilde{\xi}\frac{1-\tilde{\xi}}{\tilde{\xi''^2}} - 1\right), \\ s &= r\frac{1-\tilde{\xi}}{\tilde{\xi}}, \end{aligned} \tag{118}$$

where $\Gamma(x) = \int_0^\infty t^{x-1}e^t dt$ is the Gamma function. Both $\tilde{\xi}$ and $\tilde{\xi''^2}$

are positive quantities, and it can be shown that the range of variation of the mixture fraction variance is:

$$0 < \tilde{\xi}^{\tilde{\prime\prime}2} < \tilde{\xi}(1-\tilde{\xi}). \tag{119}$$

The previous relation is equivalent to say that $r > 0$ and $s > 0$. If $\tilde{\xi}(\mathbf{x}, t)$ and $\tilde{\xi}^{\tilde{\prime\prime}2}$ are such that both $r > 1$ and $s > 1$, the Beta FDF assumes a Gaussian-bell shape centered in $\tilde{\xi}$. This becomes larger or narrower as the variance $\tilde{\xi}^{\tilde{\prime\prime}2}$ increases or decreases respectively. If $\tilde{\xi}$ and $\tilde{\xi}^{\tilde{\prime\prime}2}$ are such that both $0 < r < 1$ and $0 < s < 1$, then the Beta FDF is bi-modal, as shown in Fig.2.

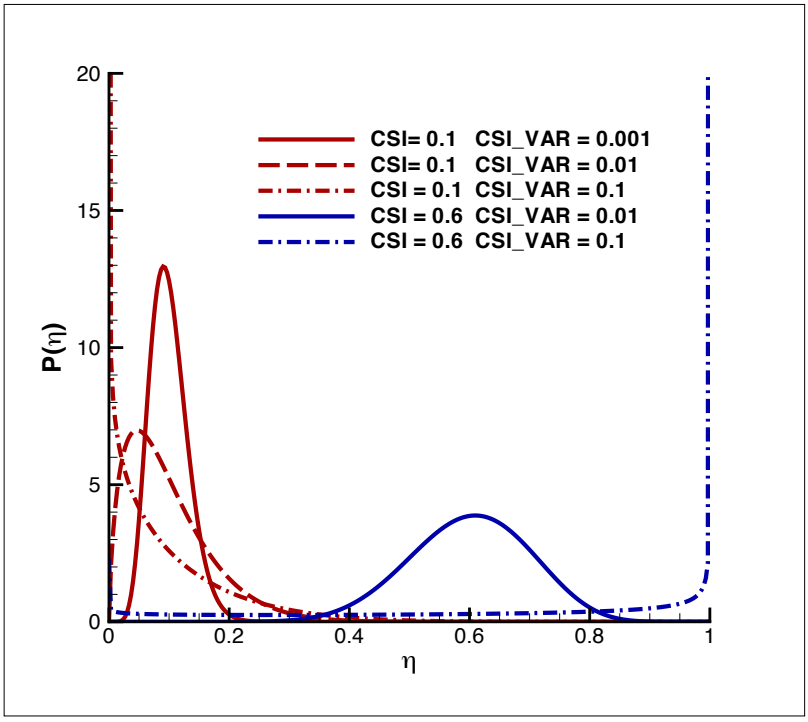


Figure 2: The Beta-FDF for several values of $\widetilde{\xi}$ and its variance $\tilde{\xi}^{\tilde{\prime\prime}2}$

### 4.2.3 *Sub-models of Closure*

#### 4.2.3.1 *Flow scales and numerical scales*

In the numerical implementation of the LES-CMC methodology, the CMC equations are usually discretized on a computational mesh with resolution $\Delta_{CMC}$. The CMC grid should be coarser than the mesh employed to discretize the LES equations, which has resolution $\Delta_{LES}$. This is to ensure the possibility of performing reliable conditional averages, required on the CMC mesh, on the basis of the LES scaler fields. As known, by definition the LES mesh is not fine enough to be resolve the sub-grid turbulent flow dynamics, which need to be modeled, i.e. $\Delta_{LES}$ is larger than the Kolmogorov scale. This is because the LES approach relies on the assumption that the smallest scales of the turbulent field are assumed to be independent from the larger scales and hence have be modeled. However, the conditional filtered values are less variable in space than the corresponding unconditionally filtered ones, and this is why $\Delta_{CMC}$ can be higher than $\Delta_{LES}$. The CMC equations written for the LES case in (111), like the RANS-CMC equations, include some terms that need to be modeled. The LES modeling options are very similar to those adopted for the RANS-CMC equations. So, once the $\widetilde{u_i|\eta}$, $\widetilde{N|\eta}$, and $e_y$ are provided from informations available at the LES level, then the CMC equations are closed can be evolved in time. The exchange of information from LES to CMC takes place through the calculation of $\widetilde{u_i|\eta}$, $\widetilde{N|\eta}$, $e_y$, and by means of the presumed-shape FDF which is a function of the filtered mixture fraction $\widetilde{\xi}$ and of his variance $\widetilde{\xi''^2}$ as illustrated in Eqns. (116 and (117).

#### 4.2.3.2 *Mixture fraction sub-grid scale variance*

In addition to the transport equation for $\widetilde{\xi}(\mathbf{x},t)$ in (68), an evolution equation for the mixture fraction variance $\widetilde{\xi''^2}(\mathbf{x},t)$ can be derived:

$$\frac{\partial \bar{\rho}\widetilde{\xi''^2}}{\partial t}+\frac{\partial \bar{\rho}\widetilde{u}_i\widetilde{\xi''^2}}{\partial x_i}=-\frac{\partial}{\partial x_j}\left(\widetilde{\bar{\rho}u_i''\xi''^2}\right)+2\bar{\rho}(-\widetilde{u_i''\xi''})\left(\frac{\partial\widetilde{\xi}}{\partial x_i}\right)-\bar{\rho}(\widetilde{D\nabla\xi\nabla\xi}). \tag{120}$$

Anyway the terms $\widetilde{u_i''\xi''^2}$ and $\widetilde{u_i''\xi''}$ are unclosed and should be modeled. For this reason, the mixture fraction variance is often directly modeled by means of a gradient type model as follows:

$$\widetilde{\xi''^2}=C_V\Delta^2\left(\frac{\partial\widetilde{\xi}}{\partial x_i}\frac{\partial\widetilde{\xi}}{\partial x_i}\right), \tag{121}$$

where $C_V$ is a suitable coefficient chosen coherently with the Smagorisky sub-grid model [48].

#### 4.2.3.3 *Conditional Velocity*

As already said, in the LES context, the sub grid field values are unknown, hence the conditionally filtered value of the velocity $\widetilde{u|\eta}(\mathbf{x},t,\eta)$ should be written as a function of the filtered value $\widetilde{u}(\mathbf{x},t)$. While in RANS approaches a linear model for conditional velocity is used, in LES equation it has not still validated, and instead, the use of a constant value $\widetilde{u|\eta}$ has been advocated, to obtain:

$$\widetilde{u_i|\eta}=\widetilde{u}_i. \tag{122}$$

#### 4.2.3.4 *Scalar dissipation rate*

The basic assumption is that the filtered scalar dissipation rate may be regarded as the sum of its resolved and sub-grid scale components:

$$\widetilde{N}=\widetilde{N}_{res}+\widetilde{N}_{sgs}, \tag{123}$$

where:

$$\widetilde{N}_{res} = D\left(\frac{\partial\widetilde{\xi}}{\partial x_i}\frac{\partial\widetilde{\xi}}{\partial x_i}\right), \tag{124}$$

while the sub-grid contribution $\widetilde{N}_{sgs}$ needs to be modeled. An often used model is:

$$\widetilde{N}_{sgs} = \frac{1}{2}C_N D_t\left(\frac{\partial\widetilde{\xi}}{\partial x_i}\frac{\partial\widetilde{\xi}}{\partial x_i}\right). \tag{125}$$

This model is based on the hypothesis that the sub-grid scales are in equilibrium with the larger scales. The coefficient $C_N$ was found by Garmory and Mastorakos [49, 44] to give good match to Sandia flame D [4] experimental results, when set equal to 42. However, the previous model can not be used if the sub-grid variance is calculated from Eq. (120), since it would become a convection-diffusion equation, which is far away from its physical behavior [44]. To bypass this problem, a different model can be adopted, which relies on the assumption that a characteristic mixing time-scale $\tau_\xi = \widetilde{\xi''^2}/\widetilde{N}_{sgs}$ is proportional to a characteristic velocity time-scale $\tau_t = \nu_t/\Delta^2$, leading to the expression:

$$\widetilde{N}_{sgs} = \frac{\nu_t}{\Delta^2}\widetilde{\xi''^2}. \tag{126}$$

#### 4.2.3.5 *Conditionally filtered scalar dissipation rate*

To relate the filtered value of the scalar dissipation $\widetilde{N|\eta}(\mathbf{x},t,\eta)$ to its unconditional value $\widetilde{N}(\mathbf{x},t)$, the Amplitude Mapping Closure (AMC) approach can be used to model the conditionally filtered scalar dissipation rate:

$$\widetilde{N|\eta} = N_0\lambda(\eta), \tag{127}$$

$$\lambda(\eta) = exp(-2[erf^{-1}(2\eta-1)]^2),$$

$$N_0 = \frac{\widetilde{N}}{\int_0^1 \widetilde{P}(\eta)\lambda(\eta)d\eta}, \tag{128}$$

where $erf$ is the error function. This assumption means that, within an LES cell, the scalar dissipation conditional distribution is considered to be $\lambda(\eta)$-shaped.

### 4.2.4 *Sub-grid fluxes*

The terms $e_y$ and $e_h$, that account for fluctuations around the conditional mean, defined in Eq. (112) can be modeled by a gradient approach:

$$e_y \simeq -\nabla(D\nabla Q_\alpha). \tag{129}$$

These terms can become important under certain flame conditions such as local extinction and reignition. In the present formulation, they are neglected [34].

### 4.2.5 *Boundary and initial conditions for CMC*

The CMC model, which is composed of conditional averaged equations for species and temperature (or enthalpy) needs boundary conditions on conditionally filtered species mass fractions $\widetilde{Y_\alpha|\eta}$ and conditional averaged temperature $\widetilde{T|\eta}$ as well. Boundary conditions have to be imposed on the CMC equations. In the mixture fraction space, pure oxidizer and pure fuel conditions must be imposed at $\eta = 0$ and $\eta = 1$ respectively. The convective fluxes boundary conditions vary with the problem of interest.

# 5

# LES/CMC COUPLING STRATEGIES

## 5.1 PROBLEM DECOUPLING

The main principles of the CMC method has been introduced in Eq. (81). The conditional filtering procedure has been defined in sec. 4.2.1, and the transport equations for the conditionally filtered species mass fraction have been derived, leading to the Eq. (111).
Chemical reactions affect the flow field in terms of thermal expansion (associated to the heat release), and change in chemical composition. In the system in Eqns. (1-7), these two mechanisms are described by the chemical source term in the species transport equations and by the energy source term in the energy equations. Moreover, the variable mixture composition affects the equations of state and the thermo chemical and transport properties of the flow system. As explained above, in the LES context, the chemical source term cannot be expressed in terms of unconditionally filtered values, because of its strong sensitivity to the sub-grid scale fluctuations. Anyway, since its conditionally filtered value can be reasonably expressed in terms of conditionally filtered values of the species mass fractions, the CMC method overcomes the chemical closure problem by evolving the conditionally filtered species equations in the CMC space. So, while the mass and momentum equations are filtered and solved in the physical space $(\mathbf{x}, t)$, the species mass fractions are conditionally filtered and solved in the CMC space $(\mathbf{x}, t, \eta)$, as discussed in section 4.2.1.
A special role is played by the energy equation in the context of a compressible LES formulation. Indeed, the energy equation is tightly coupled on one hand to the mass and momentum equations to describe the compressible flow acoustic behavior, while, on the other

hand, it accounts for the change in sensible energy caused by the variable composition, which is known only in terms of conditionally filtered values. To respect the dual role of the energy equation, we will discuss two two-way coupling strategies between the LES and the CMC systems.

## 5.2 VECTOR FIELD UPDATE

In the present approach, the "full system", Eq. (1-7), is partitioned in two sub-sets: one, named "mixing system", is filtered and solved in the LES space, the other, referred to as "reaction system", is conditionally filtered and solved in the CMC space. Mass and momentum equations are part of the LES sub-set, while the species evolution equations are found only in the CMC sub-set. The the processes driving the sensible energy equation are split into two contributions: (i) the heat release rate due to chemical reactions, which is conditionally filtered and solved in the CMC space, and (ii) the transport, convective and diffusive, of sensible energy in a fully compressible frozen mixture, which is filtered and solved in the LES space. This way, the LES sub-set describes a fully compressible frozen mixture mixing problem, while the CMC sub-set describes, for a given (LES generated) pressure field, the change in mixture composition and the energy rise owing to chemical reactions. A two-way coupling between the LES and CMC sub-sets is obtained by updating the LES temperature and composition field with the information coming from the CMC sub-set, while the conditional pressure and velocity fields, needed to solve the CMC sub-set, are obtained from the LES sub-set. Formally, the present formulation aims at solving the full system for the filtered variables $\mathbf{v} = \widetilde{\mathbf{w}} = \{\overline{\rho}, \widetilde{\mathbf{u}}, \widetilde{E}, \widetilde{T}, \overline{p}, \widetilde{\xi}, \widetilde{Y_\alpha}\}$ :

$$\frac{\partial \mathbf{v}}{\partial t} = F(\mathbf{v}); \qquad \mathbf{v}(0) = \mathbf{v}_0, \tag{130}$$

numerically by means of an operator splitting technique as follows:

$$a) \qquad \mathbf{v}_m^* = \mathbf{v}^{(n)} + F_m(\mathbf{v}_m^{(n)}; U_m^{(n)})\Delta t, \tag{131}$$

$$b) \qquad \mathbf{q}_r^* = f(\widetilde{\mathbf{v}_m^*|\eta}), \quad U_r^* = U_r^*(\widetilde{\mathbf{v}_m^*|\eta}) \tag{132}$$

$$c) \qquad \mathbf{q}_r^{(n+1)} = \mathbf{q}_r^* + F_r(\mathbf{q}_r^*; U_r^*)\Delta t, \tag{133}$$

$$d) \qquad \mathbf{v}^{(n+1)} = \mathbf{v}_m^{(n+1)} = convol(\mathbf{q}_r^{(n+1)})$$

$$U_m^{(n+1)} = U_m^{(n+1)}(\mathbf{v}_m^{(n+1)}), \tag{134}$$

where $\mathbf{v}^{(n)} = \mathbf{v}(t_n)$, $\mathbf{v}^{(n+1)} = \mathbf{v}(t_{n+1})$, while the superscript asterisk stands for intermediate computational value. The vectors $\mathbf{v}_m$ and $\mathbf{q}_r$ are the state vectors of the mixing and the reaction system, and are defined in the following. The operator $F(\_)$ indicates symbolically the full system, while $F_m(\_)$ and $F_r(\_)$ indicate symbolically the "LES mixing system", and the "CMC reaction system" operators, respectively; $\Delta t = t^{(n)} - t^{(n-1)}$ is a time interval of integration which is defined on the basis of a CFL condition for the "LES mixing system". As already presented in sec.4.2.3, the operator $F_r(\_)$ depends on conditionally filtered parameters here indicated with $U_r$, such as the conditional velocity and the conditional scalar dissipation, which are function of the conditionally filtered values of the vector field $\mathbf{v}^{(n)}$, and hence have to be updated at each iteration as will be discussed in detail later on. Similarly, the operator $F_m(\_)$, representing the "LES mixing system", depends on parameter indicated symbolically with $U_m$, such as the mixture specific heat $C_{v,mix}$ and $C_{p,mix}$, as well as the gas constant $R_{mix}$, which have to be updated at each time-step with the informations obtained from the "CMC reactive system". The operator $convol(\cdot)$ stands for the convolution operator reported in Eq. (117).

### 5.2.1 *The Mixing System*

The first sub-set, the "mixing system", has $\mathbf{w}_m = \{\rho_m, \mathbf{u}_m, E_m, T_m, p_m, \xi_m, Y_{\alpha,m}\}$ as state vector describing a chemically frozen flow, with the passive scalar $\xi = \xi(Y_\alpha)$ associated with the mixing processes:

$$\frac{\partial \rho_m}{\partial t} + \frac{\partial \rho_m u_{m,j}}{\partial x_j} = 0, \tag{135}$$

$$\frac{\partial \rho_m u_{m,j}}{\partial t} + \frac{\partial \rho_m u_{m,j}}{\partial x_j} + \frac{\partial p_m}{\partial x_j} - \frac{\partial \tau_{ij}}{\partial x_j} = 0, \tag{136}$$

$$\frac{\partial E_m}{\partial t} + \frac{\partial (E_m + p_m) u_{m,j}}{\partial x_j} - \frac{\partial \tau_{ij} u_{m,j}}{\partial x_i} + \frac{\partial}{\partial x_j}\left[k \frac{\partial T_m}{\partial x_j}\right] = 0, \tag{137}$$

$$\frac{\partial \rho_m \xi_m}{\partial t} + \frac{\partial (\rho_m u_{m,j} \xi)}{\partial x_j} + \frac{\partial}{\partial x_j}\left(D \frac{\partial \xi_m}{\partial x_j}\right) = 0. \tag{138}$$

It is derived from the "full system", Eq. (1-7), under the assumption of frozen composition. Hence the chemical source term in the energy equation can be set to zero, and the species evolution equations can be replaced by a transport equation of the mixture fraction $\xi$; here $\rho_m, T_m, E_m$ represent the density, temperature, and total sensible energy, when they are varied by fluid-dynamics alone. The "mixing system", Eqs. (135-138), is filtered according with the LES method, to yield the "LES mixing system":

$$\frac{\partial \overline{\rho}_m}{\partial t} + \frac{\partial \overline{\rho}_r \widetilde{u_{m,j}}}{\partial x_j} = 0, \tag{139}$$

$$\frac{\partial \overline{\rho}_m \widetilde{u_{m,j}}}{\partial t} + \frac{\partial \overline{\rho_m} \widetilde{u_{m,i}} \widetilde{u_{m,j}}}{\partial x_j} + \frac{\partial \overline{p}_m}{\partial x_j} - \frac{\partial \breve{\tau}_{ij}}{\partial x_j} = 0, \tag{140}$$

$$\frac{\partial \breve{E}_m}{\partial t} + \frac{\partial (\breve{E}_m + \overline{p}_m) \widetilde{u_{m,j}}}{\partial x_j} - \frac{\partial \breve{\tau}_{ij} \widetilde{u_{m,j}}}{\partial x_i} + \frac{\partial}{\partial x_j}\left[\widetilde{k} \frac{\partial \widetilde{T}_m}{\partial x_j}\right] = 0, \tag{141}$$

$$\frac{\partial \widetilde{\xi_m}}{\partial t} + \widetilde{u_{m,j}} \frac{\partial \widetilde{\xi}_m}{\partial x_j} - \frac{\partial}{\partial x_j}\left[ D \frac{\partial \widetilde{\xi}_m}{\partial x_j} \right] = 0. \tag{142}$$

The "LES mixing system" is represented by the operator $F_m(\_)$ in Eq. (131), and has a state vector $\mathbf{v}_m = \{\overline{\rho}_m, \widetilde{\mathbf{u}}_m, \breve{E}_m, \widetilde{T_m}, \overline{p}_m, \widetilde{\xi_m}, \widetilde{Y}_{\alpha,m}\}$, where the energy $\breve{E}_m$ is the filtered total sensible energy of the frozen mixture. Closure models are required for the sub-scale stress tensor $\sigma_{ij}$, the thermal term $\Theta_j$, as well as for the transport coefficients, the Smagorinsky sub-grid scale model can be used as shown in sec. 4.1.1.

### 5.2.2 *The Reactive System*

The second sub-set, the "reactive system", has a state vector $\mathbf{w}_r = \{\rho_r, \mathbf{u}_r, E_r, T_r, p_r, \xi_r, Y_{\alpha,r}\}$, whose evolution is controlled by the equations of the species mass fractions, Eq. (4), and by the energy equation obtained by subtracting Eq. (137) from Eq. (3) and combining these with Eq. (7), to yield:

$$\frac{\partial \rho_r e_{s,r}}{\partial t} + \sum_{\alpha=1}^{N} [\rho_r \dot{\omega}_\alpha \Delta h_{0_\alpha}] = 0, \tag{143}$$

$$\frac{\partial \rho Y_{r,\alpha}}{\partial t} + \frac{\partial (\rho_r u_{r,j} Y_{r,\alpha})}{\partial x_j} = -\frac{\partial}{\partial x_j}\left( \rho_r D \frac{\partial Y_{r,\alpha}}{\partial x_j} \right) + \dot{\omega}_\alpha, \quad \alpha = 1, N, \tag{144}$$

where:

$$\rho_r e_{s,r} = E_r - \frac{1}{2} \rho_r u_{r,j} u_{r,j}. \tag{145}$$

Here $e_{s,r}$ and $T_r$ are the sensible energy and temperature, whose variation is due to chemical reactions alone, while the velocity field $\mathbf{u}_r$ and the pressure field $\overline{p}_r$ will be assumed to constant during the time integration interval $\Delta t$. A conditionally filtered reaction system, referred to as the "CMC reaction system", is derived from the "reaction system" in Eq. (143-144), by recasting the energy equation in

terms of temperature, and following a CMC conditional filtering approach, to yield:

$$\frac{\partial Q_{\alpha,r}}{\partial t} + \widetilde{u_{r,i}|\eta}\frac{\partial Q_{\alpha,r}}{\partial x_i} = \widetilde{N|\eta}\frac{\partial^2 Q_{\alpha,r}}{\partial \eta^2} - \widetilde{\dot{\omega}_\alpha|\eta} + e_Y, \qquad \alpha = 1,..,N \quad (146)$$

$$\frac{\partial Q_{T_r}}{\partial t} = \widetilde{\dot{\omega}_{T_r}|\eta}. \quad (147)$$

The " CMC reactive system" in Eqns. (146) and (147) corresponds to the operator $F_r(\_)$ in Eq. 133: Eq. (146) is derived from Eq. (4) as shown in section 4.2.1, while Eq. (147) is obtained by conditionally filtering the source term $\overline{\sum_{\alpha=1}^{N}[\rho w_\alpha \Delta h_{0_\alpha}]/C_{p,mix}}$ of the energy equation, Eq. (3). The CMC space involves the physical space $\mathbf{x}$ as well as the mixture fraction $\eta$ as additional dimension. The " CMC reactive system" state vector $\mathbf{q}(\mathbf{x},t,\eta) = \{\widetilde{Y_{r,\alpha}|\eta}, \widetilde{T_r|\eta} = \{Q_\alpha, Q_{T_r},\}$, is obtained by conditionally filtering a part of the vector $\mathbf{w}_r$, i.e. the temperature $T_r$ and the species mass fraction $Y_\alpha$. The velocity field $\mathbf{u}_r$ and the scalar dissipation $\widetilde{N} = f(\widetilde{\xi}_r)$ are conditionally filtered to held the CMC diffusive and convective coefficients: $\widetilde{N|\eta}$ and $\widetilde{\mathbf{u}|\eta}$. The conditionally filtered pressure field $\widetilde{p_r|\eta}$ is employed for the computation of the conditionally filtered source terms, $\widetilde{\dot{\omega}_\alpha|\eta}$. All these conditionally filtered quantities are required to close the "CMC reactive system", and are indicated with $U_r$ in Eq. (131).

### 5.2.3 *VFU coupling algorithm*

Once the operators $F_m(\_)$, and $F_r(\_)$, and the vectors $\mathbf{v}_m$ and $\mathbf{q}_r$, have been defined, the operator splitting-based algorithm of the VFU in Eqns.(131-134) can be reported in detail as follows:

o) The initial conditions for both the "LES mixing system" and "CMC reactive system" are provided.

o-a) Initial condition for "LES mixing system" , i.e. $\mathbf{v}_m(t = t_0) = \mathbf{v}_{m,0}$:

$$\begin{pmatrix} \overline{\rho}_m(\mathbf{x}, t_0) \\ \overline{\rho}_m \widetilde{u}_{m,i}(\mathbf{x}, t_0) \\ \overline{\rho}_m \breve{E}_m(\mathbf{x}, t_0) \\ \overline{\rho}_m \widetilde{\xi}_m(\mathbf{x}, t_0) \\ \widetilde{Y_{m,\alpha}}(\mathbf{x}, t_0) \end{pmatrix} = \begin{pmatrix} \overline{\rho}_{m,0}(\mathbf{x}) \\ \overline{\rho}_{m,0}(\mathbf{x}) \widetilde{u}_{i,0}(\mathbf{x}) \\ \overline{\rho}_{m,0}(\mathbf{x}) \breve{E}_0(\mathbf{x}) \\ \overline{\rho}_{m,0}(\mathbf{x}) \widetilde{\xi}_0(\mathbf{x}) \\ \widetilde{Y}_{\alpha,m,0}(\mathbf{x}) \end{pmatrix}$$

o-b) Initial conditions for "CMC reactive system", i.e. $\mathbf{q}_r(t = t_0) = \mathbf{q}_{r,0}$:

$$\begin{pmatrix} Q_\alpha(\mathbf{x}, t_0, \eta) \\ Q_T(\mathbf{x}, t_0, \eta) \end{pmatrix} = \begin{pmatrix} Q_{\alpha,0}(\mathbf{x}, \eta) \\ Q_{T,0}(\mathbf{x}, \eta) \end{pmatrix} = \begin{pmatrix} \widetilde{Y_{\alpha,m,0}|\eta} \\ \widetilde{T_{m,0}|\eta} \end{pmatrix}$$

n) The $n$-th time step is composed of the following phases:

a) The information on the mixture composition are known from the previous step as function of the mixture fraction:

$$R, mix^{(n)} = R(\widetilde{Y}_\alpha^{(n)}(\widetilde{\xi}^{(n)})), \quad C_v^{(n)} = C_{(v)}(T^{(n)}, \widetilde{Y}_\alpha^n(\widetilde{\xi}^{(n)})), \quad C_p^{(n)} = C_p(T^{(n)}, \widetilde{Y}_\alpha^{(n)}(\widetilde{\xi}^{(n)})).$$

Hence the parameter $U_m^{(n)}$ is known and the "LES mixing system" is evolved in time:

$$\begin{pmatrix} \overline{\rho}_m^* \\ \overline{\rho}_m^* \widetilde{u}_{m,i}^* \\ \overline{\rho}_m^* \breve{E}_m^* \\ \overline{\rho}_m^* \widetilde{\xi}_m^* \end{pmatrix} = \begin{pmatrix} \overline{\rho}_m^{(n)} \\ \overline{\rho}_m^{(n)} \widetilde{u}_{m,i}^{(n)} \\ \overline{\rho}_m^{(n)} \breve{E}_m^{(n)} \\ \overline{\rho}_m^{(n)} \widetilde{\xi}_m^{(n)} \end{pmatrix} + F_m \begin{pmatrix} \overline{\rho}_m^{(n)} \\ \overline{\rho}_m^{(n)} \widetilde{u}_{m,i}^{(n)} \\ \overline{\rho}_m^{(n)} \breve{E}_m^{(n)} \\ \overline{\rho}_m^{(n)} \widetilde{\xi}^{(n)} \end{pmatrix} \Delta t$$

b) Temperature field is obtained by inverting the caloric equation of state:

$$\widetilde{T}^* = f(\breve{E}^*, \widetilde{Y}_\alpha^{(n)}(\widetilde{\xi}^*)).$$

The scalar dissipation field is obtained as function of mixture fraction gradients:

$$\widetilde{N}^* = f(\nabla(\widetilde{\xi}^*)).$$

The initial condition for $F_r(\_)$ in terms of temperature field are computed:

$$Q_T^* = cond\_filter(T^*),$$

and the conditionally filtered values, $U_r^*$, required to close the reacting system $F_r(\_)$:

$$\begin{aligned}
\widetilde{N^*|\eta} &= cond_filter(N^*),\\
\widetilde{\mathbf{u}^*|\eta} &= cond_filter(\mathbf{u}^*),\\
\widetilde{p^*|\eta} &= cond_filter(p^*),
\end{aligned} \tag{148}$$

where the operator $cond\_filter(\cdot)$ stand for the conditional filtering operation in Eq. (117).

c) The "CMC reactive system", $F_r(\_)$, is then evolved in time:

$$\begin{pmatrix} Q_\alpha^{(n+1)} \\ Q_T^{(n+1)} \end{pmatrix} = \begin{pmatrix} Q_\alpha^{(n+1)} \\ Q_T^* \end{pmatrix} + F_r \begin{pmatrix} Q_\alpha^{(n)} \\ Q_T^* \end{pmatrix} \Delta t$$

d) The species mass fraction and temperature LES fields are updated as follows:

$$\begin{aligned}
\widetilde{Y}_\alpha^{(n+1)} &= convol(Q_\alpha^{(n+1)})\\
\widetilde{T}^{(n+1)} &= convol(Q_T^{(n+1)}).
\end{aligned}$$

Where variables $\mathbf{q}_r(\mathbf{x}, t, \eta)$ and the LES physical filtered variables $\mathbf{v}_m$ are linked by the convolution operations in Eq. (116), here indicated with the operator $convol(\cdot)$, and

a presumed-shape pdf is employed as explained in section 4.2.2. The vector field $\mathbf{v}$ is then updated as follows:

$$\overline{R}_{av}^{(n+1)} = \sum (R_{\alpha}^{(n+1)} \widetilde{Y}_{\alpha}^{(n+1)}),$$

$$\overline{\rho}^{(n+1)} = \frac{\overline{P}^{(n)}}{\overline{R}_{mix}^{(n+1)} \overline{T}^{(n+1)}},$$

$$(\overline{\rho}\widetilde{u})^{(n+1)} = (\overline{\rho}\widetilde{u})^{(n)} \frac{\overline{\rho}^{(n+1)}}{\overline{\rho}^{(n)}},$$

$$(\overline{\rho}\check{E})^{(n+1)} = \frac{\overline{\rho}^{(n+1)}}{\overline{\rho}^{(n)}} \check{E}^{(n)} + \overline{\rho}^{(n+1)} \int_{T^{(n)}}^{T^{(n+1)}} \hat{C}_{v,mix}^{(n+1)} dT + \frac{(\overline{\rho}\widetilde{u})^{(n+1)}}{\overline{\rho}^{(n+1)}},$$

$$(\overline{\rho}\widetilde{\xi})^{(n+1)} = (\overline{\rho}\widetilde{\xi})^{(n)} \frac{\overline{\rho}^{(n+1)}}{\overline{\rho}^{(n)}}$$

n+1) .....

It should be noted that the global time interval of integration, defined on the basis of a CFL condition over acoustics for the LES mixing system, is usually larger than the time interval required to integrate the CMC reaction system. Hence, although multiple CMC time-steps are required per each LES time-step, the assumption of constant pressure is still reasonable since the LES time interval is the acoustic one. The VFU algorithm is summarized, by means of a diagram, in fig. 3.

## 5.3 ENERGY SOURCE UPDATE

The ESU approach is substantially different from the VFU approach. The VFU approach relies on the splitting of the "full system" into two sub-systems, hence the time evolution of the state vector is due to the contribution of the two sub-systems, which are evolved in time sequentially by means of an operator splitting technique, Eqns. (130). Following the ESU approach [42], the evolution of the state vector $\mathbf{v}$ is totally described by a properly defined system, named "LES main system". The "main system" is composed of mass, momentum, energy, and mixture fraction equations. The species equations are substituted

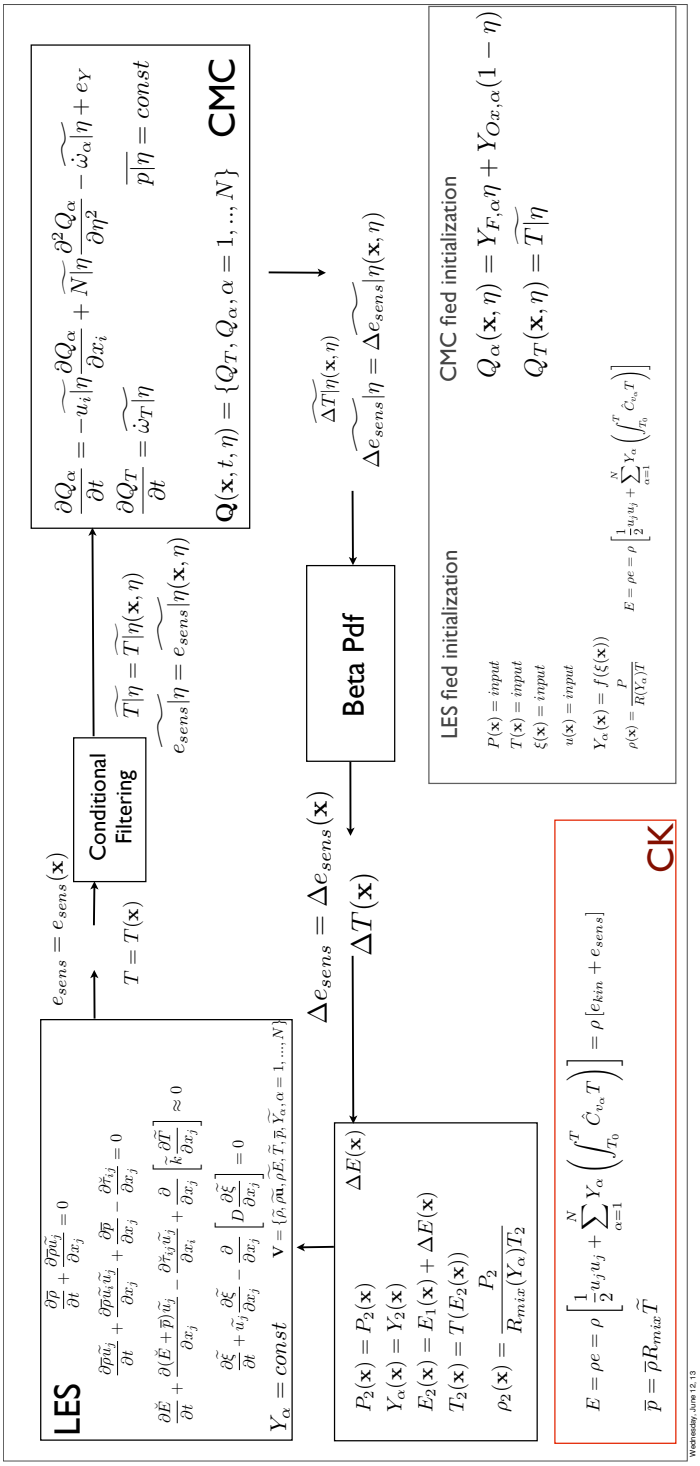


Figure 3: CMC/LES Vector Field Update (VFU) coupling

by the mixture fraction equation, while an energy source term in the energy equation describes the thermal effects due to chemical processes. The energy source term is function of temperature, pressure, and species mass factions, so it is unclosed. The "main system" is filtered accordingly to the LES technique, while the evolution of the species mass fractions and an additional energy equation are conditionally filtered accordingly to the CMC technique. The energy source term and the change in composition resulting from the evolution of the CMC system, constitute the closure model for the "main system". Formally, the present formulation aims at solving the full system for the filtered variables $\mathbf{v}$ as follows:

$$\frac{\partial \mathbf{v}}{\partial t} = F_M(\mathbf{v}; U)\Delta t; \qquad \mathbf{v}(0) = \mathbf{v}_0, \tag{149}$$

where $F_M$ stands for the "LES main system", while the parameter $U = U(\mathbf{v})$, representing the energy source term and the change in composition, is unclosed and is obtained from the evolution of the CMC equations by means of Eq. (117). Like in the VFU formulations, the conditional pressure and velocity fields, required to solve the CMC equations, are known from the LES sub-set, by means of the relations in Eq. (116).

### 5.3.1 *Main System*

The "main system" is derived from the "full system", Eq. (1-7), by replacing the species evolution equations by a transport equation of the mixture fraction $\xi$. The "LES main system" is obtained by filtering the "main system" accordingly with the LES technique, and has a state vector $\mathbf{v}$, which is identical to the one introduced for the previous formulation. Finally the "LES main system" takes the form:

$$\frac{\partial \overline{\rho}}{\partial t} + \frac{\partial \overline{\rho}\widetilde{u_j}}{\partial x_j} = 0, \tag{150}$$

$$\frac{\partial \overline{\rho}\widetilde{u_j}}{\partial t} + \frac{\partial \overline{\rho}\widetilde{u_i}\widetilde{u_j}}{\partial x_j} = -\frac{\partial \overline{p}}{\partial x_j} + \frac{\partial \check{\tau}_{ij}}{\partial x_j}, \tag{151}$$

$$\frac{\partial \check{E}}{\partial t} + \frac{\partial (\check{E} + \overline{p})\widetilde{u_j}}{\partial x_j} - \frac{\partial \check{\tau}_{ij}\widetilde{u_j}}{\partial x_i} + \frac{\partial}{\partial x_j}\left[\widetilde{k}\frac{\partial \widetilde{T}}{\partial x_j}\right] = \widetilde{\dot{\omega}_h}, \tag{152}$$

$$\frac{\partial \widetilde{\xi}}{\partial t} + \widetilde{u_j}\frac{\partial \widetilde{\xi}}{\partial x_j} - \frac{\partial}{\partial x_j}\left[D\frac{\partial \widetilde{\xi}}{\partial x_j}\right] = 0. \tag{153}$$

The "LES main system" is unclosed, since the energy source term and specific heats of the mixture, indicated symbolically with $U$ in Eq. (149), are unknown. The energy source term $\widetilde{\dot{\omega}_h} = \overline{\sum_{\alpha=1}^{N}[\rho\dot{\omega}_\alpha \Delta h_{0_\alpha}]}$ is provided from the temporal integration of the CMC equations over a time interval $\Delta t$. Moreover, the specific heats are provided by the CMC closure, being functions of the mixture composition through the mixture fraction $\widetilde{\xi}$ as well.

### 5.3.2 *CMC Closure*

The energy source term $\widetilde{\dot{\omega}_h}$ and the species mass fractions $\widetilde{Y}_\alpha$, required to compute $C_{v,mix}$, $C_{p,mix}$, and $R_{mix}$, being necessary to close the "LES main system", are obtained from the time integration of the conditionally filtered counterpart of the species and energy equations, Eqns. (3) and (4) written in terms of temperature $T$, to yield the "closure system" as follows:

$$\frac{\partial Q_\alpha}{\partial t} + \widetilde{u_i|\eta}\frac{\partial Q_\alpha}{\partial x_i} = \widetilde{N|\eta}\frac{\partial^2 Q_\alpha}{\partial \eta^2} - \widetilde{\dot{\omega}_\alpha|\eta} + e_Y, \qquad \alpha = 1, .., N \tag{154}$$

$$\begin{aligned}&\frac{\partial Q_T}{\partial t} + \widetilde{u_x|\eta}\frac{\partial Q_T}{\partial x_i} - \widetilde{N|\eta}\frac{\partial^2 Q_T}{\partial \eta^2} + \\ &+ \widetilde{N|\eta}\left[\frac{1}{\widetilde{c_p|\eta}}\left(\frac{\partial \widetilde{c_p|\eta}}{\partial \eta} + \sum_\alpha c_{p,\alpha}\frac{\partial Q_\alpha}{\partial \eta}\right)\right]\frac{\partial^2 Q_\alpha}{\partial \eta^2} + e_T + \widetilde{\dot{\omega}_h|\eta} = 0,\end{aligned} \tag{155}$$

The state vector associated to the above equations is defined as $\mathbf{q}(\mathbf{x}, t, \eta) = \{Q_\alpha, Q_{T,r}\} = \{\widetilde{Y_{r,\alpha}|\eta}, \widetilde{h_r|\eta}\}$, while the velocity field $\widetilde{\mathbf{u}}$ and the pressure field $\overline{p}$ are assumed constant in time. As in the previous formulation, the conditionally filtered variables $\mathbf{q}(\mathbf{x}, t, \eta)$ and the unconditionally filtered variables $\mathbf{v}$ are related by the convolution operations in eqns. (116-117).

At each time step, a time averaged conditionally filtered source term can be written as:

$$\widetilde{\dot{\omega}_T|\eta}^{(n+1)} = \frac{1}{\Delta t}\int_{t_n}^{t^n+\Delta t} \widetilde{\dot{\omega}_T|\eta} dt, \tag{156}$$

The term $\widetilde{\dot{\omega}_T|\eta}$ as well as the updated mass fractions $\widetilde{Y}_\alpha$ and specific heats, are formally indicated with $U$ in Eq. (149), and represent a closure for the system $F_M(\_)$.

### 5.3.3 *ESU coupling algorithm*

The ESU coupling algorithm can be summarized as follows:

o) The initial conditions for both the LES "main system" and "CMC closure systems" are provided.

o-a) Initial condition for LES, i.e. $\mathbf{v}(t = t_0) = \mathbf{v}_0$:

$$\begin{pmatrix} \overline{\rho}(\mathbf{x}, t_0) \\ \overline{\rho}\widetilde{u}_i(\mathbf{x}, t_0) \\ \overline{\rho}\breve{E}(\mathbf{x}, t_0) \\ \overline{\rho}\widetilde{\xi}(\mathbf{x}, t_0) \\ \widetilde{Y_\alpha}(\mathbf{x}, t_0) \end{pmatrix} = \begin{pmatrix} \overline{\rho}_0(\mathbf{x}) \\ \overline{\rho}_0(\mathbf{x})\widetilde{u}_{i,0}(\mathbf{x}) \\ \overline{\rho}_0(\mathbf{x})\breve{E}_0(\mathbf{x}) \\ \overline{\rho}_0(\mathbf{x})\widetilde{\xi}_0(\mathbf{x}) \\ \widetilde{Y}_{\alpha,0}(\mathbf{x}) \end{pmatrix}$$

o-b) Initial conditions for CMC, i.e. $\mathbf{q}(t = t_0) = \mathbf{q}_0$

$$\begin{pmatrix} Q_\alpha(\mathbf{x}, t_0, \eta) \\ Q_T(\mathbf{x}, t_0, \eta) \end{pmatrix} = \begin{pmatrix} Q_{\alpha,0}(\mathbf{x}, \eta) \\ Q_{T,0}(\mathbf{x}, \eta) \end{pmatrix} = \begin{pmatrix} \widetilde{Y_{\alpha,0}|\eta} \\ \widetilde{T_0|\eta} \end{pmatrix}$$

n) The $n$-th time step is composed of the following phases:

a) Since the unclosed terms of the "LES main system", $F_M(\_)$, are known,

$$U: \quad \widetilde{\omega}_T^n; \quad R_{mix}^n = R(\widetilde{Y}_\alpha^n(\widetilde{\xi}^{(n)})), \quad C_{v,mix}^n = C_{v,mix}(T^n, \widetilde{Y}_\alpha^n(\widetilde{\xi}^{(n)})).$$

The system in evolved in time:

$$\begin{pmatrix} \overline{\rho}^{(n+1)} \\ \overline{\rho}^{(n+1)}\widetilde{u}_i^{(n+1)} \\ \overline{\rho}^{(n+1)}\breve{E}^{(n+1)} \\ \overline{\rho}^{(n+1)}\widetilde{\xi}^{(n+1)} \end{pmatrix} = \begin{pmatrix} \overline{\rho}^{(n)} \\ \overline{\rho}^{(n)}\widetilde{u}_i^{(n)} \\ \overline{\rho}^{(n)}\breve{E}^{(n)} \\ \overline{\rho}^{(n)}\widetilde{\xi}^{(n)} \end{pmatrix} + F_M \begin{pmatrix} \overline{\rho}^{(n)} \\ \overline{\rho}^{(n)}\widetilde{u}_i^{(n)} \\ \overline{\rho}^{(n)}\breve{E}^{(n)} \\ \overline{\rho}^{(n)}\widetilde{\xi}^{(n)} \end{pmatrix}$$

b) A temperature field is obtained by inverting the caloric equation of state:

$$\widetilde{T}^{(n+1)} = f(\breve{E}^{(n+1)}, \widetilde{Y}_\alpha^{(n)}(\widetilde{\xi}^{(n+1)})).$$

The scalar dissipation field is obtained as function of mixture fraction gradients:

$$\widetilde{N}^{(n+1)} = f(\nabla(\widetilde{\xi}^{(n+1)}))$$

the initial condition, in terms of temperature field, for "CMC closure system" are computed:

$$Q_T^{(n+1)} = cond\_filter(T^{(n+1)}),$$

and the conditionally filtered values required to close the "CMC closure system" are deduced:

$$\begin{aligned} \widetilde{N^{(n+1)}|\eta} &= cond\_filter(N^{(n+1)}), \\ \widetilde{\mathbf{u}^{(n+1)}|\eta} &= cond\_filter(\mathbf{u}^{(n+1)}), \\ \widetilde{p^{(n+1)}|\eta} &= cond\_filter(p^{(n+1)}), \end{aligned} \tag{157}$$

where the operator $cond\_filter(\cdot)$ stand for the conditional filtering operation in Eq. (117).

c) The "CMC closure system" is evolved in time:

$$\begin{pmatrix} Q_\alpha^{(n+1)} \\ Q_T^{(*)} \end{pmatrix} = \begin{pmatrix} Q_\alpha^{(n)} \\ Q_T^{(n+1)} \end{pmatrix} + F_r \begin{pmatrix} Q_\alpha^{(n)} \\ Q_T^{(n+1)} \end{pmatrix} \Delta t$$

d) The conditionally filtered energy source term is known :

$$\widetilde{\dot{\omega}_h|\eta}(t) = \sum_\alpha (\widetilde{\dot{\omega}_\alpha|\eta}(t)\Delta h_{0,\alpha})$$

A time average over $\Delta t$ is performed:

$$\widetilde{\overline{\dot{\omega}_h|\eta}}^{(n+1)} = \frac{1}{\Delta t}\int_{t^n}^{t^{n+1}} \widetilde{\dot{\omega}_h|\eta}(t)dt$$

d) While the new temperature value $Q_T^*$ is discarded, the species mass fraction LES fields , and the energy source terms is computed are updated as:

$$\begin{aligned} &\widetilde{Y}_\alpha^{n+1} = convol(Q_\alpha^{n+1}). \\ &\widetilde{\dot{\omega}}_h^{n+1} = convol(\widetilde{\overline{\dot{\omega}_h|\eta}(t)}). \end{aligned} \tag{158}$$

Here the conditionally filtered variables $\mathbf{q}_r(\mathbf{x}, t, \eta)$ and the LES physical filtered variables $\mathbf{v}_m$ are linked by the convolution operations in Eq. (116), here indicated with the operator $convol(\cdot)$, and a presumed-shape pdf is employed as explained in section 4.2.2.

n+1) The next iteration can be performed, since both the energy source term and the new species mass fraction fields are known:

$$R^{(n+1)} = R(\widetilde{Y}_\alpha^{(n+1)}(\widetilde{\xi}^{(n+1)})), \quad C_v^{(n+1)} = C_v(T^{(n+1)}, \widetilde{Y}_\alpha^{(n)}(\widetilde{\xi}^{(n+1)})) \tag{159}$$

...)

The ESU coupling approach is summarized by means of the diagram in fig. 4.

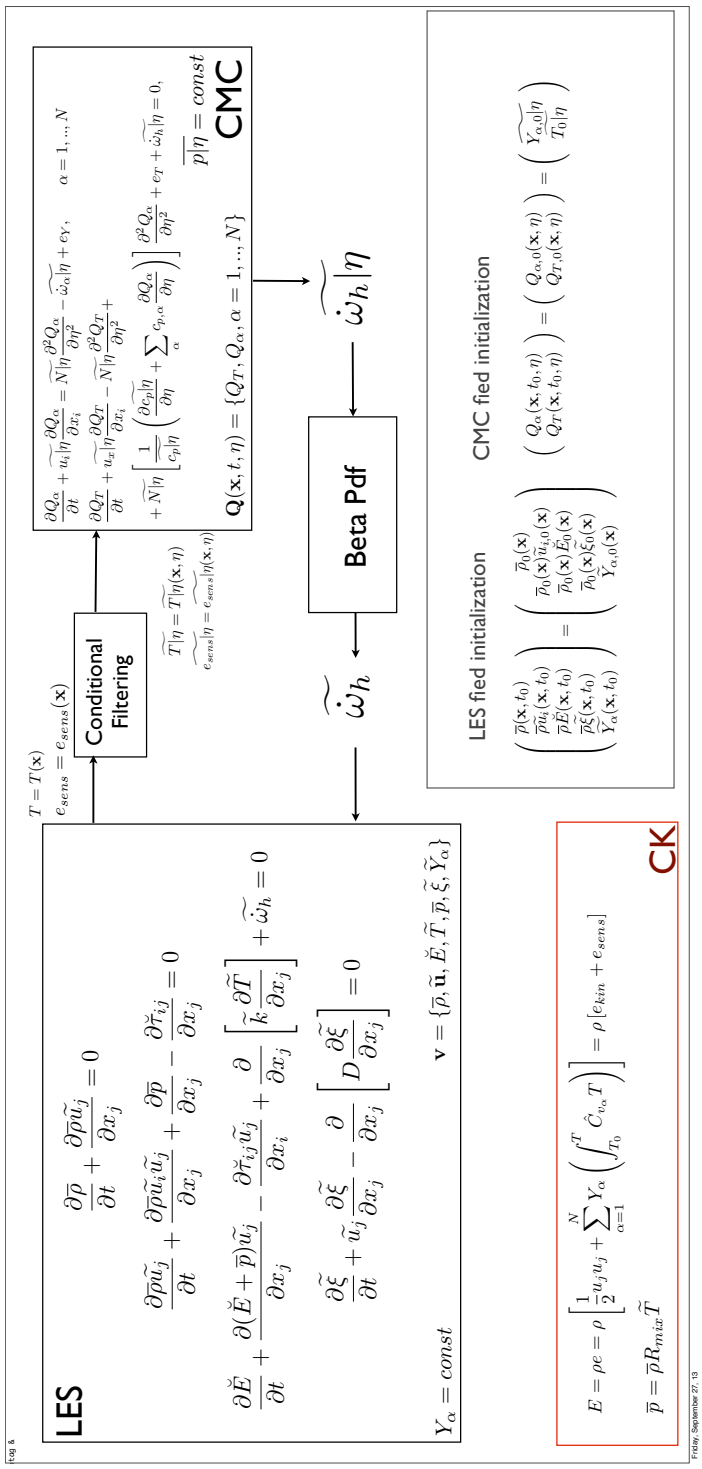


Figure 4: CMC/LES Energy Source Update (ESU) coupling

# 6

# NUMERICAL DISCRETIZATION

According with the problem decoupling illustrated in Chap. 5.1, two different LES/CMC coupling approaches have been presented, the Vector Field Update (VFU) and the Energy Source Update (ESU). From an analytical point of view, the two approaches substantially differ: the first is based on an operator splitting, while the latter is a closure method. On the other hand, both the approaches require the temporal evolution of two systems: an unconditionally filtered one, defined in the LES physical space, and a conditionally filtered one, defined in the CMC space. In other words, the numerical implementation of the 'mixing system' in VFU and of the 'main system' in the ESU are similar and will be discussed together referring to both these system as *'LES system'*. The same will be done for the 'reacting system' in the VFU and for the 'closure system' in the ESU, which will be referred to as the*'CMC system'*. Hence for the sake of brevity, in this chapter, the numerical implementation if the two 'LES systems' and the two 'CMC systems' will be discussed jointly, and the differences between the VFU and the ESU approaches will be highlighted only when necessary.

The thermal and caloric equations of state in Eqns.(6-7) respectively, as well as the filtered chemical source terms are obtained by means of the CHEMKIN libraries [50].

## 6.1 THE 'LES SYSTEM'

The LES system can be introduced, once the source term $\mathcal{S}$ is defined as:

$$\mathcal{S} = \begin{cases} 0 & \text{in VFU} \\ \\ \widetilde{\dot{\omega}}_T & \text{in ESU} \end{cases}. \tag{160}$$

So the 'mixing system' in Eq. (139-142) and the 'main system' in Eq. (150-153) can be recast as follows:

$$\frac{\partial \overline{\rho}}{\partial t} + \frac{\partial \overline{\rho}\widetilde{u}_i}{\partial x_i} = 0, \tag{161}$$

$$\frac{\partial \overline{\rho}\widetilde{u}_i}{\partial t} + \frac{\partial \overline{\rho}\widetilde{u}_i\widetilde{u}_j}{\partial x_j} + \frac{\partial \overline{p}}{\partial x_i} - \frac{\partial \breve{\tau}_{ij}}{\partial x_j} = 0, \tag{162}$$

$$\frac{\partial \breve{E}}{\partial t} + \frac{\partial (\breve{E} + \overline{p})\widetilde{u}_j}{\partial x_j} - \frac{\partial \sigma_{ij}\widetilde{u}_i}{\partial x_j} - \frac{\partial}{\partial x_i} k \frac{\partial \widetilde{T}}{\partial x_i} = \mathcal{S}, \tag{163}$$

$$\frac{\partial \widetilde{\xi}}{\partial t} + \frac{\partial \widetilde{\xi}\widetilde{u}_j}{\partial x_j} - \frac{\partial}{\partial x_i} D_{\widetilde{\xi}} \frac{\partial \widetilde{\xi}}{\partial x_i} = 0. \tag{164}$$

Where $\overline{\rho}$, $\widetilde{p}$, $\widetilde{T}$ and $\widetilde{u}_i$ are density, pressure, temperature and the velocity component in the $i-$th direction; $\mu$ and $k$ are the dynamic viscosity and thermal conductivity respectively, while $D$ stands for the diffusion coefficient, which, under the unity Lewis number assumption, is equal to the species diffusive coefficients $D_\alpha$. The stress tensor is then defined as:

$$\breve{\tau}_{ij} := \mu \left[ \left( \frac{\partial \widetilde{u}_i}{\partial x_j} + \frac{\partial \widetilde{u}_j}{\partial x_i} \right) - \frac{2}{3} \delta_{ij} \frac{\partial \widetilde{u}_k}{\partial x_k} \right]. \tag{165}$$

It should be recalled that the transport coefficients $\mu$, $k$ and $D_\xi$ are the summation of a molecular and a turbulent transport contribution according to the Smagorinsky's fluid-dynamic sub-grid closure model, briefly presented in Eqns. (70-77). The dissipative effects

arising from the sub-grid motions are accounted for by means of a turbulent viscosity, as shown in Eqns. (74-76). The thermic diffusion coefficients $k$ and the diffusion coefficient $D$ are related to the viscosity $\mu$ throughout the Prandtl and Schmidt number, $Pr$ and $Sc$, as well as their turbulent counterpart, $Pr_t$ and $Sc_t$, as already mentioned in sec. 4.1.1.

The LES code originally written for compressible single specie non reacting flows[53, 54, 55], has been implemented starting from a non-dimension form of the Navier-Stokes equations, as reported in detail in the appendix A.2.

### 6.1.1 *Convective term discretization*

The non-dimensional system in Eqns. (297-300) is discretized on a Cartesian mesh and solved by means of a conservative finite-difference approach. The flow solver relies on central up-to sixth-order discretization of the convective terms of the Navier-Stokes equations. This is realized through a central discretization of the convective terms cast in fully split form [51]:

$$\begin{aligned}\frac{\partial \rho u_i \phi}{\partial x_i} =& \frac{1}{4}\frac{\partial \rho u_i \phi}{\partial x_i} + \\ &+ \frac{1}{4}\left(u_j \frac{\partial \rho \phi}{\partial x_i} + \rho \frac{\partial u_i \phi}{\partial x_i} + \phi \frac{\partial \rho u_i}{\partial x_i}\right) + \\ &+ \frac{1}{4}\left(u_j \phi \frac{\partial \rho}{\partial x_i} + \rho u_i \frac{\partial \phi}{\partial x_i} + \phi \rho \frac{\partial u_i}{\partial x_i}\right),\end{aligned} \tag{166}$$

where $\phi$ represents the transported quantity in Eqns. (1-4), i.e.$\phi = 1$ in the continuity equation, $\phi = u_j$ in the momentum equations, and $\phi = E$ for the energy equation. This arrangement leads to a locally conservative formulation, and guarantees discrete conservation of the total kinetic energy in the limit case of inviscid, incompressible flow, also in the presence of grid stretching in the coordinate directions.

Pirozzoli [52] showed that The Eq. (166) can be cast in conservation form by applying a discrete central difference operators of the type:

$$Df_i = \sum_{l=1}^{L} \frac{a_l}{h}(f_{i+\frac{1}{2}} - f_{i-\frac{1}{2}}), \tag{167}$$

where the coefficients $a_l$ maximize the formal order of accuracy of the approximation, i.e. 2L, and an equally spaced grid with nodes $xk = kh$ is employed. In other words, if the (167) is applied, the (166) can be written as:

$$\frac{\partial \rho u_i \phi}{\partial x_i}|_{x=x_k} \simeq \frac{1}{h}\left(\hat{f}_{k+\frac{1}{2}} - \hat{f}_{k-\frac{1}{2}}\right), \tag{168}$$

with numerical flux defined as:

$$\hat{f}_{k+\frac{1}{2}} = 2\sum_{l=1}^{L} a_l \sum_{m=0}^{l-1} (\overline{\rho, y, \phi})_{k-m,l}, \tag{169}$$

where $(\overline{\rho, y, \phi})_{k,l}$ is a two-point, three-variable discrete averaging operator:

$$(\overline{\rho, y, \phi})_{k,l} = \frac{1}{8}(\rho_k + \rho_{k+l})(u_k + u_{k+l})(\phi_k + \phi_{k+l}). \tag{170}$$

This flux splitting arrangement in Eq. (168) guarantees semi-discrete preservation of the total kinetic energy in the limit case of inviscid, incompressible flow (also in the presence of Cartesian grids with stretching in some directions), thus allowing for a robust spatial discretization of the convective terms without the addition of spurious numerical dissipation [52]. The approach has already successfully employed in several contexts [53, 54, 55].

A total variation diminishing (TVD) scheme has been used for the convective flux of the mixture fraction $\widetilde{\xi}$ only, this to prevent spurious oscillations which would otherwise lead to the non-physical values $\widetilde{\xi} > 1$ or $\widetilde{\xi} < 0$.

### 6.1.2 *Diffusive terms discretization*

The diffusive terms in the Navier-Stokes equations are expanded to Laplacian form for improved numerical stability, and approximated with sixth-order central difference formulas as in Eq. (167), to guarantee proper action of molecular viscosity at the smallest scales resolved on the computational mesh.

### 6.1.3 *Time integration*

The resulting semi-discrete system of equations is advanced in time by means of a standard, fully explicit third-order Runge-Kutta algorithm. Once discretized in space, the system of the Navier-Stokes equations, is reduced to a system of ODE, which can be formally written as:

$$\frac{\partial \mathbf{u}}{\partial t} = \mathcal{F}(\mathbf{u}), \tag{171}$$

where the operator $\mathcal{F}$ results from the approximation of the right hand side of the LES system. In the present work, we employ a standard fourth-order Runge-Kutta [56] algorithm for time integration:

$$\mathbf{u}^{(1)} = \mathbf{u}^{(n)} + \frac{1}{2}\Delta t \mathcal{F}(\mathbf{u}^{(n)}), \tag{172}$$

$$\mathbf{u}^{(2)} = \mathbf{u}^{(n)} + \frac{1}{2}\Delta t \mathcal{F}(\mathbf{u}^{(1)}), \tag{173}$$

$$\mathbf{u}^{(3)} = \mathbf{u}^{(n)} + \frac{1}{2}\Delta t \mathcal{F}(\mathbf{u}^{(2)}), \tag{174}$$

$$\mathbf{u}^{(n+1)} = \frac{1}{3}\left(-\mathbf{u}^{(n)} + \mathbf{u}^{(1)} + 2\mathbf{u}^{(2)} + \mathbf{u}^{(3)}\right) + \frac{1}{6}\Delta t \mathcal{F}(\mathbf{u}^{(3)}). \tag{175}$$

The stability criterion is based on the CFL condition.

### 6.1.4 *Initial conditions*

Imposing the initial conditions requires the choice of the initial values of $\rho(\mathbf{x})$, $\mathbf{u}(\mathbf{x})$, $E(\mathbf{x})$, and $\xi(\mathbf{x})$. It is important to stress the fact that, at least for the initial condition, a given mixture fraction distribution $\xi(\mathbf{x})$ corresponds to a given mixture composition, and a relation of the kind $Y_\alpha = Y_\alpha(\xi)$ must be chosen. This relation between mixture fraction, temperature, and species composition is tightly linked to the CMC initial condition and can vary between two limit cases, as already mentioned in sec. 3.4.0.1. The first limit case, the Burke-Schumann limit, corresponds to the steady solution of the equations (56) and (56), user the assumption of one-way, infinitely fast chemistry. The resulting temperature and species mass fractions profiles are linear with a slope discontinuity in $z = z_{st}$, as follows:

$$
\begin{aligned}
Y_O(\xi) &= 0 && \xi > \xi_{st}, \\
Y_O(\xi) &= 1 - \xi && \xi < \xi_{st}, \\
Y_F(\xi) &= 0 && \xi < \xi_{st}, \\
Y_F(\xi) &= \xi && \xi > \xi_{st}, \\
Y_P(\xi) &= \xi && \xi < \xi_{st}, \\
Y_P(\xi) &= 1 - \xi && \xi > \xi_{st}, \\
T(\xi) &= T_O + (T_{ad} - T_O)\xi && \xi < \xi_{st}, \\
T(\xi) &= T_{ad} - (T_{ad} - T_F)\xi && \xi > \xi_{st}.
\end{aligned} \tag{176}
$$

The second second limit case, the case of pure mixing of fuel and oxidizer, corresponds to the trivial solution of the equations (56) and (56) where any reaction occurred, and the solution is still linear, with constant slope, and reads:

$$
\begin{aligned}
Y_O(\xi) &= \xi && 0 < \xi < 1 \\
Y_F(\xi) &= 1 - \xi && 0 < \xi < 1 \\
Y_P(\xi) &= 0 && 0 < \xi < 1 \\
T(\xi) &= T_0 && 0 < \xi < 1
\end{aligned} \tag{177}
$$

So, once the initial pressure field is imposed, and the relation between temperature, composition and mixture fractions are defined, the whole field of density $\rho(\mathbf{x})$ and sensible energy $E(\mathbf{x})$ are automatically defined as function of pressure and mixture fraction.

### 6.1.5 *Boundary conditions*

The employed boundary conditions are the Generalized Characteristic Relaxation Boundary Conditions (GRCBC) for unsteady, compressible flow simulations proposed by Pirozzoli and Colonius in 2013 [57]. The GRCBC hinges on Locally One-DImensional characteristic projection (LODI) at the computational boundaries [58], supplemented with available information from the flow exterior [59]. Similarly to the approach proposed by Thompson [58], the NS system is written in one dimensional form, for example in the $x$ direction for a boundary normal to the x direction:

$$
\frac{\partial \mathbf{u}}{\partial t} + \mathbf{R}_x \mathbf{\Lambda}_x \mathbf{L}_x \frac{\partial \mathbf{u}}{\partial x} = \mathbf{C}, \tag{178}
$$

where the contributions of the transverse inviscid fluxes and the viscous fluxes are lumped together in the right-hand-side term $\mathbf{C}$, and the Jacobian matrix $\mathbf{A}_x$ is defined as follows [60, 58]:

$$
\mathbf{A}_x = \frac{\partial \mathbf{f}_x}{\partial \mathbf{u}} = \mathbf{R}_x \mathbf{\Lambda}_x \mathbf{L}_x, \tag{179}
$$

and $\mathbf{\Lambda}_x$ is the diagonal matrix of the eigenvalues:

$$
\lambda_1 = u - c, \quad \lambda_2 = \lambda_3 = \lambda_4 = \lambda_6 = u, \quad \lambda_5 = u + c. \tag{180}
$$

The main idea of the Navier–Stokes characteristic boundary conditions (NSCBC) approach, is to isolate the contribution of waves exiting the computational domain, which can therefore be extrapolated from the interior, from those associated with incoming waves, whose amplitude depends on the flow properties outside the computational domain [57]. To isolate the two contributions, the $l$-th eigenvalue can always be written as:

$$\lambda_l^{o,i} = \frac{1}{2}(\lambda_l \pm n_x|\lambda_l|), \tag{181}$$

where $n_x = \pm 1$ for the right and left boundaries respectively. The purely non-reflecting boundary conditions [58], consist in canceling all that waves coming from outside the domain, whose value is unknown, that is $\lambda_l^i = 0$. This results in the following relation in the boundary:

$$\frac{\partial \mathbf{u}_b}{\partial t} = -\mathbf{R}_{b,x}\mathbf{\Lambda}^o_{x,b}\mathbf{L}_{x,b}D_b\mathbf{u}_b + \mathbf{C}_b, \tag{182}$$

where the subscript $b$ means that the quantity has been computed in the boundary $x = x_b$; while $D_b$ stand for the one-sided derivatives computed in the inner nodes. However, following this approach, all the waves coming from the outside are neglected, and any information on the physical conditions can be imposed, this being a cause of possible numerical drifts. If some information on the behavior of the true solution outside the computational domain is known, a common strategy is to estimate the contribution of the incoming waves was proposed by Poinsot and Lele [59]. This approach can be formalized starting from the system in Eq. (178) written in terms of conservative variables $\mathbf{v}$, which is straightforward once the matrix $\mathbf{P} = \partial\mathbf{u}/\partial\mathbf{v}$ is defined. Substituting $\partial\mathbf{u} = \mathbf{P}\partial\mathbf{v}$ in Eq. (178) leads to:

$$\frac{\partial \mathbf{v}}{\partial t} + \mathbf{P}^{-1}\mathbf{R}_x\mathbf{\Lambda}_x\mathbf{L}_x\mathbf{P}\frac{\partial \mathbf{v}}{\partial x} = \mathbf{P}^{-1}\mathbf{C}, \tag{183}$$

that is:

$$\frac{\partial \mathbf{v}}{\partial t} + \mathbf{P}^{-1}\mathbf{R}_x\mathcal{L} = \mathbf{P}^{-1}\mathbf{C}, \tag{184}$$

with:

$$\mathcal{L} = \mathbf{\Lambda}_x \mathbf{L}_x \mathbf{P} \frac{\partial \mathbf{v}}{\partial x} = \mathbf{\Lambda}_x \mathbf{L}_x \frac{\partial \mathbf{u}}{\partial x}. \tag{185}$$

Here $\mathcal{L}_i$ represent the amplitudes of the characteristic waves associated with the characteristic velocity $\lambda_i$ [59]. This is clear if the vector $\partial \mathbf{w} = \mathbf{L}_x \partial \mathbf{u}$ is defined, and the Eq. (178) is pre-multiplied by $\mathbf{L}_x$, leading to the new relation:

$$\mathbf{L}_x \frac{\partial \mathbf{u}}{\partial t} + \mathbf{L}_x \mathbf{R}_x \mathbf{\Lambda}_x \mathbf{L}_x \frac{\partial \mathbf{u}}{\partial x} = \mathbf{L}_x \mathbf{C}, \tag{186}$$

which can be recast as:

$$\frac{\partial \mathbf{w}}{\partial t} + \mathbf{\Lambda}_x \frac{\partial \mathbf{w}}{\partial x} = \frac{\partial \mathbf{w}}{\partial t} + \mathcal{L} = \mathbf{L}_x \mathbf{C}. \tag{187}$$

The wave amplitude [58] are:

$$\mathcal{L} = \mathbf{\Lambda}_x \mathbf{L}_x \mathbf{P} \frac{\partial \mathbf{v}}{\partial x} = \begin{bmatrix} \lambda_1 \left( \frac{\partial p}{\partial x} - \rho c \frac{\partial u}{\partial x} \right) \\ \lambda_2 \left( c^2 \frac{\partial \rho}{\partial x} - \frac{\partial p}{\partial x} \right) \\ \lambda_3 \frac{\partial v}{\partial x} \\ \lambda_4 \frac{\partial w}{\partial x} \\ \lambda_5 \left( \frac{\partial p}{\partial x} - \rho c \frac{\partial u}{\partial x} \right) \\ \lambda_6 \frac{\partial \xi}{\partial x} \end{bmatrix}. \tag{188}$$

The main idea of the locally inviscid one dimensional (LODI) approach [59], is to write the relation for the primitive variable in Eq. (184) discarding the viscous and transversal contribution. i.e.:

$$\frac{\partial \mathbf{v}}{\partial t} + \mathbf{P}^{-1} \mathbf{R}_x \mathcal{L} = 0. \tag{189}$$

These are solved at the boundary, the resulting wave amplitudes estimation $\mathcal{L}_l$ are then used model incoming waves which would be otherwise neglected as in Eq. (182). A different approach, is to model the amplitude of the incoming characteristic waves assuming relaxation to the far field conditions, referred to as target conditions to

prevent drifts on pressure, as proposed by Rudy and Strikwerda [61]. According to the Rudy and Strikwerda approach, the first wave aptitude as function of a target pressure $p_{tg}$, by means of a properly defended constant $K_p$, that is:

$$\mathcal{L}_1 = K_p(p_b - p_{tg}). \tag{190}$$

The basic idea of the GRCBC [57] is to combine the decomposition in Eq. (181) and relaxation methods starting from the wave decomposition in incoming and outgoing part, as in Eq. (181), then modeling the outgoing part $\mathcal{L}^o$ as in Eq. (182), and the incoming $\mathcal{L}^i$ according to the relaxation method. This can be written as:

$$\frac{\partial \mathbf{u}_b}{\partial t} = -\mathbf{R}_{b,x}\mathbf{\Lambda}^o_{x,b}\mathbf{L}_{x,b}D_b\mathbf{u}_b + n_x\mathbf{R}_{b,x}\mathbf{\Lambda}^i_{x,b}\mathbf{L}_{x,b}\mathbf{P}\frac{\mathbf{v}_b - \mathbf{v}_g}{\Delta} + \mathbf{C}_b. \tag{191}$$

Here $\mathbf{v_g}$ represents the values of primitive variables, used as target value, and assigned in the first ghost none outside the boundary, and $\Delta = x_b - x_g$. In the case one or more elements of $\mathbf{v}_g$ are unknown, it is sufficient to set to zero the corresponding $\mathbf{v}_b - \mathbf{v}_g$. The practical effectiveness of this approach has been documented through numerical simulations in [57].

Moreover, the nonreflecting performance of numerical boundary conditions can be significantly enhanced by suitably damping the amplitude of disturbances before they hit the boundary, such as the use of sponge layers [62], whereby forcing terms are added to the governing equations, to cause the flow to relax to prescribed target conditions.

## 6.2 THE 'CMC SYSTEM'

The 'CMC systems' has been implemented in one-dimensional, axial form, to reduce the computational load. It has been demonstrated that the conditional averages have a very weak dependence on the cross stream position in recirculation regions [20], and that the radially averaged CMC, is able to accurately predict the lift-off height

of a lifted flame [24]. Moreover this one-dimensional approximation has already been implemented with satisfactory accuracy for the Sandia Flame-D simulation [34] as well as the HM1 bluff-body flame [35]. Moreover the energy equation has been recast in terms of conditionally filtered temperature [26], and the pressure work has been neglected. Once introduced the term $\mathcal{M}_{\mathcal{T}}$:

$$\begin{aligned}\mathcal{M}_{\mathcal{T}} =&\widetilde{u_x|\eta}\frac{\partial Q_T}{\partial x_i} - \widetilde{N|\eta}\frac{\partial^2 Q_T}{\partial \eta^2} + \\ &+\widetilde{N|\eta}\left[\frac{1}{\widetilde{c_p|\eta}}\left(\frac{\partial \widetilde{c_p|\eta}}{\partial \eta} + \sum_\alpha c_{p,\alpha}\frac{\partial Q_\alpha}{\partial \eta}\right)\right]\frac{\partial^2 Q_\alpha}{\partial \eta^2} + e_T,\end{aligned} \tag{192}$$

the CMC systems of both the VFU and ESU formulations can be written in a compact form as follows:

$$\frac{\partial Q_\alpha}{\partial t} + \widetilde{u_x|\eta}\frac{\partial Q_\alpha}{\partial x} - \widetilde{N|\eta}\frac{\partial^2 Q_\alpha}{\partial \eta^2} + e_y + \widetilde{\dot{\omega}_\alpha|\eta} = 0, \tag{193}$$

$$\frac{\partial Q_T}{\partial t} + \mathcal{M} + \widetilde{\dot{\omega}_h|\eta} = 0. \tag{194}$$

Where the term $\mathcal{M}$ is defined as:

$$\mathcal{M} = \begin{cases} 0 & \text{in VFU} \\ \mathcal{M}_{\mathcal{T}} & \text{in ESU .} \end{cases} \tag{195}$$

The conditionally filtered pressure $\widetilde{p|\eta}$ is weakly dependent on the mixture fraction $\widetilde{\xi}$ and hence is kept constant in $\eta$ and equal to its average value over a CMC cell. The terms $e_y$ and $e_h$ take into account the fluctuations around the conditional mean, defined in Eq. (112) and can be modeled by the gradient approach as briefly presented in 4.2.4, but in the present formulation they are neglected [34]. The scalar dissipation $\widetilde{N|\eta}$ is modeled accordingly to the amplitude mapping closure briefly, presented in sec. 4.2.3.5. The conditional velocity $\widetilde{u_x|\eta}$ has been chosen as the averaged value of $\widetilde{u}_x$. The variance value $\widetilde{\xi''}$ is modeled according to Eq. (121).

### 6.2.1 *Conditional Moment Closure operator splitting*

The CMC system in Eqns. (193-194), is numerically integrated in time by means of an operator splitting. To prevent spurious oscillations of the conditionally filtered reactive scalars, the convective term is discretized in space by means of a second order upwind scheme, and integrated in time explicitly with a fully explicit fourth-order Runge-Kutta method. The diffusive terms are discretized in space by means of a second order, central differences scheme, and are integrated in time together with the source term by means of a BDF implicit technique using DVODE [63], a variable-coefficient ordinary differential equation solver. The time step for explicit time integration of the convective term is the same used for the time integration of the LES system, since it will be consistent with the LES CFL criteria. The characteristic times of the source and diffusive terms are usually much smaller than the fluid-dynamic one, and this motivated the use of a backward differentiation formula method like DVODE which allows to perform a time integration with a prescribed accuracy. The choice of integrating the source and the diffusive terms together is motivated by the need of reproducing the tight coupling of the two phenomena, especially in the case of local quenching and reignition, where an hysteresis behavior exists.

### 6.2.2 *Initial and boundary conditions*

The initial conditions for the conditionally filtered species mass fractions depend on the investigated problem and are tightly linked to the choice of the LES initial conditions. More specifically, defining $Y_{\alpha,O}$ and $Y_{\alpha,F}$ as pure oxidizer and pure fuel composition respectively, we have $Q_\alpha(\eta = 0) = Y_{\alpha,O}$ and $Q_\alpha(\eta = 1) = Y_{\alpha,F}$ by definition. For $\eta \in (0,1)$ the initial condition depends on whether in the initial condition the mixture is already reacting or not. Hence the choice of a

profile $Q_\alpha(\eta) = f(Y_{\alpha,O}, Y_{\alpha,F}, Y_{\alpha,P})$ must be chosen among the possible conditions between the mixing limit and the Burke-Schumann limit, and coherently with the choice of the LES initial and boundary conditions, as explained in sec.6.1.4.

It should be noted that, while the conditionally filtered species mass fractions evolution are controlled by the CMC species equations only, the temperature field is updated at each time step since it is known from the LES field. A conditional filtering operation is pursued at each time step, by means of a conditional averaging procedure, like:

$$\widetilde{T|\eta} = \langle T|\eta \rangle. \tag{196}$$

This is a preliminary solution and a more accurate reconstruction can be envisaged.

### 6.2.3 *ESU coupling discretization*

In the ESU approach, the CMC system is used as a closure, so that it provides the source term $\mathcal{S} = \widetilde{\dot{\omega}_T} = \sum_\alpha \widetilde{\dot{\omega}}_\alpha \Delta h_{0,al}$. At each time step, a time averaged conditionally filtered source term can be written as:

$$\widetilde{\dot{\omega}_T|\eta} = \frac{1}{\Delta t} \int_{t_n}^{t^n+\Delta t} \widetilde{\dot{\omega}_T|\eta} dt, \tag{197}$$

and its unconditionally filtered counterpart can be obtained by a convolution operation:

$$\mathcal{S} = \widetilde{\dot{\omega}_T} = \int_0^1 \overline{\widetilde{\dot{\omega}_T|\eta}} p(\eta) d\eta. \tag{198}$$

However the estimation of the integral in Eq.(197) can be computationally demanding, and in a preliminary formulation the quantity in Eq.(197) can be substituted by its approximated form:

$$\overline{\widetilde{\dot{\omega}_T|\eta}} = \frac{1}{\Delta t} \frac{\widetilde{\dot{\omega}_T|\eta}(t) - \widetilde{\dot{\omega}_T|\eta}(t+\Delta t)}{2}, \tag{199}$$

while higher order approximations can be envisaged.

# 7

# RESULTS AND DISCUSSION

## 7.1 CMC 0D - A STANDALONE SYSTEM

In the following section, the predictive capabilities of the CMC approach are inquired. The first step has been to define a zero-dimensional CMC system starting form Eqns. (111 -113), and solving this independent system by providing the scalar dissipation distribution over the mixture fraction $\eta$ as an input. The sensitivity of the scalar dissipation distribution on both the steady state and transients solution has been assessed. Moreover, the SANDIA flame D [4] dynamics have been reproduced by presuming a scalar dissipation field and a mean flow axial velocity distribution. The impact of assuming constant specific heats on the solution accuracy has been quantified.

### 7.1.1 *The oD equations*

The CMC equations have been presented in Eqns. (111) and (113); their counterparts, written in terms of temperature under the assumption of constant pressure, have been presented in sec. 6.2 and are reported here for the reader convenience:

$$\frac{\partial Q_\alpha}{\partial t} + \widetilde{u_x|\eta}\frac{\partial Q_\alpha}{\partial x} - \widetilde{N|\eta}\frac{\partial^2 Q_\alpha}{\partial \eta^2} + e_y + \widetilde{\dot{\omega}_\alpha|\eta} = 0 \tag{200}$$

$$\begin{aligned}&\frac{\partial Q_T}{\partial t} + \widetilde{u_x|\eta}\frac{\partial Q_T}{\partial x_i} - \widetilde{N|\eta}\frac{\partial^2 Q_T}{\partial \eta^2} + \\ &+ \widetilde{N|\eta}\left[\frac{1}{\widetilde{c_p|\eta}}\left(\frac{\partial \widetilde{c_p|\eta}}{\partial \eta} + \sum_\alpha c_{p,\alpha}\frac{\partial Q_\alpha}{\partial \eta}\right)\right]\frac{\partial^2 Q_\alpha}{\partial \eta^2} + e_T + \widetilde{\dot{\omega}_h|\eta} = 0\end{aligned} \tag{201}$$

The solution of these equations depends on the fluid dynamic fields through the terms $\widetilde{N|\eta}$, $\widetilde{u|\eta}$, $e_y$ and $e_T$, as already discussed in the previous section. If the terms $e_y$ and $e_T$ are neglected, the CMC equations in Eq. (200) can be reduced to:

$$\frac{DQ_\alpha}{Dt} - \widetilde{N|\eta}\frac{\partial^2 Q_\alpha}{\partial \eta^2} + \widetilde{\dot{\omega}_\alpha|\eta} = 0 \tag{202}$$

$$\frac{DQ_T}{Dt} - \widetilde{N|\eta}\frac{\partial^2 Q_T}{\partial \eta^2} + \tag{203}$$

$$+ \widetilde{N|\eta}\left[\frac{1}{\widetilde{c_p|\eta}}\left(\frac{\partial \widetilde{c_p|\eta}}{\partial \eta} + \sum_\alpha c_{p,\alpha}\frac{\partial Q_\alpha}{\partial \eta}\right)\right]\frac{\partial^2 Q_\alpha}{\partial \eta^2} + \widetilde{\dot{\omega}_h|\eta} = 0.$$

The terms $e_y$ and $e_T$ can be modeled as shown in 4.2.4, and are neglected as introduced in sec. 6.2, according with the hypothesis of having small values of $e_y$ and $e_T$ in the flows of typical interest, which is exactly true in the limit of laminar flows. The terms $\widetilde{u_x|\eta}\frac{\partial Q_\alpha}{\partial x}$ and $\widetilde{u_x|\eta}\frac{\partial Q_T}{\partial x_i}$ are absorbed in the total derivative terms like:

$$\begin{aligned}\frac{DQ_\alpha}{Dt} &= \frac{\partial Q_\alpha}{\partial t} + \widetilde{\mathbf{u}|\eta}\frac{\partial Q_\alpha}{\partial x} \\ \frac{DQ_T}{Dt} &= \frac{\partial Q_T}{\partial t} + \widetilde{\mathbf{u}|\eta}\frac{\partial Q_T}{\partial x}\end{aligned} \tag{204}$$

The resulting equations are very similar to the Lagrangian flamelet equations [11], this meaning that the equations in Eqns. (202) and (202) describe the evolution of a flamelet in a Lagrangian frame of reference flowing with the flow, where the gradients normal to the flame front are mapped in the mixture fraction space, while the gradients in the directions tangential to the flame surface are negligible, as already discussed in sec. 3.4.0.1. The equations in (202) and (202) have been discretized numerically, as explained in sec. 6.2, under the assumption of constant velocity in the mixture fraction space, normal to the flame front, i.e. $\widetilde{\mathbf{u}|\eta}(\mathbf{x}, t, \eta) = u_x(t)$. This hypothesis allows to have a one-to-one mapping between time and axial position, $x = x(t)$, this meaning that the total derivative in Eqns. (204) can be replaced by ordinary time derivatives, eliminating the physical space dependency of the problem. So the solutions of the new system are function of time and mixture fraction only, i.e. $Q_\alpha = Q_\alpha(t, \eta)$ and $Q_T = Q_T(t, \eta)$,

while the space dependence can be retrieved by the cinematic relation $u_x = x/t$, where $u_x(t)$ is known as an input of the problem. A computational code has been developed, and both steady state solutions and time evolving solutions have been found numerically under several conditions. If the conditional velocity is assumed to be constant in time or, at least zero, the only input of the flamelet system is the scalar dissipation $N|\eta$, as already mentioned in sec. 3.4.

In the steady flamelet approach [1], the scalar dissipation is usually assumed to be constant in the mixture fraction space and equal to the value assumed at the stoichiometric surface, i.e., $\widetilde{N|\eta} = N_{st}$. However, in the following test cases, unless otherwise specified, the bell-shaped distribution shown in sec. 4.2.3.4 is adopted:

$$\widetilde{N|\eta} = N_{max}\lambda(\eta), \tag{205}$$

$$\lambda(\eta) = exp(-2[erf^{-1}(2\eta - 1)]^2) \tag{206}$$

here the maximum scalar dissipation value $N_{max}$ is an input of the problem and the only responsible for the fluid mechanic influence on the flame behavior.

The solution of the flamelet system can be useful for the comprehension of the flame sensitivity on the fluid dynamics, that is the sensitivity of the solution on the scalar dissipation distribution over the flame front, both in terms of transients and steady state solution. Moreover, if the scalar dissipation distribution is known, say as an output of a CFD computation, the system in Eqns. (202) and (202) can be solved for diagnostic purposes, in order to have a rough prediction, of the flow regions where ignition can take place, and on temperature and species mass fractions fields.

### 7.1.2 *Effects of the scalar dissipation on the steady state solutions*

If the convective terms are neglected, the system in Eqns.(202) describes a dynamical system characterized by the competition between transport and chemical reactions. The first is described by the diffusive term, whose strength is ruled by the scalar dissipation, the latter is described by the chemical source term, which, for a given pressure value, is a function of temperature and composition.

The steady state solutions of the set of Eqns. (202) and (202), for the case of a $CH_4$/Air system ($\eta_{st} = 0.055$), obtained for a number of maximum scalar dissipation values. The boundary conditions of the problem are pure oxidizer (Air) at $\eta = 0$ and pure fuel ($CH_4$) at $\eta = 1$, temperature is the same and equal to $291K$ in both the fuel and oxidizer fronts, pressure is constant and equal to $1\ Atm$. The chemical mechanism is the 49 species 277 reactions gri-2.11 [64]. The steady state condition is found by marching in time starting from the Burke-Schumann limit as initial condition, while the discretization in the mixture fraction space in obtained by means of a uniform computational mesh with 64 points in $\eta$.

From the results shown in figs. 5-12, it is clear that the solution for temperature, is influenced by the scalar dissipation $\widetilde{N|\eta}$, with the maximum temperature being a decreasing function of the scalar dissipation maximum value. For very high values of the scalar dissipation the flame is quenched and the solution is the pure mixing solution. This means that, if turbulence is so intense that Kolmogorov eddies become smaller than the flame surface, i.e. if the scalar dissipation reaches a limit value $N_q$, the flame front gets destroyed and a local quench occurs [1]. The cases for $N_{max} > 125 s^{-1}$ corresponds to the pure mixing conditions after quenching, and are reported in red in figs. 5-12. The effects of the scalar dissipation are also evident for the NO mass fraction which is a decreasing function of the scalar dissipation. This means that in a burning flame, a local rise in scalar

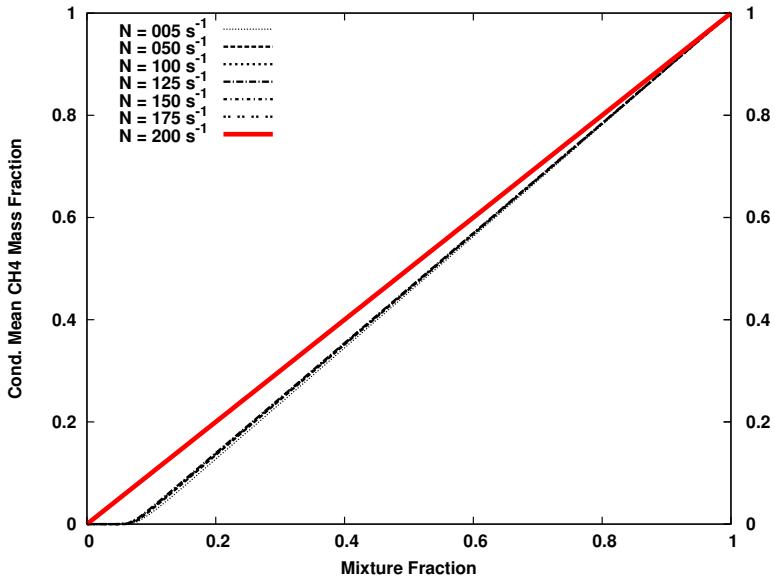


Figure 5: Steady-State solution sensitivity to scalar dissipation: $Y_{CH_4}(\eta)$

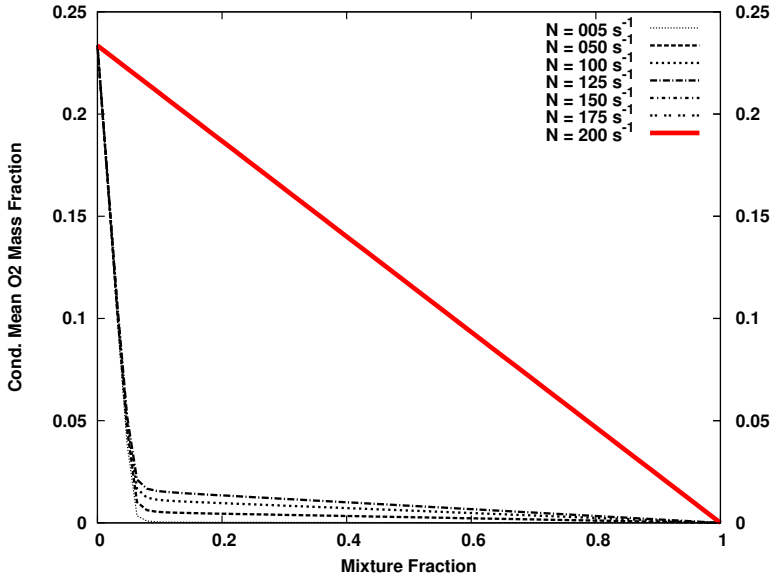


Figure 6: Steady-State solution sensitivity to scalar dissipation: $Y_{O_2}(\eta)$

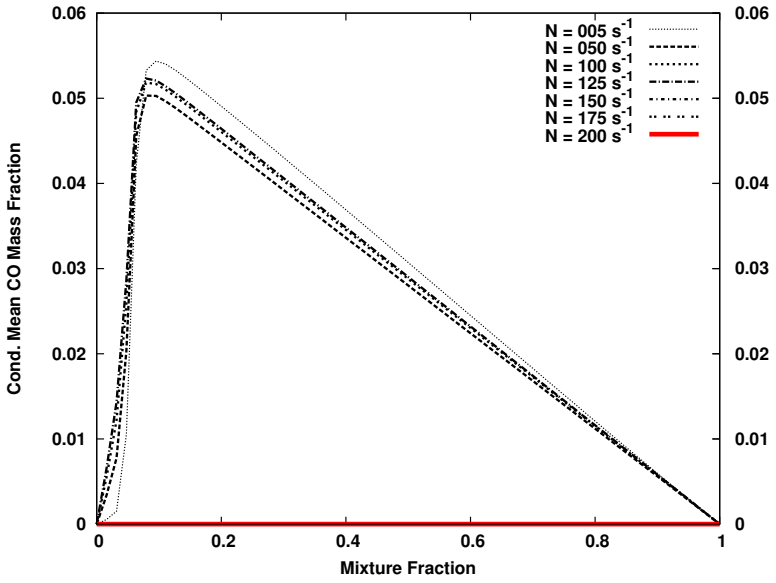


Figure 7: Steady-State solution sensitivity to scalar dissipation: $Y_{CO}(\eta)$

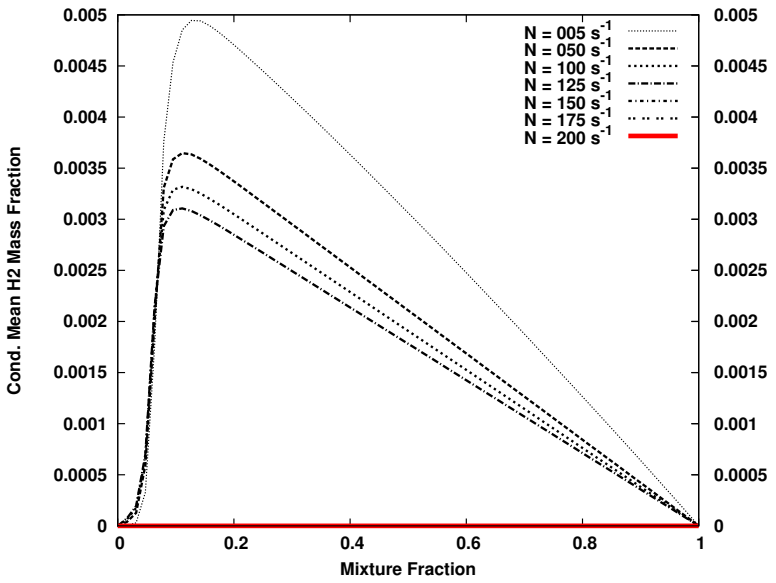


Figure 8: Steady-State solution sensitivity to scalar dissipation: $Y_{H_2}(\eta)$

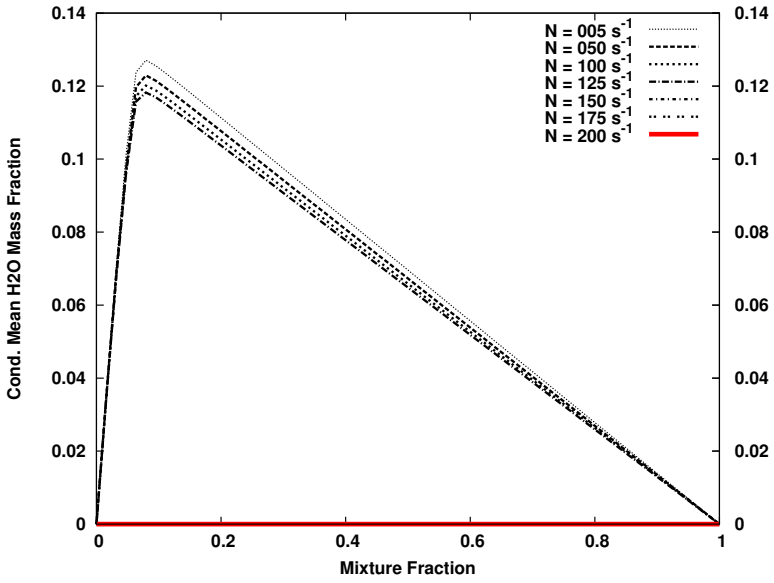


Figure 9: Steady-State solution sensitivity to scalar dissipation: $Y_{H_2O}(\eta)$

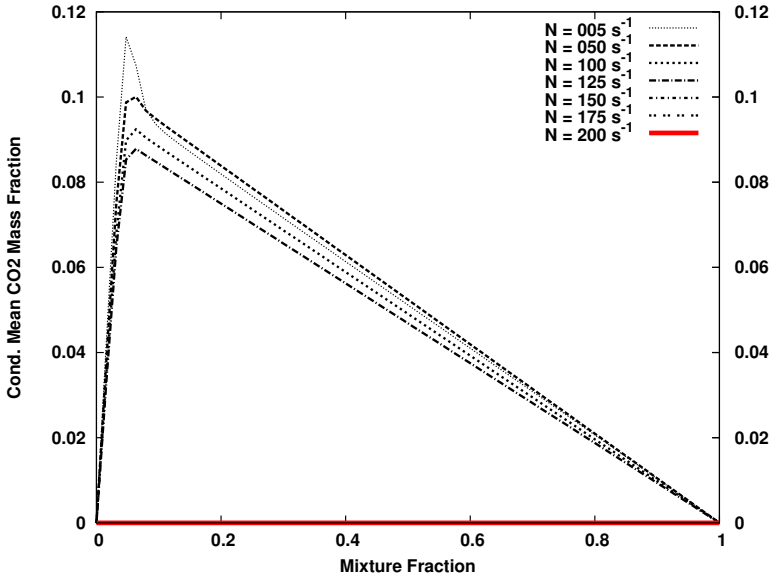


Figure 10: Steady-State solution sensitivity to scalar dissipation: $Y_{CO_2}(\eta)$

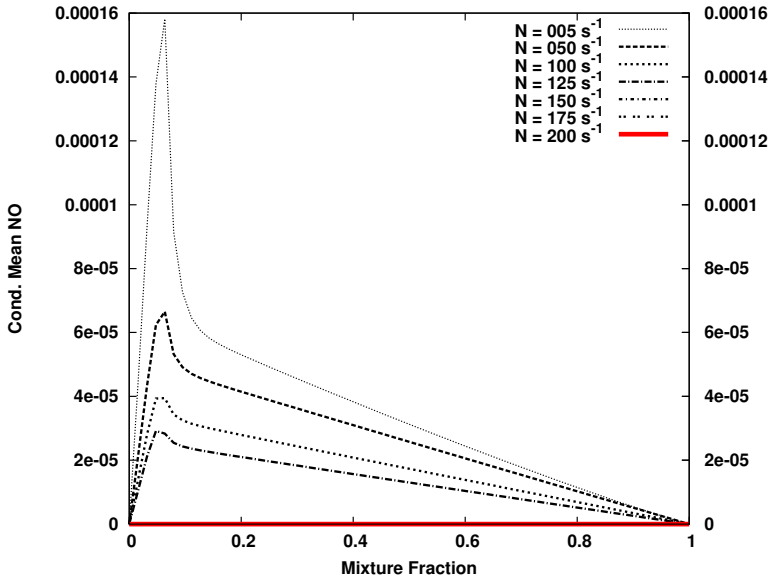


Figure 11: Steady-State solution sensitivity to scalar dissipation: $Y_{NO}(\eta)$

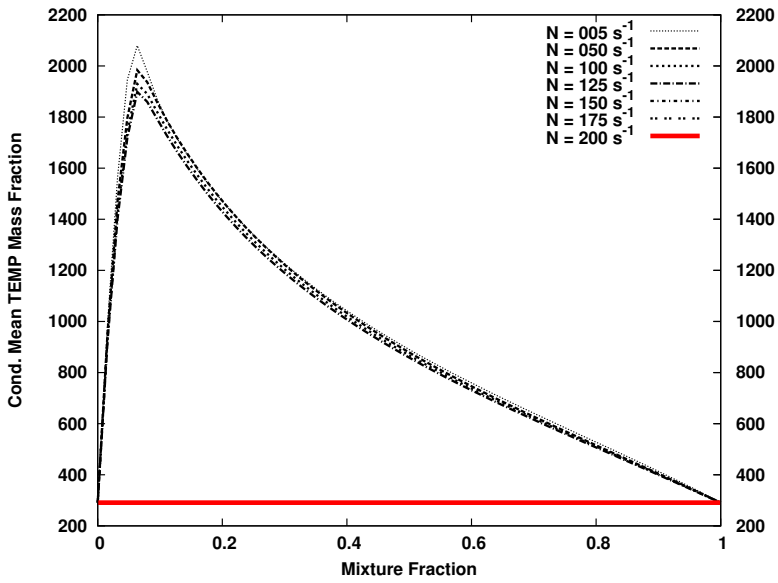


Figure 12: Steady-State solution sensitivity to scalar dissipation: $T(\eta)$ [K]

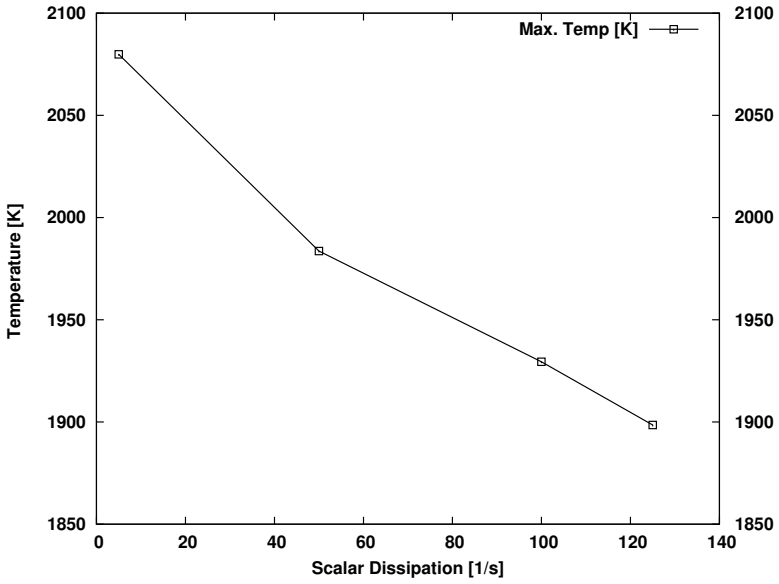


Figure 13: Steady state solution, maximum Temperature varyng scalar dissipation

dissipation, perhaps due to local rise of the mixture fraction gradients, will result in both a lowering of the flame temperature and of the NO mass fraction.

The sensitivity of maximum values of Temperature,$Y_{NO}$, $Y_{CO_2}$, $Y_{CO}$, and $Y_{H_2}$ are reported in figs. 13-15 respectively, showing that temperature is weakly influenced by the maximum scalar dissipation value, so long as the scalar dissipation is lower than the limit quenching value. The $CO$ mass fraction seems to be independent on the scalar dissipation, while $Y_{CO_2}$, $Y_{H_2}$, $Y_{NO}$ are decreasing functions of the scalar dissipation, with $Y_{NO}$ being the more sensitive on it, as shown in fig.15.

### 7.1.3 *Ignition transients in mixture fraction space*

The flamelet system is capable to describe most of the ignition transient phenomena as shown in figs. 18-21.

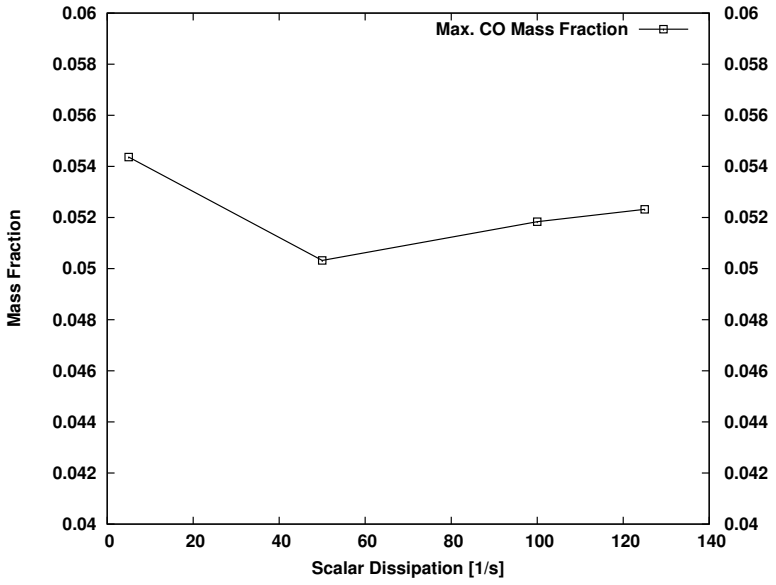


Figure 14: Steady state solution, maximum $Y_{CO}$ varying scalar dissipation

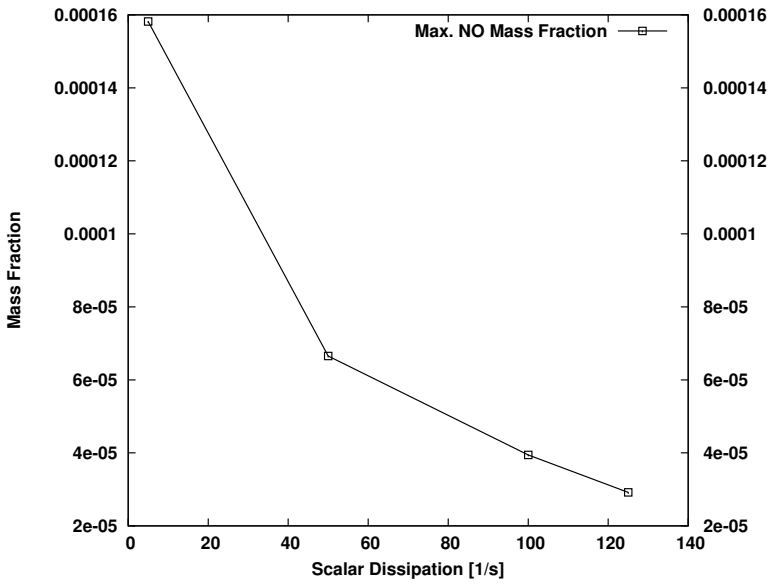


Figure 15: Steady state solution, maximum $Y_{NO}$ varying scalar dissipation

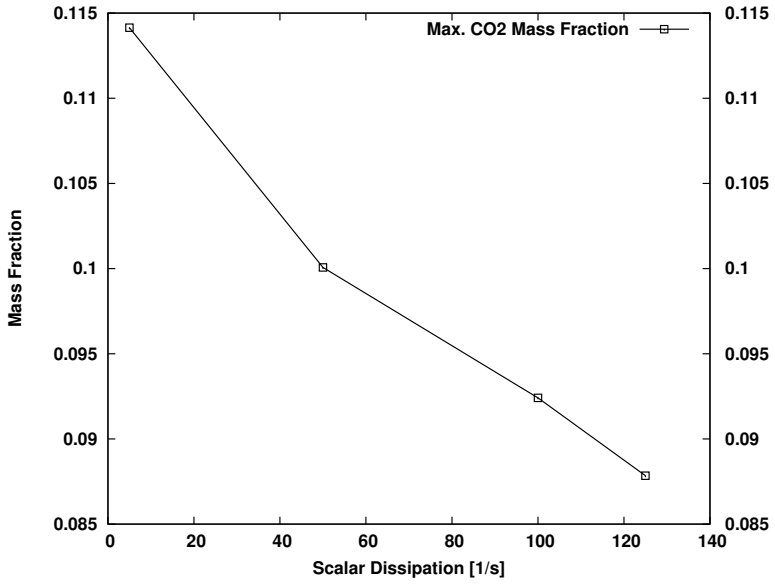


Figure 16: Steady state solution, maximum $Y_{CO_2}$ varying scalar dissipation

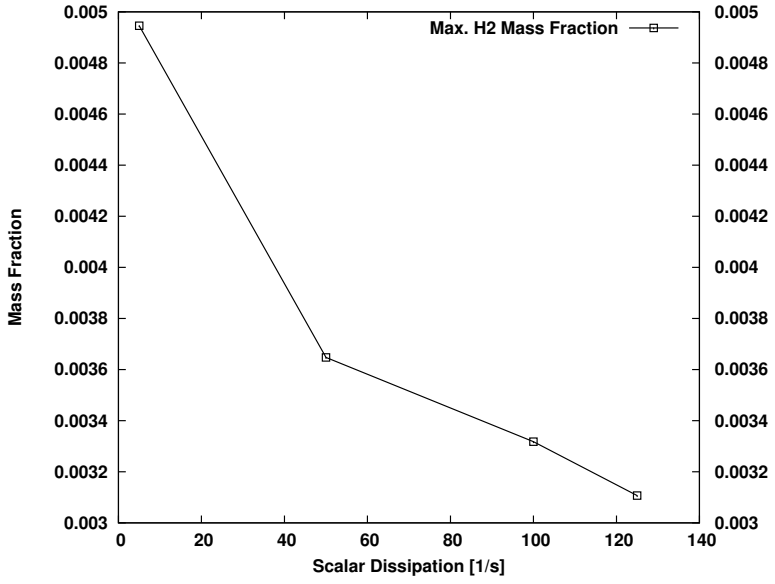


Figure 17: Steady state solution, maximum $Y_{H_2}$ varying scalar dissipation

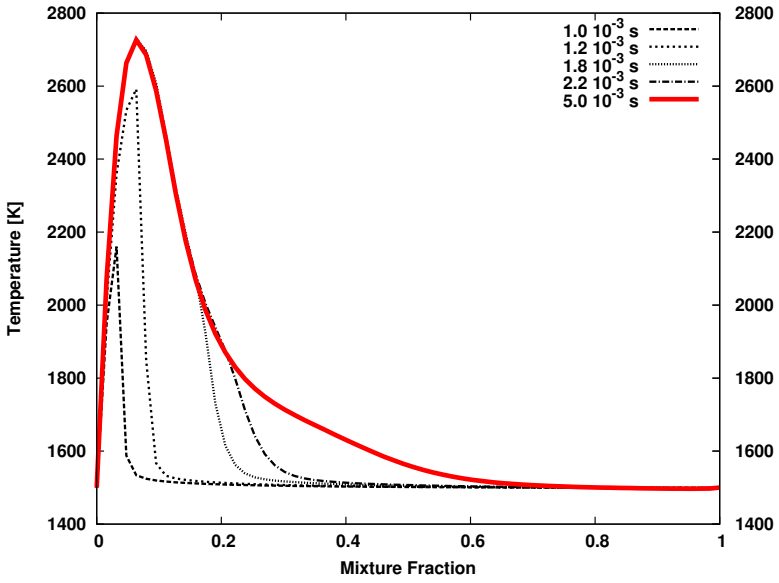


Figure 18: Autoignition Transients, $N_{max} = 5s^{-1}, T = T(\eta, t)$

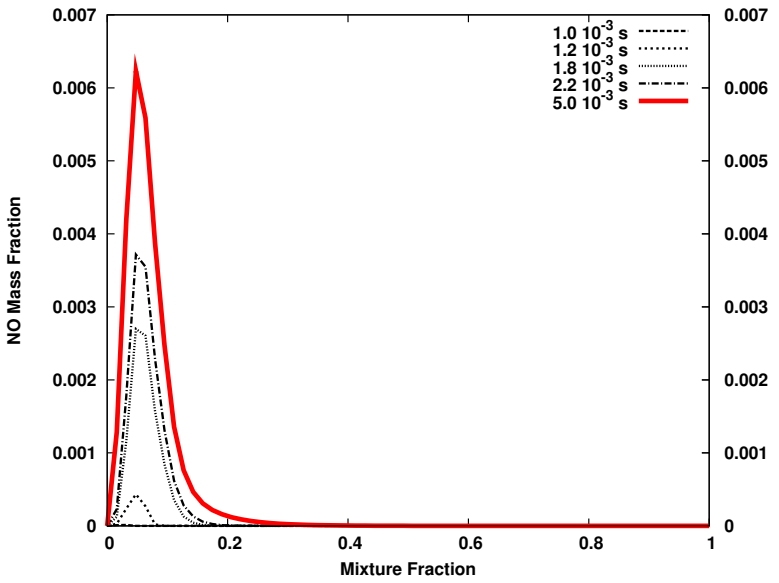


Figure 19: Autoignition Transients, $N_{max} = 5s^{-1}, Y_{NO} = Y_{NO}(\eta, t)$

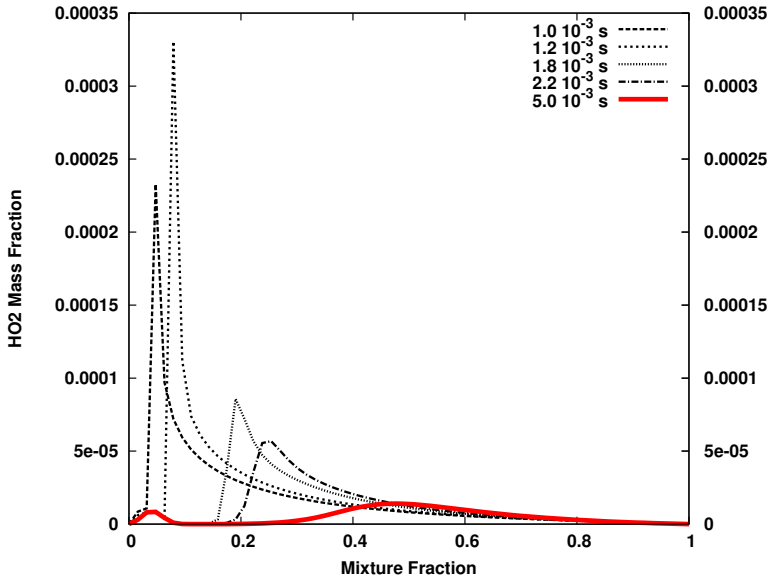


Figure 20: Autoignition Transients, $N_{max} = 5s^{-1}, Y_{HO_2} = Y_{HO_2}(\eta, t)$

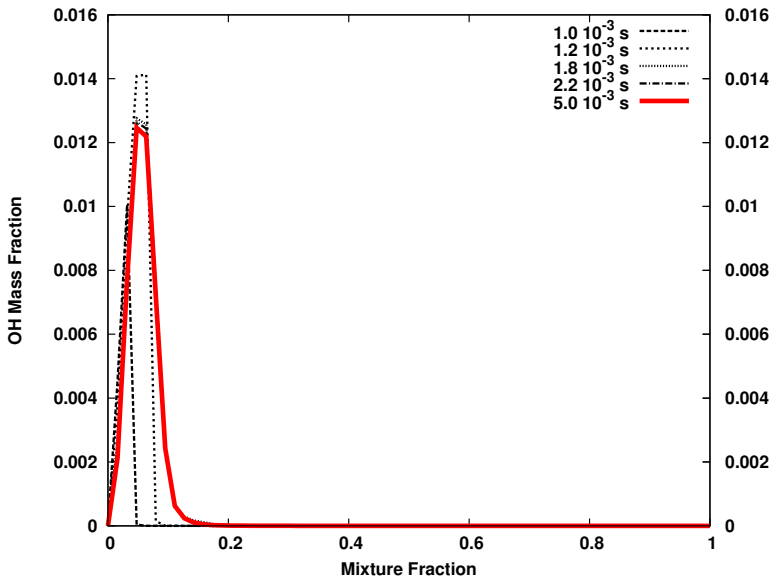


Figure 21: Autoignition Transients, $N_{max} = 5s^{-1}, Y_{OH} = Y_{OH}(\eta, t)$

The problem is similar to the one studied in the previous section: a $CH_4$/Air flame, $\eta_{st} = 0.055$, $N_{max} = 5s^{-1}$, but in this case the initial temperature is constant, $T(\eta) = 1500K$, and only fuel and oxidizer are not null in the initial condition. The same discretization with 64 points is used for the mixture fraction $\eta$. So differently from what has been done in the previous section, the initial temperature is higher than the auto ignition temperature to ensure the autoignition with several maximum scalar dissipations rate values.

The temperature evolution in fig. 18 clearly shows that ignition takes place in the stoichiometric region, and then the flame front moves towards the reach region. In fig.

Moreover, from the $HO_2$ mass fraction evolution in fig. 20, it should be noted that in the early ignition phases, the $Y_{HO_2}$ peak value is located in the stoichiometric region, while later on two peaks form. These two peaks leave the stoichiometric region and move towards the rich and lean regions, where a local minimum is formed near the stoichiometric values, as expected. These kind of predictive capabilities are crucial for the description of edge flames, such as triple flames [65].

### 7.1.4 *Effects of initial temperature on chemical transients*

The sensitivity of ignition transients to initial temperature can be easily inquired by means of numerical integration of the system in Eqns. 202. In particular, the ignition delay as function of the initial temperature is reported in fig. 22, where, for a given scalar dissipation $\widetilde{N|\eta} = 5s^{-1}$ the ignition delay time is clearly visible as decreasing function of the initial temperature, while, as expected, the steady state temperature is an increasing function of the initial temperature. The peak in the production of the radical OH and HO2, are observable in fig. 23 and 24, as well as the dependence of its amount on initial and final temperature. The radical NO formation in time has a differ-

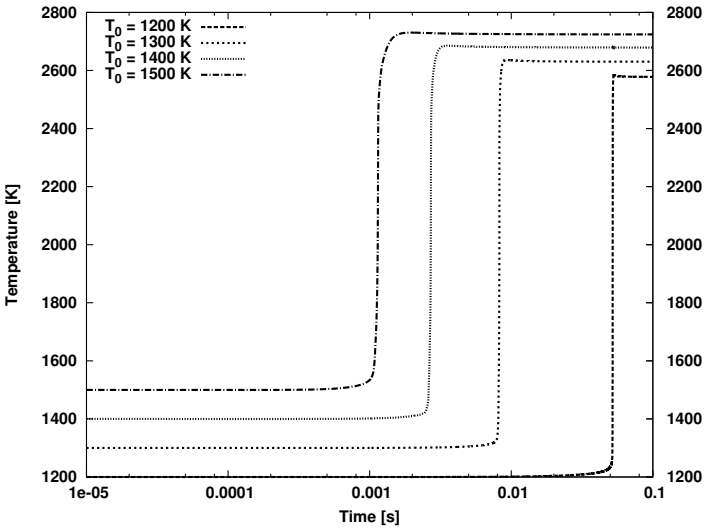


Figure 22: Autoignition transients varying $T_0$, $N_0 = 5s^{-1}$, $T = T(\eta_{st}, t)$

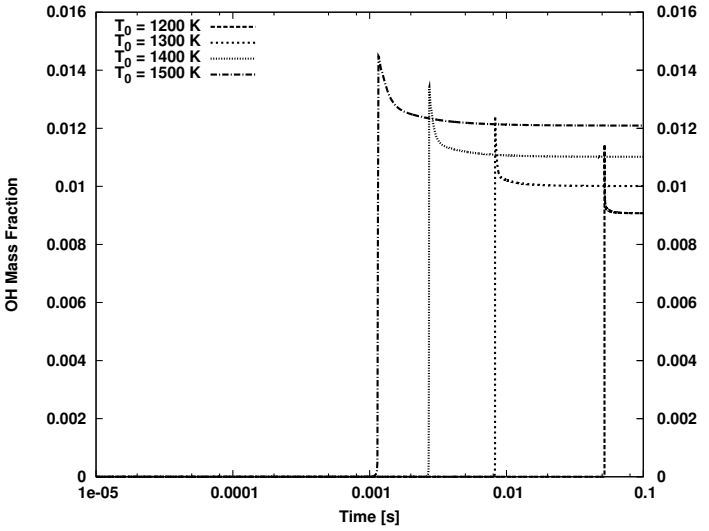


Figure 23: Autoignition transients varying $T_0$, $N_0 = 5s^{-1}$, $Y_{OH} = Y_{OH}(\eta_{st}, t)$

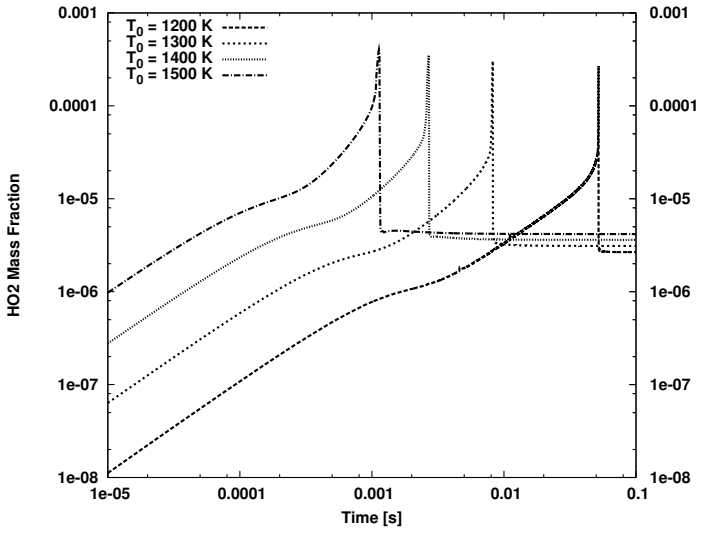


Figure 24: Autoignition transients varying $T_0$, $N_0 = 5s^{-1}$, $Y_{OH} = Y_{HO_2}(\eta_{st}, t)$

ent dynamics with respect to OH, as shown in fig 25, where the NO formation dependence on the residence time at high temperature is observed.

### 7.1.5 *Effects of scalar dissipation on chemical transients*

In order to test the sensitivity of the ignition delay time on the scalar dissipation distribution $N(\eta)$, the ignition delay time for a given initial temperature $T(\eta) = 1500K$, and for various distributions of scalar dissipation, is reported in fig. 27.

In fig.27, the black lines are obtained by imposing a bell-shaped distribution of scalar dissipation, while the red lines are obtained by imposing a constant value of scalar dissipation over the mixture fraction space $\eta$ as shown in fig. 26. While the constant scalar dissipation distribution assumption is often made in laminar flamelet closures [1], a bell shaped distribution is closer to the expected physical behavior, being able to describe the zero mixture fraction gradients at

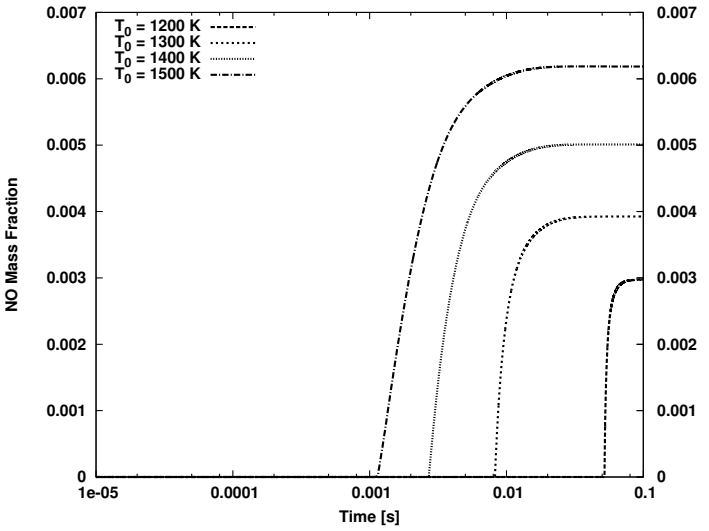


Figure 25: Autoignition transients varying $T_0$, $N_0 = 5s^{-1}$, $Y_{NO} = Y_{NO}(\eta_{st}, t)$

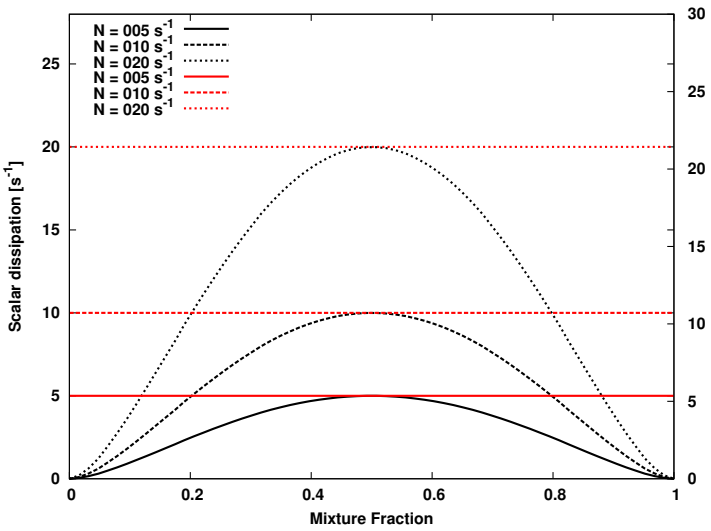


Figure 26: Amplitude Mapping Closure versus constant value of $N(\eta)$

$\eta = 0$ and $\eta = 1$, and a maximum value for intermediate values on mixture fraction, in $\eta \neq \eta_{st}$, where the mixture fraction gradients are more intense.

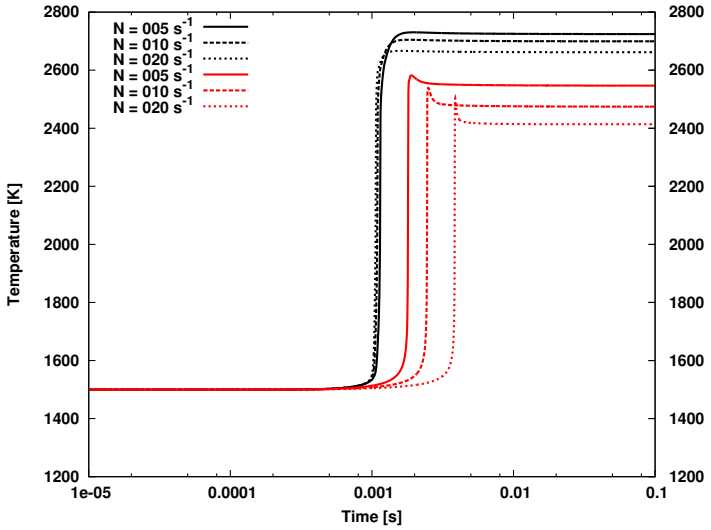


Figure 27: Autoignition time delay in the case of AMC (black lines) and constant (red lines) scalar dissipation distributions, $T_0 = 1500K$

In the case of the bell-shaped distribution (black lines in fig. 27), the sensitivity of the ignition delay time over the maximum scalar dissipation is very weak, while it can be noticed a slight decrease of the flame temperature. This can explained by the fact that, as shown previously, ignition takes place nearby the stoichiometric region, $\eta = 0.055$ in our case, where the bell-shaped scalar dissipation is weakly dependent on its maximum value, located at $\eta = 0.5$, as shown in fig. 26. Hence the ignition occurs almost simultaneously in the three cases, then, when the flame dynamics move toward reacher regions, the influence of the scalar dissipation on the fully developed flame is weak but clearly observable. On the contrary, in the case of constant scalar dissipation, represented by the red curves in fig. 26, the scalar dissipation difference in the three cases is high in the whole mixture fraction range, this explaining the high sensitivity of the ignition delay time and maximum temperature on scalar dissipation in this case.

This test highlights the importance of the scalar dissipation modeling especially in term of accuracy of transients description.

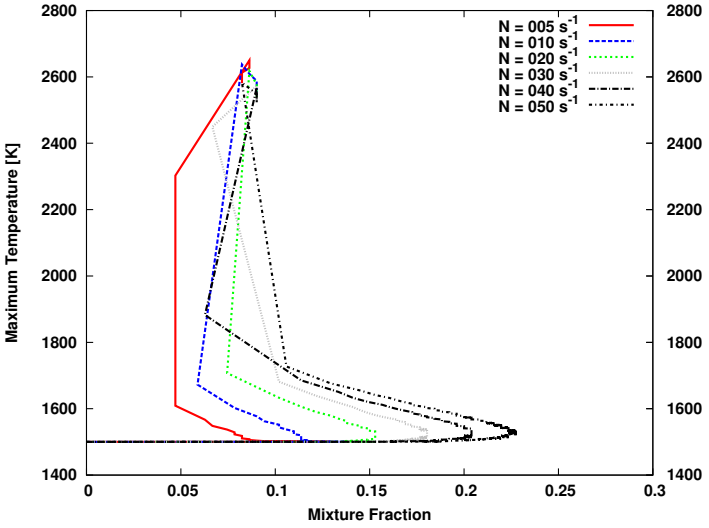


Figure 28: Temeperature Peak in Autoignition transients, $T_0 = 1500$

Finally, the position in the mixture fraction space, of the maximum temperature value is reported in fig. 28. The test has been performed inquiring the autoignition if the same $CH_4/Air$ test-case employed so far, with initial temperature $T_0 = 1500K$, and under the assumption of constant value of scalar dissipation over the mixture fraction space. The results in fig. 28, confirm that the final temperature a weakly decreasing function of the scalar dissipation, and its steady state, peak value position in the mixture fraction space is weakly influenced by scalar dissipation. On the other hand, the temperature peak trajectories, show that the higher is the scaler dissipation, the richer is the ignition point, which later moves closer to the stoichiometric region.

### 7.1.6 *A priori testing of a SANDIA flame D*

The predictive capabilities of Eqns. (202), has been assessed by means of an 'a priori' test over the experimental data of the Sandia D flame

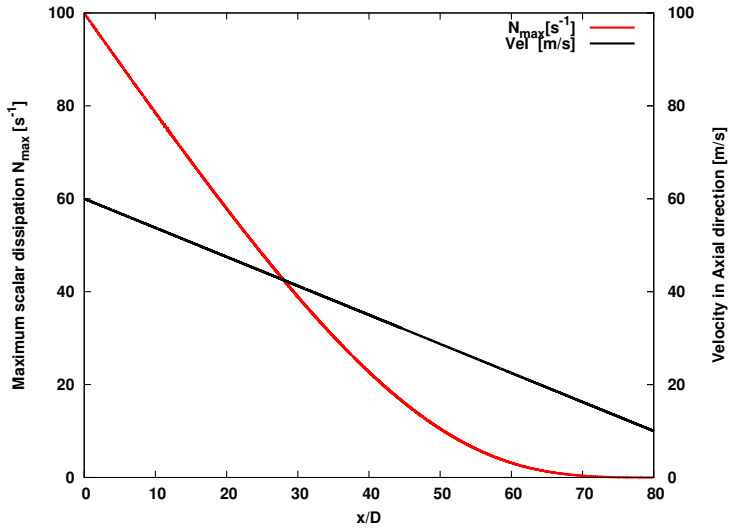


Figure 29: Presumed Axial distribution of axial velocity and scalar dissipation

[4]. The Sandia D flame is a co-flow piloted jet flame, nozzle diameter $7.2mm$, pilot diameter $18.2mm$, average axial velocity of the jet of $50m/s$, and co-flow average velocity is $0.9m/s$. The main jet composition is 25%$CH4$ and 75% Air by volume, resulting in a stoichiometric mixture fraction $\xi_{st} = 0.37$; both ambient and main jet temperature are $291K$. The co-flow pilot flame is a lean mixture ($\phi = 0.77$) of $C_2H_2$, $H_2$, Air, $CO_2$ and $N_2$ with the same nominal enthalpy and equilibrium composition as methane/air at this equivalence ratio [4]. The numerical test consists in prescribing the space evolution of both the axial velocity and the maximum scalar dissipation in space; the axial velocity has been presumed to be a linear decreasing function of the axial position, with $U(X/D = 0) = 50m/s$ and $U(X/D = 80) = 10m/s$. The scalar dissipation profile in the mixture fraction space has been modeled to have a gaussian shape like as in Eqns.(205) and (206), while its maximum value $N_{max}(x)$, has been chosen to be an exponential decreasing function, chosen in order to have $N_{max}(X/D = 0) = 100s^{-1}$, $N_{max}(X/D = 30) = 40s^{-1}$, and $N_{max}(X/D > 60) \simeq 0$, consistently with experimental measurements [4]. The maximum scalar dissipa-

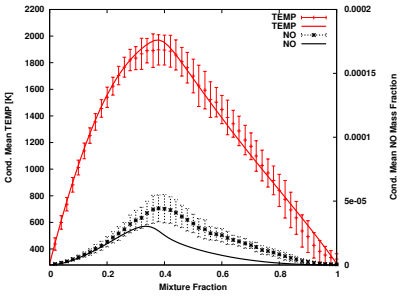


Figure 30: Sandia D $x/D = 7.5$

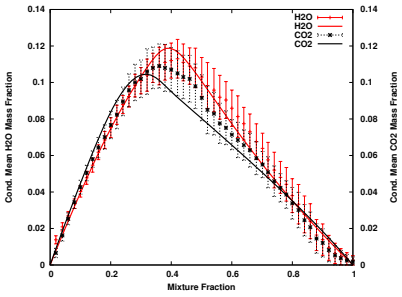


Figure 31: Sandia D $x/D = 7.5$

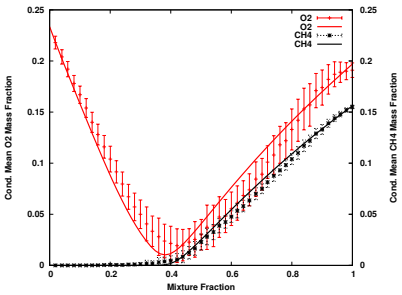


Figure 32: Sandia D $x/D = 7.5$

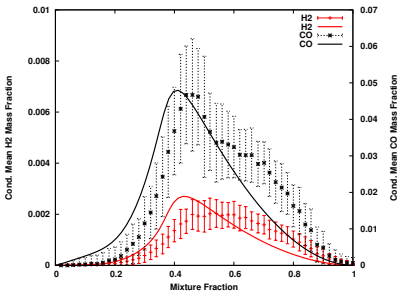


Figure 33: Sandia D $x/D = 7.5$

tion and axial velocity trends as function of the axial direction $N_{max}$ and $\widetilde{u_x(x,\eta)}|\eta = U(x)$ are shown in fig. 29.

For the sake of simplicity, the initial condition fir the CMC unsteady calculations has been chosen to be the Burke-Shumann limit of a flame generating from air and the $CH_4$/Air mixture of the sandia main jet. The resulting stoichiometric mixture fraction, following the Bilger's definition [8], is $\xi_{st} = 0.37$. The plots in figs. 30 to 53 show

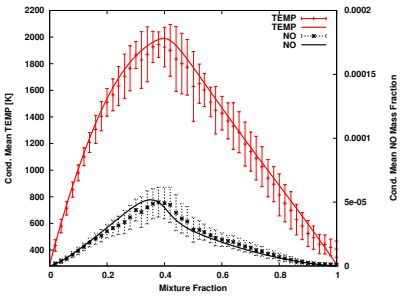


Figure 34: Sandia D $x/D = 15$

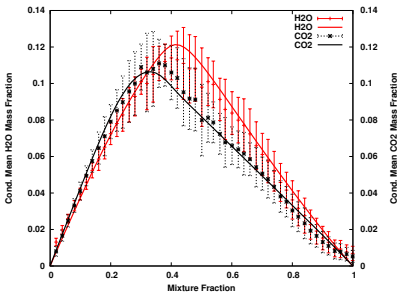


Figure 35: Sandia D $x/D = 15$

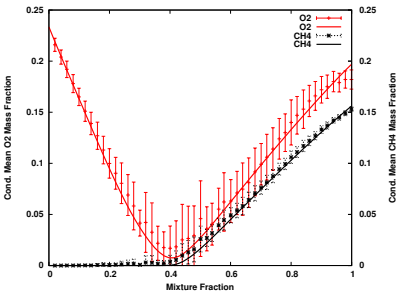


Figure 36: Sandia D $x/D = 15$

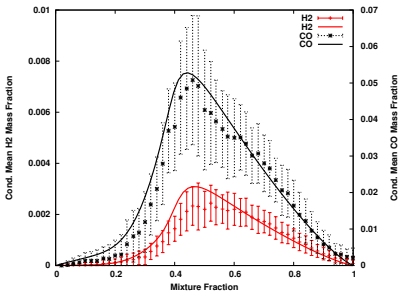


Figure 37: Sandia D $x/D = 15$

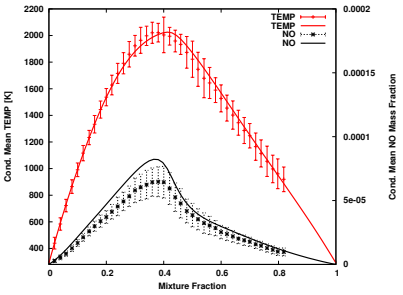


Figure 38: Sandia D $x/D = 30$

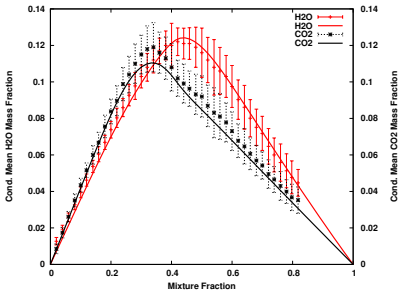


Figure 39: Sandia D $x/D = 30$

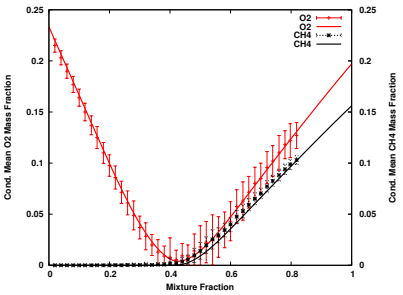


Figure 40: Sandia D $x/D = 30$

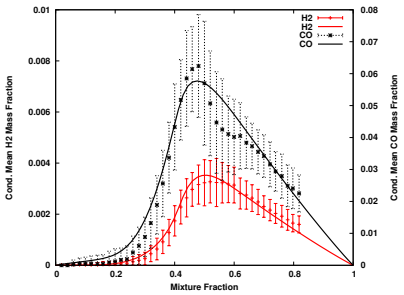


Figure 41: Sandia D $x/D = 30$

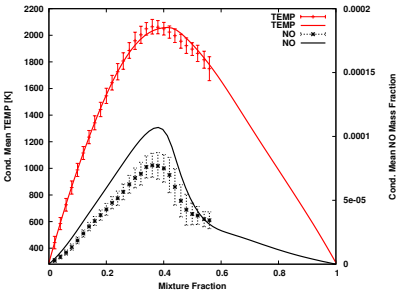


Figure 42: Sandia D $x/D = 45$

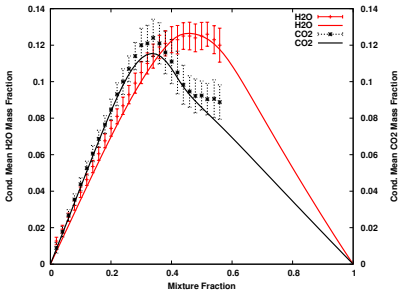


Figure 43: Sandia D $x/D = 45$

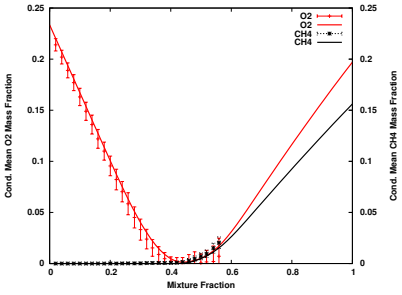


Figure 44: Sandia D $x/D = 45$

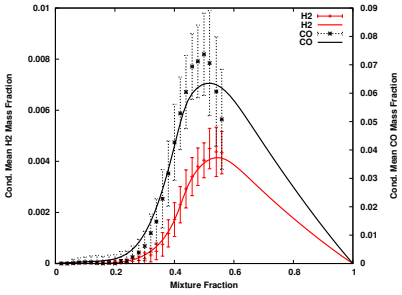


Figure 45: Sandia D $x/D = 45$

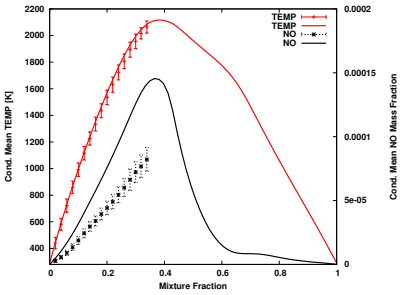


Figure 46: Sandia D $x/D = 60$

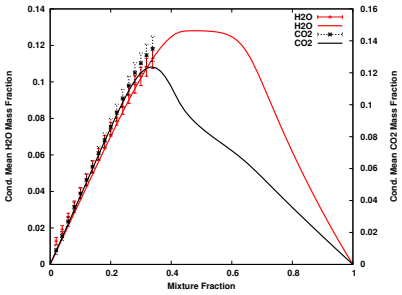


Figure 47: Sandia D $x/D = 60$

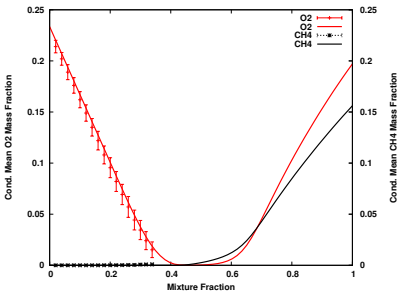


Figure 48: Sandia D $x/D = 60$

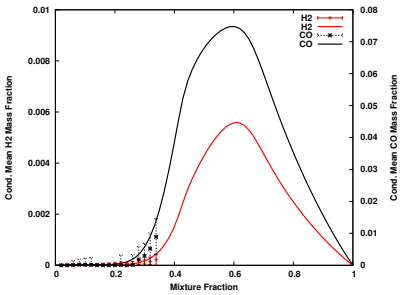


Figure 49: Sandia D $x/D = 60$

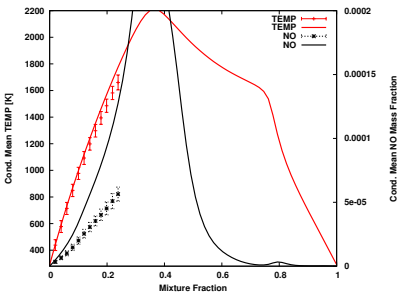


Figure 50: Sandia D $x/D = 75$

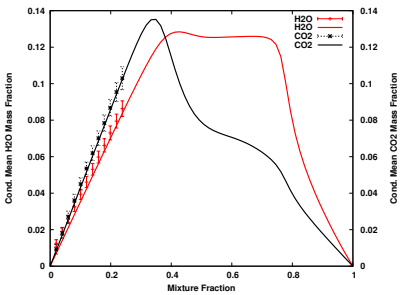


Figure 51: Sandia D $x/D = 75$

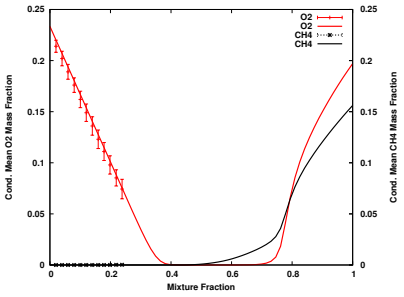


Figure 52: Sandia D $x/D = 75$

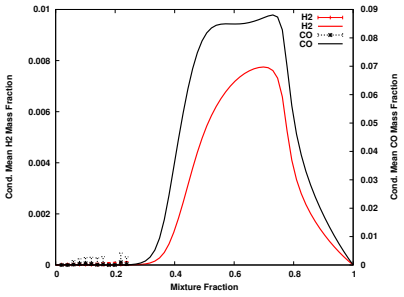


Figure 53: Sandia D $x/D = 75$

a very good agreement between the numerical test and experimental data until $x/D = 75$. The main differences between the numerical and the experimental results are in the $NO$ mass fractions prediction, possibly caused by the employed chemical mechanism, coherently with the findings available in the open literature [34, 11].

### 7.1.7 *Constant vs variable specific heats*

Finally, Eqns. in (202) have been employed to quantify the impact of the constant specific heat assumption on the steady state flame prediction.

Two steady-state solutions for the same Methane/air test case studied in sec.7.1.2, with the same chemical mechanism and discretization in the mixture fraction space $\eta$, have been compared with $N_{max} = 100s^{-1}$. The first solution has been obtained for $C_p = C_p(Y_\alpha, T)$, while the second has been computed under the assumption of having $C_p = const$. The comparison between the constant and variable specific heats results is presented in fig. 54-57, showing the importance of the specific heat dependence on temperature and composition for an accurate prediction of the flame behavior, both in terms of temperature distribution and product prediction.

The temperature prediction, in particular, shows a mostly linear behavior in the case of constant specific heat, this being due to the fact that the temperature Eq. (113), for $C_p = const$, becomes a reactive

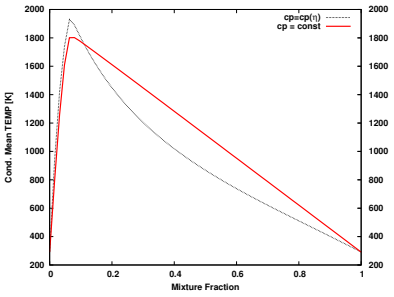


Figure 54: Temperature

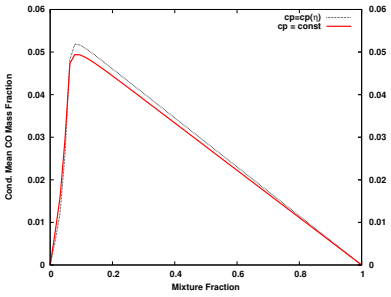


Figure 55: CO Mass Fraction

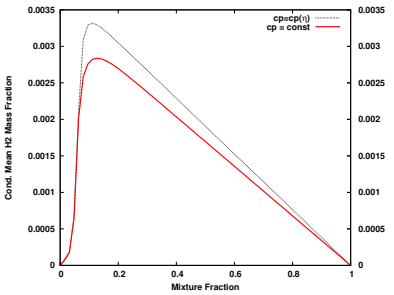


Figure 56: H2 Mass Fraction

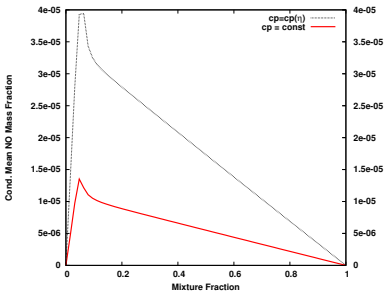


Figure 57: NO Mass Fraction

diffusive equation, similarly to the species equations, leading to linear solutions in the regions where any reaction occur, i.e. everywhere but in the stoichiometric region.

## 7.2 LES-CMC COUPLING

In this section the CMC coupling approaches presented in sec. 5.2 and in 5.3 are compared. Both the Vector Field Update (VFU) and the Energy Source Update (ESU) have been implemented as explained in detail in sec 5.3, 5.2 and 6.2. While the predictive capabilities of the CMC equations have been assessed in sec 7.1.6. The aim of this section is to understand the influence of the VFU and ESU coupling strategies on the solution accuracy.

### 7.2.1 *The test-case*

To isolate the effects of the coupling strategies on the numerical solution, a laminar test-case has been set up. The test-case is a 2D mixing layer at ambient pressure $P = 1Atm$, with a uniform axial velocity profile $u_x = 66m/s$ at the inlet, and an assigned mixture fraction profile with an hyperbolic tangent dependence on the transversal direction y as reported here:

$$\begin{aligned} \xi_{av} &= \frac{(\xi_O + \xi_F)}{2} & \Delta\xi &= \xi_O - \xi_{av} \\ \delta &= \frac{1}{2} & \xi(y) &= \xi_{av} + \tanh(\frac{y}{\delta})\Delta\xi \end{aligned} \tag{207}$$

The initial condition composition varies being a linear function of the mixture fraction as follows :

$$Y_\alpha(y) = \xi(y)Y_{\alpha,F} + (1 - \xi(y))Y_{\alpha,O} \tag{208}$$

The fuel is composed by H2 and N2 while the oxidizer is Air, with a resulting stoichiometric mixture fraction $\xi_{st} = 0.47$; the exact fuel and oxidizer compositions are reported in tab. 1. The initial temperature field is constant in space with $T_{t=0}(x, y) = 1100K$. Once the

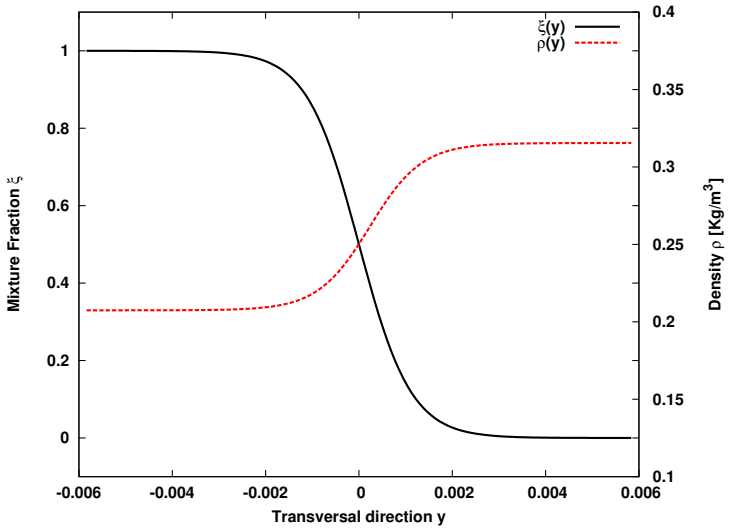


Figure 58: Mixture Fraction inlet mixture fraction and density profiles

| | $Y_O$ | $Y_F$ |
|---|---|---|
| $\xi$ | 0.0 | 1.0 |
| H2 | 0.0 | .037 |
| O2 | .234 | 0.0 |
| N2 | .766 | .963 |
| TEMP | 1100K | 1100K |

Table 1: Laminar 2D test-case Inlet Composition

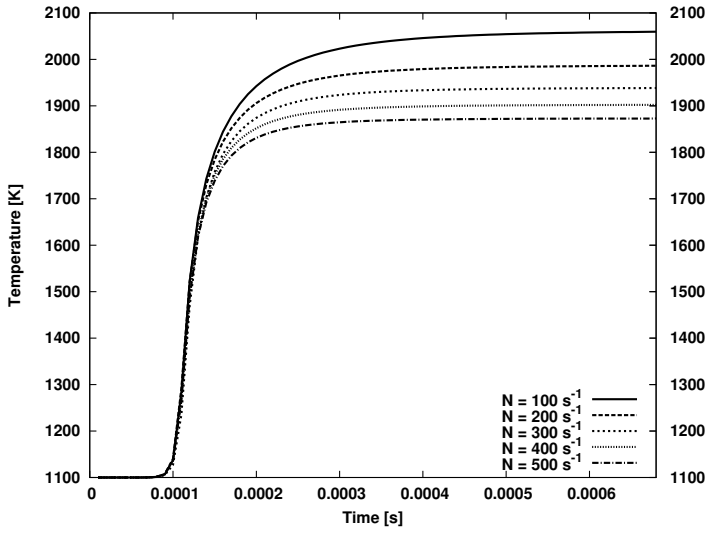


Figure 59: Temperature 0D predictions, $\eta = \eta_{st}$

species profile is known, being function of the mixture fraction $\zeta(y)$ as reported in sec 6.1.4, the density profile $\rho(y)$ is defined as function of temperature, pressure and species mass fractions as follows:

$$\rho(y) = \sum_{\alpha} Y_{\alpha}(y)\rho_{\alpha}(P(y), T(y)) \tag{209}$$

The mixture fraction and density profiles chosen for the initial and inflow boundary conditions are shown in fig. 58. The resulting problem is an autoignition problem of a mixing layer, with oxidizer in the upper stream and fuel in the lower, both at the same velocity and temperature. Since the initial temperature is higher than autoignition temperature, the fresh mixture will auto-ignite, the ignition delay time will result in space displacement from the inflow section due to the convective transport in the axial direction, which can be estimated roughly estimated to be $X_d = u_x t_{ign}$.

A 0D a priori prediction of the inquired 2D test-case has been performed assuming a bell-shaped scalar dissipation distribution over the mixture fraction $\eta$, and a constant maximum scalar dissipation value in the axial direction. The employed chemical mechanism is a 9 species and 19 reactions proposed by Yetter, et al. in [66]. The

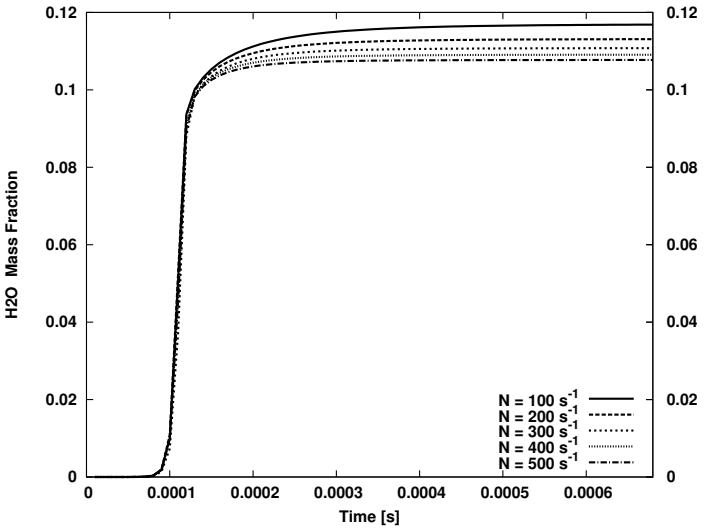


Figure 60: H2O Mass fraction 0D predictions, $\eta = \eta_{st}$

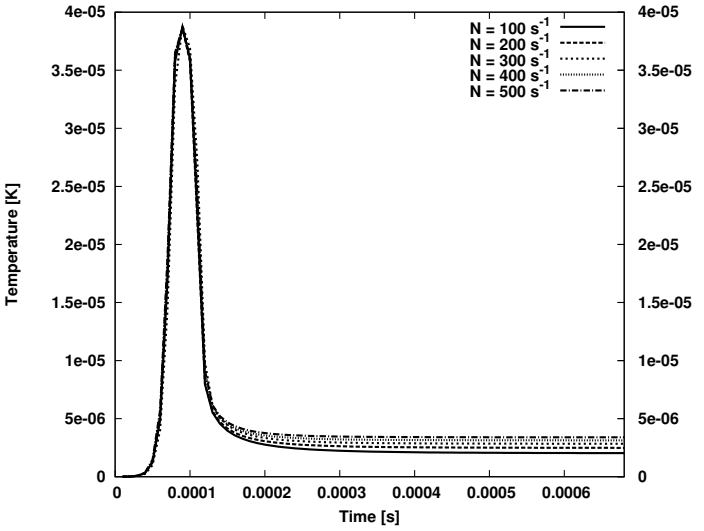


Figure 61: HO2 Mass fraction 0D predictions, $\eta = \eta_{st}$

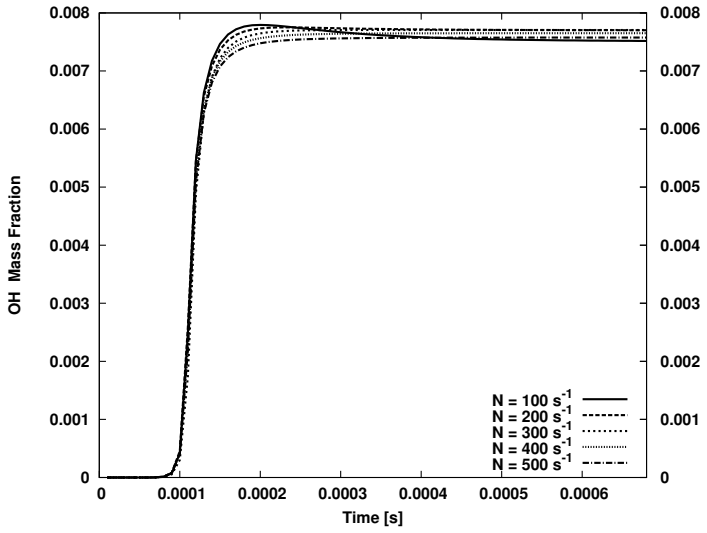


Figure 62: OH Mass fraction oD predictions, $\eta = \eta_{st}$

computational strategy is the same employed for the SANDIA D flame oD prediction in sec. 7.1.6, with a uniform initial temperature, $T_0(x,y) = 1100K$, and for a number of different scalar dissipation maximum values. The results of the oD computations are reported in fig. 59-62. The temperature and combustion products time evolutions show that, for the prescribed initial temperature and pressure, $T_0 = 1100K$ and $P_0 = 1Atm$, the ignition delay time is very weakly dependent on the maximum scalar dissipation. However, the effects of a change in the maximum scalar dissipation are observable in terms of flame temperature and combustion products, this being in accordance with the results reported in sec. 7.1.5 for methane/air flames.

### 7.2.2 *Results and discussion*

The steady state solutions of the 2D test case obtained with both the VFU and ESU coupling strategies are compared in the following. The computational physical domain dimensions are $L_x = 44.6mm$ in the axial direction and $L_y = 11.2mm$ in the transversal direction,

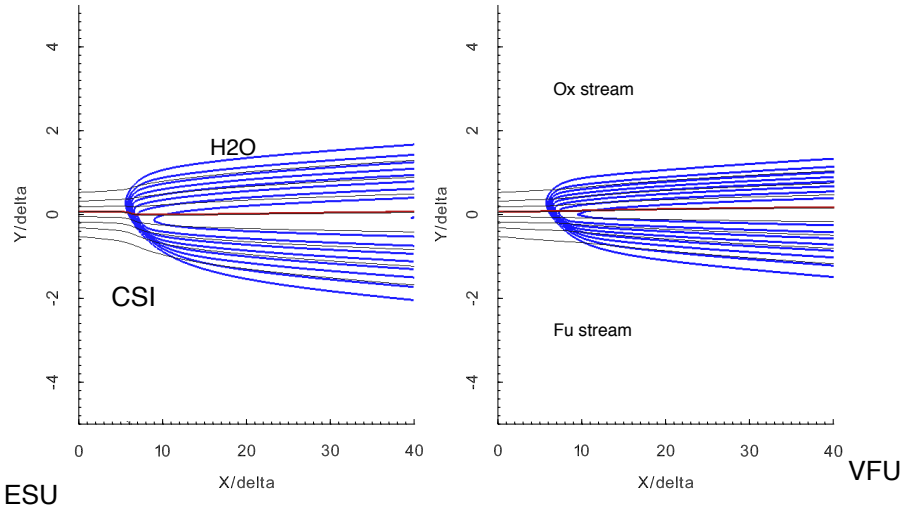


Figure 63: $\xi(x,y)$ and $Y_{H2O}$ contour lines

which are discretized with $n_x = 512$ cells in the axial direction and $n_y = 128$ cells in the transversal direction. The CMC domain has been discretized with the same number of cells in the axial direction x, while the mixture fraction space is discretized with 64 mesh cells; hence each CMC cell corresponds to $n_y$ LES cells.

The results of the two computations are reported in figs. 63- 67 with the physical axes normalized to the mixing layer thickness $\delta$. The VFU and ESU solutions are in good agreement in terms of ignition displacement in the axial direction and in terms of $H_2O$ mass fraction and temperature fields as shown in figs. 66 and 63 respectively. Moreover, the $HO_2$ and $OH$ mass fraction fields in fig. 64 demonstrate that both the two approaches are able to capture the typical triple flame configuration [65]. However, the plots in fig. 68, relative to the transversal distributions ($x = 0.022m$) call for more comments.

In fig. 68 the temperature distribution $T(y)$ shows a difference in the peak value of the order of the 4%, and the ESU approach produces a wider flame front than VFU. This difference in temperature distributions is less marked if one moves from the transversal direction $T = T(y)$ to the mixture fraction $T = T(\eta)$ as shown in fig. 69. Fur-

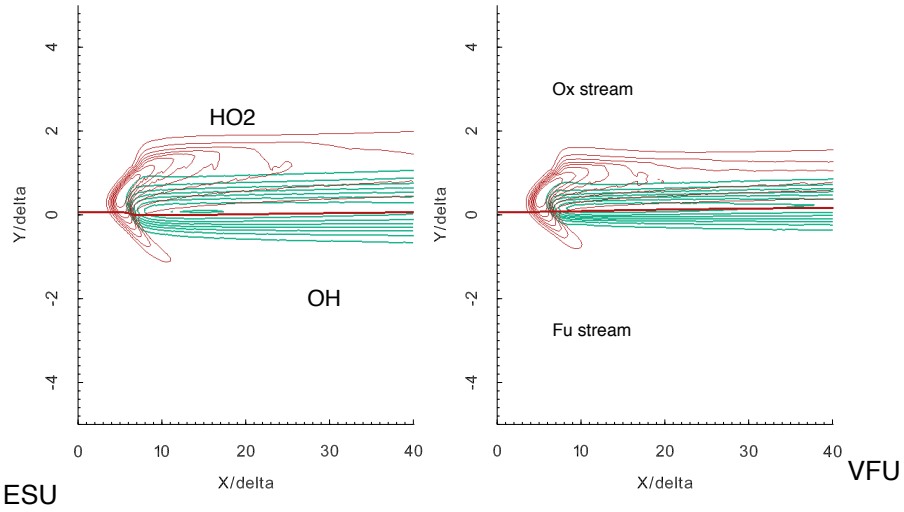


Figure 64: $Y_{HO2}$ and $Y_{OH}$ contour lines

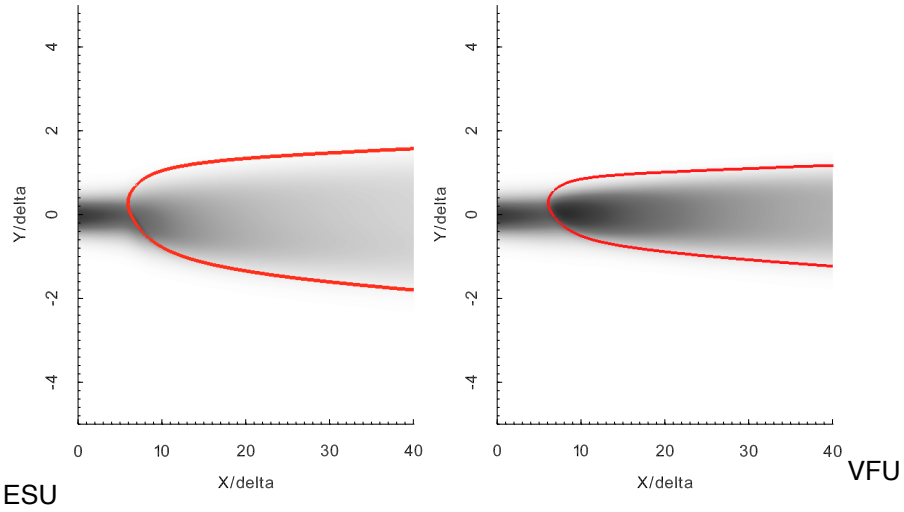


Figure 65: Scalar Dissipation field $[s^{-1}]$, and $T = 1.1T_0$ contour line (red)

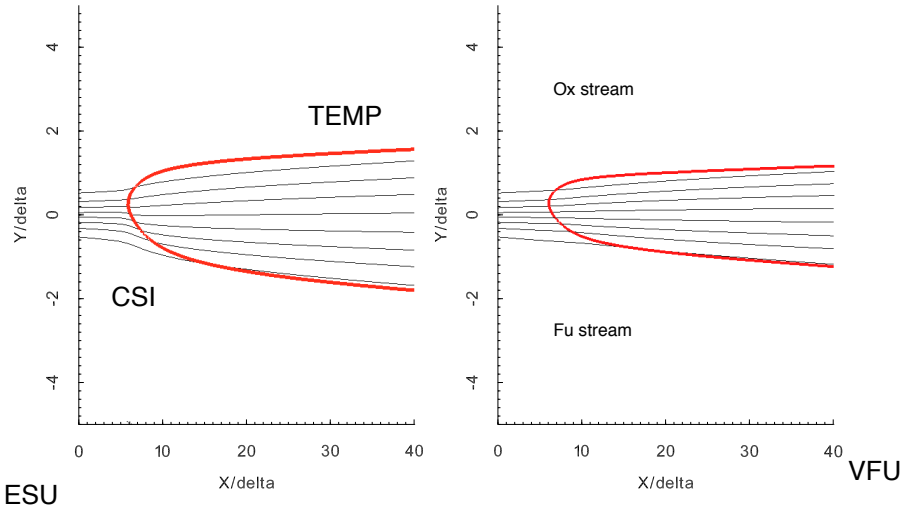


Figure 66: $\tilde{\zeta}(x,y)$ and and $T = 1.1T_0$ contour lines

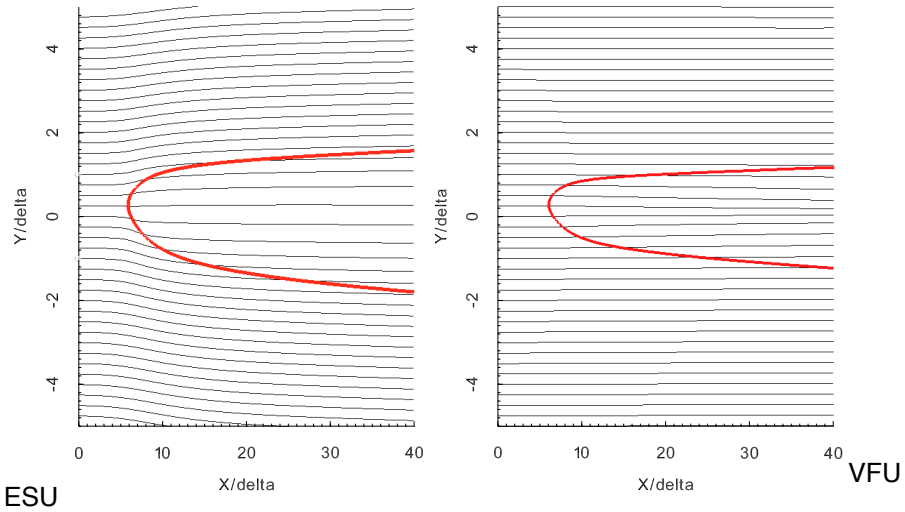


Figure 67: Steamlines and $T = 1.1T_0$ contour line (red)

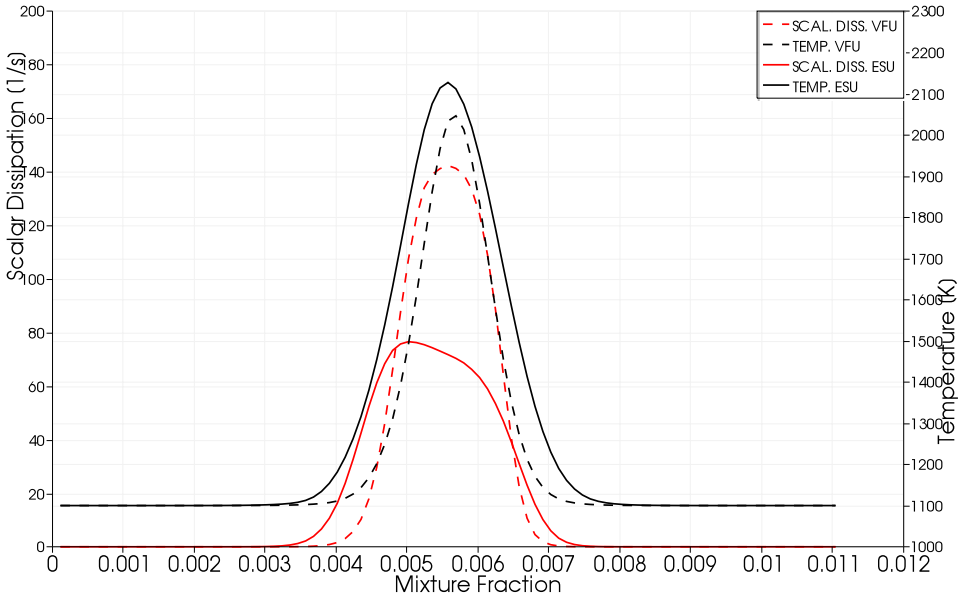


Figure 68: $T(y)$ [K] profiles at x=0.02 m

thermore, the scalar dissipation $N(\eta)$, also reported in fig. 69, shows a maximum value resulting from the VFU computations which is twice as large as the one resulting from the ESU predictions. This difference in the scalar dissipation prediction is in total agreement with the mixture fraction distribution presented in fig. 70. The difference in the mixture fraction transversal profiles $\xi(y)$ obtained from the ESU computations, results in lower mixture fraction gradients, and eventually in a lower scalar dissipation fields. This difference in the scalar dissipation distribution is observable in the whole flame front, as visible in the contour plot in fig. 65, reporting the scalar dissipation fields in the two cases.

The difference in the mixture fraction spatial distribution seems to be the effect of a different velocity field, especially in terms of the transversal velocity component $v(\mathbf{x})$, as reported in the streamline plot in fig. 67. In the ESU approach, the thermal expansion due to fresh gasses ignition, results in a slight change in the fluid direction, with a transversal velocity peak of the order of 5% of the inlet velocity. With the VFU approach, this fluid dynamic process is not described as will be discussed below.

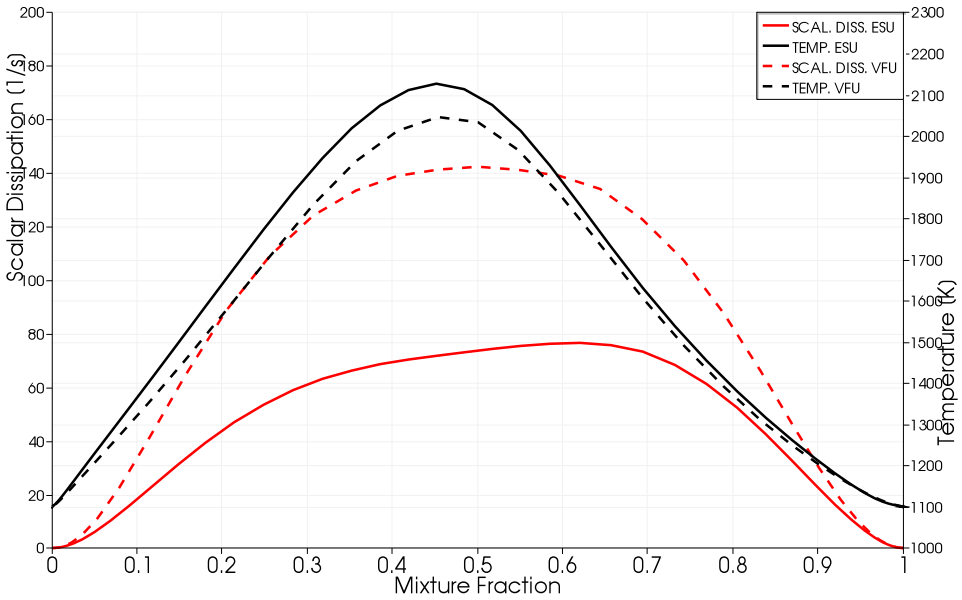


Figure 69: $\widetilde{T|\eta}$ [K] profiles at x=0.02 m

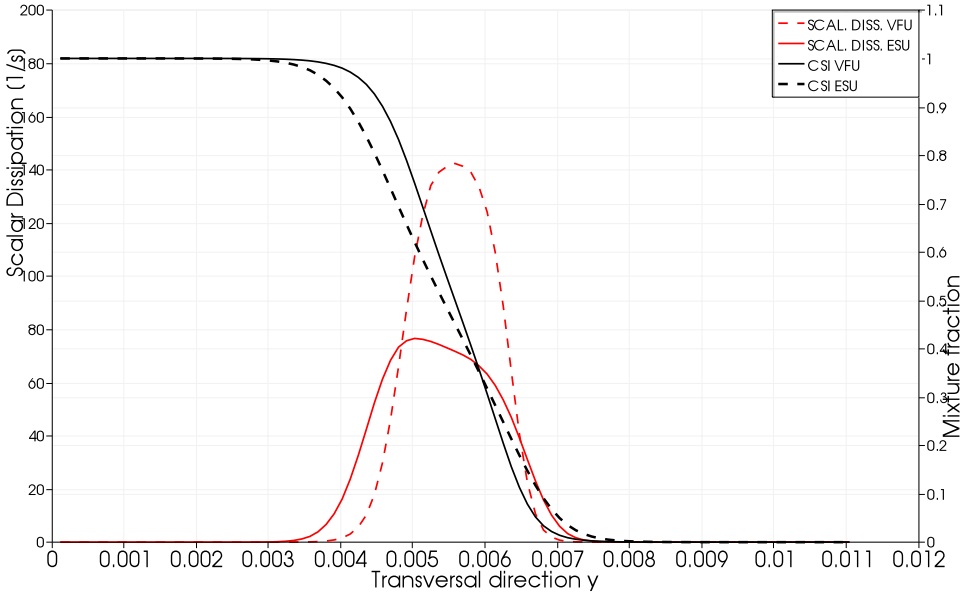


Figure 70: $\xi(y)$ profiles at x=0.02 m

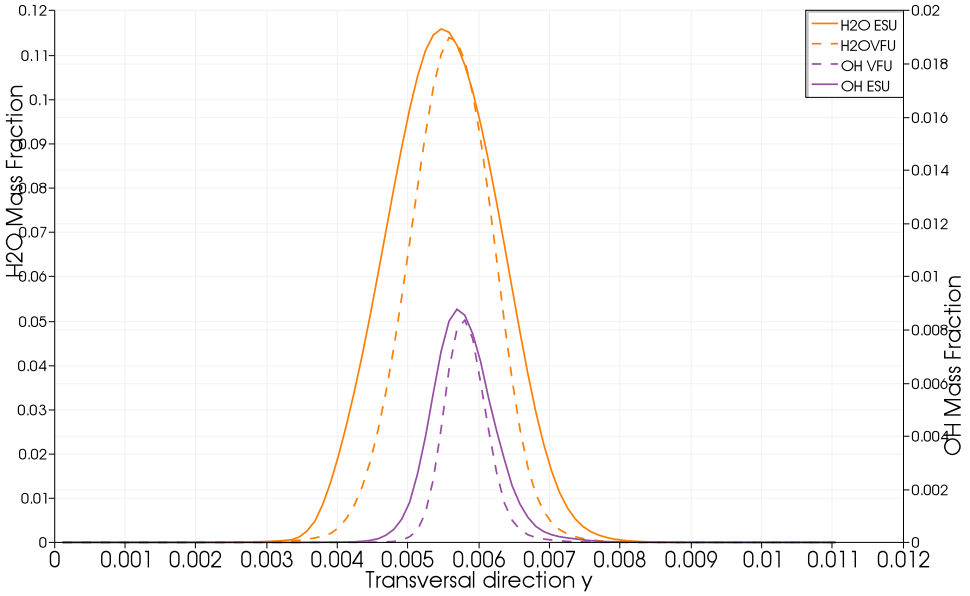


Figure 71: $Y_{H2O}(y)$ and $Y_{OH}(y)$ profiles at x=0.02 m

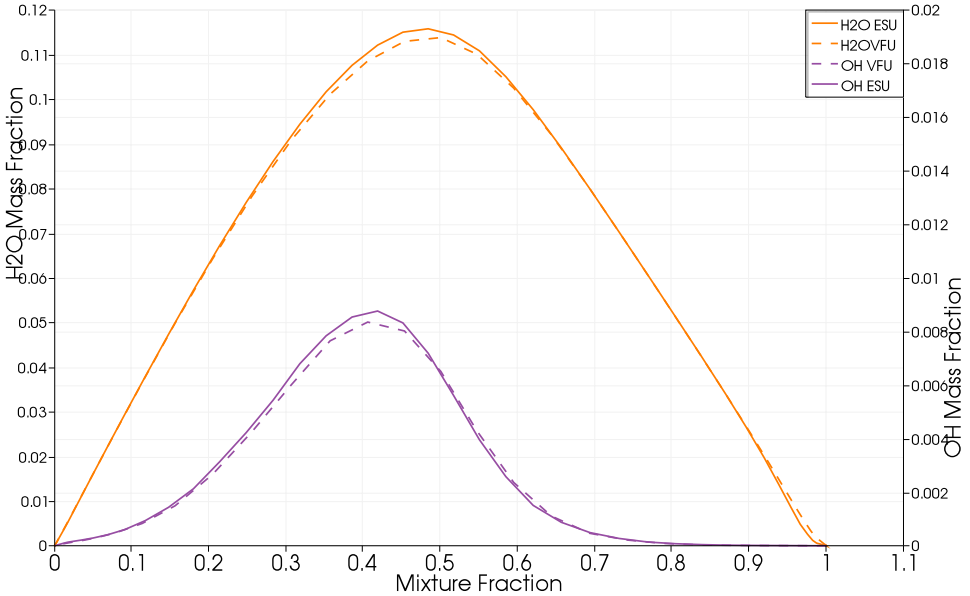


Figure 72: $\widetilde{Y_{H2O}|\eta}$ and $\widetilde{Y_{OH}|\eta}$ profiles at x=0.02 m

The mostly fluid-dynamic nature of the discrepancy between the two approaches is confirmed by the fact that, in the mixture fraction space, the two solutions are quite similar both in terms of temperature and products mass fractions distributions, as shown in figs.69 and 72 respectively. This is because, as predicted by means of the 0D computations, fig. 62 and 60, the dependence on the products to the maximum scalar dissipation is weak, while the space dependence is removed by moving from the physical space $y$ to the mixture fraction space $\eta$.

The reasons of the difference between the solution obtained with the two approaches seems to rely in the fact that, as explained in sec. 5.2, the VFU consists of an operator splitting of the full Navier-Stokes system into a 'mixing problem' and a 'reactive problem'.

Being an operator splitting, the two subsystems are then evolved in time sequentially, and, from a theoretical point of view, this should converge to the exact solution of the full system, in the limit of the integration time step going to zero. Moreover this would be true even if one of the subsystem, the reacting system in this case, is conditionally filtered and solved in a different space, with the mixture fraction as additional dimension. However, in the present formulation, the mixing system is conditionally filtered and solved and reduced to a one dimensional version under the shear layer assumption [23, 24]. Hence in the VFU approach, when the mixing system state vector is updated, the effects of the approximations operated in the reactive system formulation are entirely reflected in the final solution.

On the other hand, as explained in sec 5.3, in the ESU approach, the solution is provided by the solution of the main system, while the CMC acts only as closure model in terms of chemical source term and mixture composition. Hence, although the 'closure system' has been derived for the ESU approach, under the same hypothesis of the 'reactive system' in the VFU approach, the influence of these approximations are not strongly reflected in the final solution, which is a solution of an intrinsically multi-dimensional system, the 'main sys-

tem'. This is confirmed by the conservation tests performed in both the two solutions. While the ESU approach numerically conserves both the mass (with an error on 0.04%), and the absolute enthalpy (with an error of 2%), the VFU approach is affected by an error of 7% in the mass conservation. This makes the ESU approach a preferable choice.

| Oxid Stream | Fuel Stream |
|---|---|
| $u_O = 125\ m/s$ | $u_F = 62.5\ m/s$ |
| $v_O = 0.$ | $v_F = 0.$ |
| $w_O = 0.$ | $w_F = 0.$ |
| $p_O = 1.Atm$ | $p_F = 1.0Atm$ |
| $T_O = 1000.0K$ | $T_F = 1000.0K$ |
| $\xi_O = 0.$ | $\xi_F = 1.$ |

Table 2: Summary of the inlet conditions

## 7.3 3D MIXING LAYER

A three dimensional turbulent mixing layer has been numerically computed. Similarly to the 2D test case, the test problem is an autoignition problem: the upper stream is the oxidizer stream, while the lower stream is the fuel one. The fuel and oxidizer composition are exactly the same of the 2D laminar test case and are reported in tab. 1. All the test cases presented in the following are at ambient pressure $P_0 = 1Atm$ and with an initial temperature of $T_0 = 1000K$. Differently from the 2D test-case the fuel and oxidizer stream velocity are not the same, and a velocity ratio $V_R = u_O/u_F = 2$ is imposed. The two stream velocities are $u_O = 125m/s$ and $u_F = 62.5m/s$. The inlet conditions of the problem are reported in tab. 2.

The mixture fraction $\xi$ and the axial velocity $u$ varies along the $y$ direction as follows:

$$\xi_{av} = 0.5(\xi_O + \xi_F) \qquad \Delta\xi = \xi_O - \xi_{av}$$
$$u_{av} = 0.5(u_{av} + u_F) \qquad \Delta u = u_O - u_{av}$$
$$\delta = 0.5$$
$$\xi(y) = \xi_{av} + \tanh(\frac{y}{\delta})\Delta\xi$$
$$u(y) = u_{av} + \tanh(\frac{y}{\delta})\Delta u$$

While the composition varies as function of the mixture fraction as follows :

$$Y_\alpha(y) = \xi(y)Y_{\alpha,F} + (1 - \xi(y))Y_{\alpha,O} \tag{210}$$

As already introduced in sec. 6.1, the LES system is numerically discretized and implemented in non-dimensional form with reference to the choice of a prescribed state. The oxidizer stream provides the reference state values of temperature, pressure and transport properties. The mixing layer thickness $\delta$ has been chosen as characteristic length. A reference velocity is defined in terms of the reference pressure and density, while the reference time scale is defined as the ratio of reference length and velocity.

$$p^* = p_O \qquad T^* = T_O \tag{211}$$
$$\mu^* = \mu_O \qquad \gamma^* = \gamma_O \tag{212}$$
$$L^* = \delta \qquad u^* = \sqrt{\frac{p^*}{\rho^*}} \tag{213}$$
$$t^* = \delta / \sqrt{\frac{p^*}{\rho^*}} \tag{214}$$

The non-dimensional inputs of the problem are the Mach number and the Reynolds number defined as:

$$Re = \rho_O u_O \delta / \mu_O \quad \rightarrow \quad L^* = \delta = \frac{\mu_O Re}{\rho_O u_O} \tag{215}$$
$$M = u_O / a_O \tag{216}$$

| Re | $L_x$ [m] | $L_y$ [m] | $L_z$ [m] | $\delta$ [m] |
|---|---|---|---|---|
| 500 | 0.149 | 0.049 | 0.0245 | $0.49 \cdot 10^{-3}$ |
| 1000 | 0.299 | 0.0996 | 0.0448 | $0.996 \cdot 10^{-3}$ |
| 1500 | 0.434 | 0.149 | 0.149 | $1.49 \cdot 10^{-3}$ |

Table 3: Physical domain dimensions

Once defined the composition, temperature and pressure of the oxidizer stream, a variation of $Re$ corresponds to a length variation. A higher $Re$ results in a wider $\delta$. The three-dimensional physical domain is a parallelepiped, with the $x$-axis lying parallel to the axial direction, the $y$-axis directed normal to the mixing layer, and the $z$-axis orthogonal to the other two. The boundary conditions are the GRCBC presented in sec. 6.1.5, with the inlet profiles previously specified as inflow target values, and the ambient pressure for the other directions. The only exception are the two boundary conditions in the $z$ direction which are periodic.

Three computations have been performed, all with the same inlet Mach number and a fuel and oxidizer velocity ratio $V_R = 2$. The oxidizer inlet velocity is $u_O$, where the oxidizer inlet Mach number, $M_{in} = 0.2$, follows the definition in Eq. (215). The three test-cases differ for the imposed Reynolds number: $Re_1 = 500$, $Re_2 = 1000$, $Re_3 = 1500$. The computational domain has an overall non dimensional size of $(L_x \times L_y \times L_z) = (300\delta \times 100\delta \times 30\delta)$, where $\delta$ is the mixing layer thickness at the inlet. In accordance with the definition in Eq. (216), under the conditions previously introduced, a change in the Reynolds number results in a change of the domain size, as reported in fig. 74. The corresponding sizes of the computational domains are reported in tab.3.

The LES computational mesh is the same for all the cases, $N_x$=512, $N_y$= 129, $N_z$=64, while the CMC mesh has the same mesh points in the axial direction,$N_x$=512 , and 64 point in the mixture fraction direction

$\eta$. The computation has been fully parallelized, and 512 cores are used for each computation. A cartesian domain decomposition has been performed, which splits the entire domain in 512 sub-domains, each constituted by $n_x$ =8, $n_y$=129, and $n_z$ =8 points in the respective physical directions as shown in fig. 73.

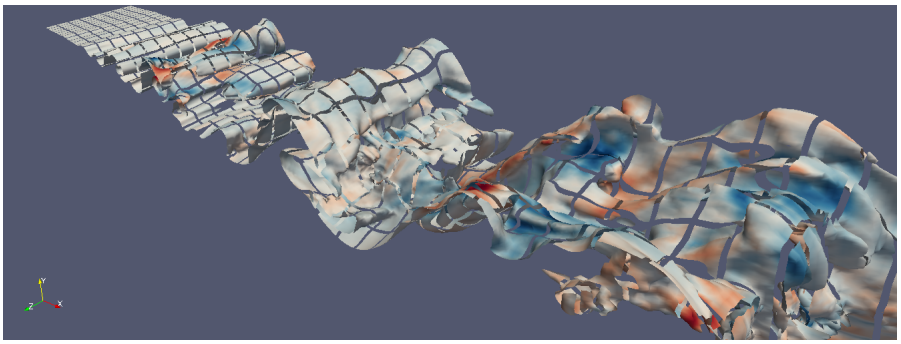

Figure 73: MPI cartesian domain decomposition example

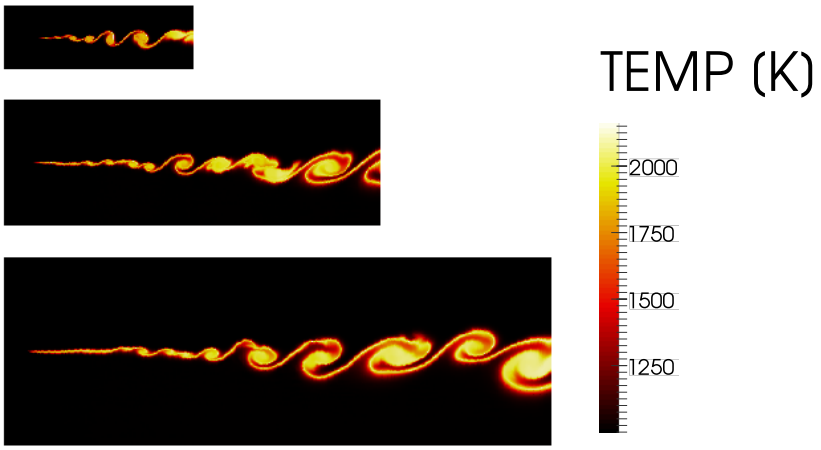


Figure 74: From the top: Re=500, Re=1000, Re=1500

The predictive capabilities of this numerical implementation still need to be verified by means of a comparison with experimental results. However, these preliminary consistency test confirmed that this LES/CMC implementation is promising and most of the expected

predictive capabilities, such as the triple flame behavior in fig. 75, are confirmed in the 3D case.

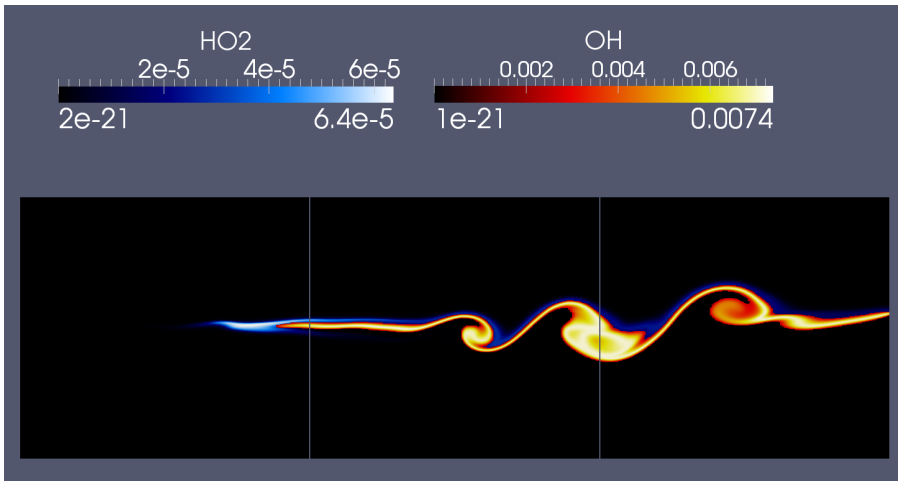


Figure 75: Edge Flame, Triple Flame

### 7.3.1 *Numerical performance*

The code has been written in Fortran 90/95 and fully parallelized. Parallelization relies on a Cartesian decomposition strategy, where the computational domain is split in various sub-domains in the coordinate directions and communication between neighboring blocks is handled by means of an efficient MPI implementation. The non-reactive LES code by Pirozzoli and Bernardini has been already tested on a variety of different architectures (IBM POWER6, IBM PLX, Opteron) with excellent performance and scalability characteristics [53, 54, 55, 52]. The present reacting LES code has been ported and tested on MATRIX (lnx86 architecture) and on FERMI (IBM Blue Gene/Q system), where both strong and weak scalability tests have been performed.

The strong scalability tests are performed by choosing a problem of interest, in terms of number of variables and space discretization. A 'reference computational time' is defined as the computational time required by 1 core, for the numerical integration over a certain pre-

scribed number of time steps. Increasing the number of cores employed to solve the same problem will typically result in a decrease of the computational time. The ideal behavior would be to have the computational time inversely proportional to the number of employed cores. This can happen if the cost of the communication operations among the computational sub-blocks is negligible when compared to the cost of the numerical integration within each sub-block. In real applications, the cost of the communications between sub-blocks is not negligible, and becomes more and more important when the number of cores and computational sub-domains increases. This is because the computational load per core lowers with the increase of the number of cores employed, and the relative importance of the communications operations rises. The closer the real behavior is to the ideal behavior, the better is the strong scaling performance of the code. It is important to underline that, if the scalability performance is inquired over thousands of cores, the reference computational time cannot be chosen as the time required to numerically solve the same problem with a single core. This is because no machine exists that could solve such a large problem with a single core. Hence, the reference problem of our test has been chosen to be a Hydrogen/Air flame, with a 9 species 13 steps chemical kinetic mechanism, on a mesh of $128^3$ points per core. The reference computational time has been chosen as the computational time required by 16 computational nodes, with 16 cores each (256 cores), to perform 10 time steps. The number of employed cores used has been doubled up to 2048 cores, and number of points per cores has been proportionally reduced. The results of the strong scalability test are reported in tab. 4, demonstrating good scalability performance. The same results are plotted in fig. 76 in terms of strong speed-up function defined as:

$$S_s = \frac{N_{core,16} \cdot t_{16}}{N_{core} \cdot t}. \tag{217}$$

| #nodes | #cores | Comp.time [s] | Speedup | #points/task | Memory/task |
|---|---|---|---|---|---|
| 16 | 256 | 2475.4 | 1 | 128x128x128 | 700 MB |
| 32 | 512 | 1261.4 | 1.96 | 64x128x128 | 350 MB |
| 64 | 1024 | 669.4 | 3.7 | 32x128x128 | 180 MB |
| 128 | 2048 | 376.9 | 7.3 | 16x128x128 | 90 MB |

Table 4: Strong scaling results

The ideal strong scaling behavior is represented by the straight line in fig. 76, while the red curve represents the real behavior.

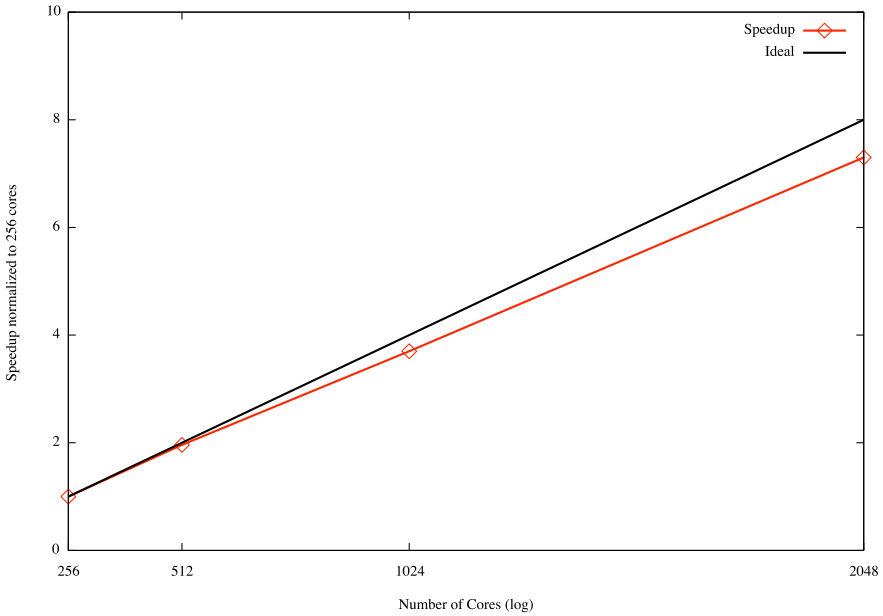


Figure 76: Strong scalability speed-up function

Similarly to what is done for the strong scalability tests, also the weak scalability tests require the choice of a reference problem of interest, in terms of number of variable and mesh points. The time required to numerically solve the problem is defined as reference computational time. However, differently from the strong scalability case, in the weak scaling tests both the number of cores and the computa-

| #nodes | #cores | # points/task | #total points | Comp.time [s] | Norm.time |
|---|---|---|---|---|---|
| 1 | 16 | 128x128x128 | $2.510^5$ | 2455.8 | 1 |
| 2 | 32 | 128x128x128 | $5.010^5$ | 2467.2 | 1.004 |
| 4 | 64 | 128x128x128 | $1.010^6$ | 2460.1 | 1.001 |
| 8 | 128 | 128x128x128 | $2.510^6$ | 2473.7 | 1.007 |
| 16 | 256 | 128x128x128 | $5.010^6$ | 2475.4 | 1.0071 |
| 32 | 512 | 128x128x128 | $1.010^9$ | 2490.1 | 1.0139 |
| 64 | 1024 | 128x128x128 | $2.010^9$ | 2524.5 | 1.0278 |
| 128 | 2048 | 128x128x128 | $4.010^9$ | 2635.9 | 1.0729 |
| 256 | 4096 | 128x128x128 | $8.0 * 10^9$ | 2719.9 | 1.1075 |

Table 5: Weak scaling results

tional domain dimensions are doubled at each test. In the ideal case, i.e. if the cost of the MPI communication operations is negligible or null, the computational time would remain constant at each doubling operations. This is because, if both the number of cores and the computational mesh points are doubled, the computational load per core remains ideally constant. In real applications, increasing the number of cores means increasing the relative cost of the communication operations on the final computational time mostly due to the all-to-all communications, this being responsible of a computational time increase at each doubling operation.

Similarly to the strong scaling case, the reference state has been chosen to be, a Methane/Air flame, with the same chemical mechanism, and16 cores with $128^3$ points per core, the number of cores and mesh point are doubled up to 4096 cores and 8 billion points. The results of the weak scaling tests are reported in tab.5, while a weak speed-up function,whose trend is reported in fig. 77, can be defined as:

$$S_w = N_c \frac{t_{ref} N_c}{t_{eff}}, \tag{218}$$

where $N_c$ is the number of cores employed, $t_{ref}$ is the computational time required for the reference test-case, and $t_{eff}$ is the effective time required for the corresponding test case.

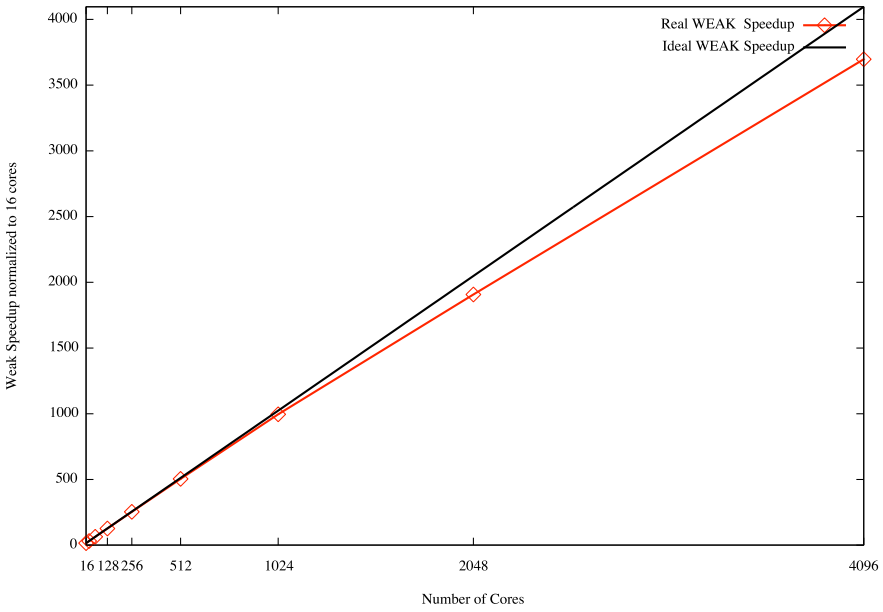


Figure 77: Weak scalability speed-up function

It is worth to note that the upper limit of the strong scalability tests is the number of mesh points per core, which cannot be too low, while in the weak scalability test there is no upper limit since the number of mesh points per cores is kept constant, while the total number of mesh points rises (up to 8Bil points in this case). This means that increasing the number of available computational resources, strictly results in the capability of studying problems with larger dimensions. On the other hand, increasing the number of available computational resources, does not ensure the capability of reducing the time required to study a fixed-size problem of interest.

| Comp. Load | Task |
|---|---|
| 12 % | $\widetilde{\cdot\|\eta}$ |
| 6 % | $\widetilde{u_x\|\eta}\frac{\partial Q_\alpha}{\partial x}$ |
| 61 % | $\widetilde{N\|\eta}\frac{\partial^2 Q_\alpha}{\partial \eta^2} + \widetilde{\dot{\omega}_\alpha\|\eta}$ |
| 21 % | $\cdot = \int_0^1 \widetilde{\cdot\|\eta} p(\eta) d\eta$ |

Table 6: Profiling of the CMC library

### 7.3.2 *Code profiling*

For the 3D version of the code, the numerical profiling of the CMC libraries, showed that a large amount of the computational load is required for the convolution operations, Eq.(116) and the conditional filtering procedures, Eq. (117). This means that the computation time required to obtain the conditionally filtered values $\widetilde{N|\eta}$, $\widetilde{u|\eta}$,$\widetilde{T|\eta}$ needed to close and integrate the CMC equations, plus the computational time required to provide the results of the CMC system integration to the LES system, are very close to the computational time required to numerically integrate the CMC equations.

The 60% of the computational time is spent by the CMC libraries, for the implicit numerical integration of the reactive and diffusive part of the CMC system, while the 6% is spent for the explicit convective term. The remaining 34% of the computational load is due to convolution operations (14%) and conditional filtering procedures (12%), as reported in tab. 6. The relative weight of the various phases of the computational integration of the CMC system integration, are weakly dependent on the chemical mechanism employed, since all the tasks get proportionally more CPU demanding when the number of species and equations rises.

The ratio between the computational time required to integrate in time over the same $\Delta t$ the LES and the CMC system varies with the number of species evolved. In the case of Hydrogen/Air, with

9 species and 19 reactions [66], the 70% of the computational time is required for the LES system, and the remaining 30% is for the CMC one. In the case of Methane/Air, with the gri2.11 mechanism , i.e. 49 species and 277 reactions [64], the overall computational time is approximately increased of a factor of six, while the CMC system and the LES require roughly the 50% of the computational time each. This is because the rise in the number of species, has a stronger impact on the CMC system, since the number of equations integrated in time rises. On the other hand, the computational load in the LES system is purely due to the equations of state, which become function of a larger number of variables.

For the 2D version of the code, the computational load is mostly due to the CMC system, this meaning that, for a given LES mesh, halving the space resolution of the CMC computational mesh, results in almost halving the computational time of the entire simulation.

### 7.3.3 *The operator splitting impact on the scalability performance*

The key features for a code to have a good scalability performance are well known. The first is to minimize the computational load due to message passing operations. The second is to balance the computational load on the employed cores, this to avoid a subset of cores waiting for other to accomplish their tasks.

In this particular case, the first issue has been addressed by means of a proper choice of the computational domain decomposition, and a proper use of the Message Passing Interface (MPI) libraries. The second issue requires more attention, since the computational load of each core depends on the number of operations to perform. In the case of a plane explicit time integration scheme, the computational load is a linear function of the number of mesh points per core, and rises with the rise of space and time accuracy of the scheme.

The CMC code implemented within this thesis relies on an operator splitting of the CMC equations, where the diffusive and source term are integrated in time implicitly by means of DVODE [63], a variable-coefficient, ordinary differential equation solver, as already introduced in sec. 6.2. Hence, the time integration is not performed in purely explicit way, and the number of time steps required for the implicit time integration are chosen by DVODE in order to comply with a prescribed solution accuracy. Hence, the smaller is the local characteristic time scale, the higher is the number of time iteration required by the implicit integrator. If some localized zones in the physical space are characterized by characteristic time scales which are smaller than in the rest of the field, e.g. in an autoignition region, the computational load required to integrate the problem in these regions would be higher than in the rest of the field, this resulting in a load unbalance among the cores. This is a potential cause of worse scalability performance of the code. However, it should be noted that, although the choice of a time explicit numerical time integrator for the whole system, would imply the use of the same time step over the whole computational field, the chosen time step would be the one able do integrate the fast chemical dynamic of the problem. So, even if this would avoid the load unbalance among the cores, it would also lead to a general worsening of the absolute performance of the code.

### 7.3.4 *Further developments*

The aim is to compute a Sandia D flame, some preliminary computations are already in progress as shown in fig. 78.

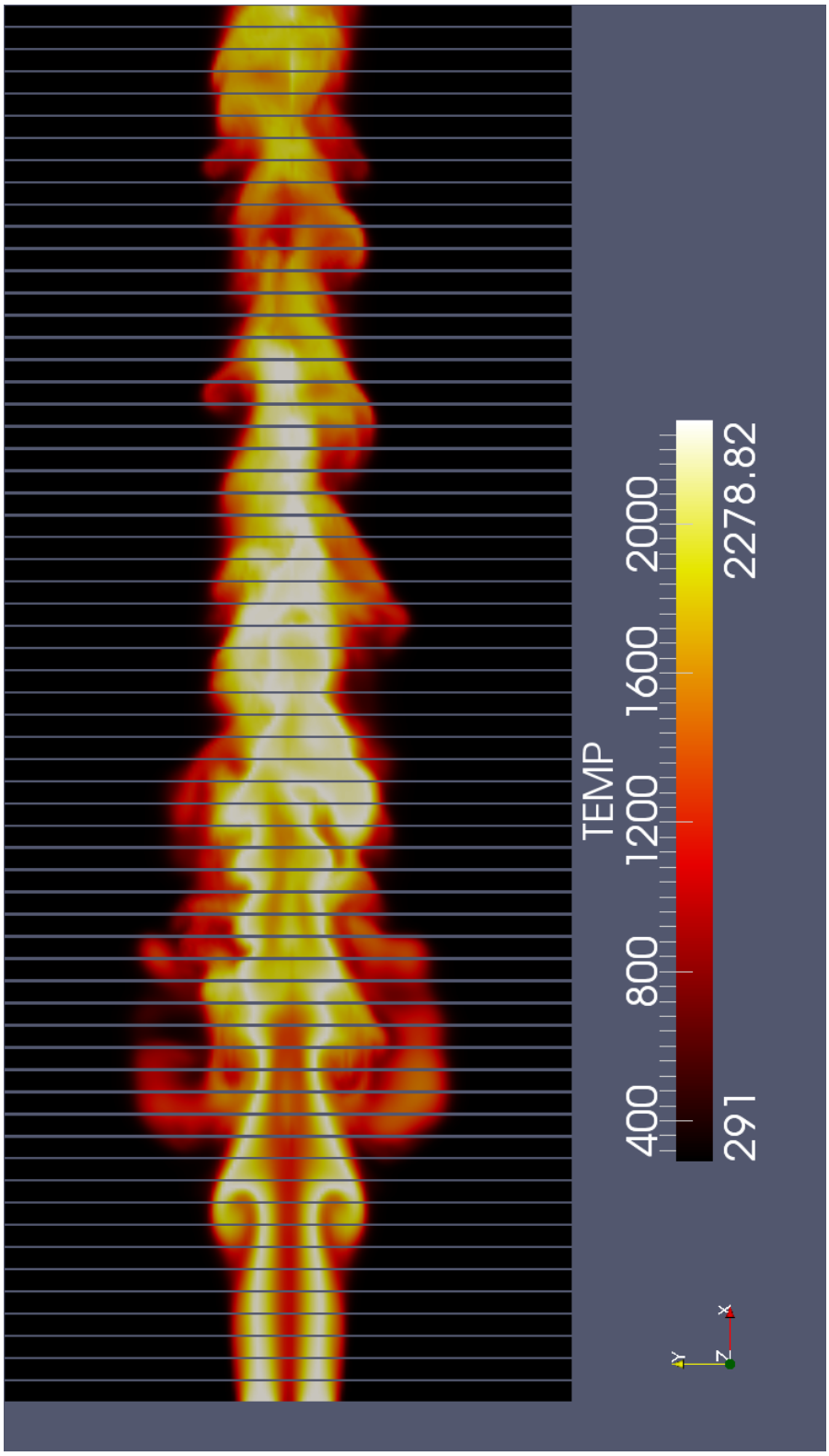


Figure 78: Sandia D flame, preliminar computation

# CONCLUSIONS

Two coupling strategies between the CMC combustion sub-grid model and the LES of compressible, turbulent, reactive flows has been presented. The two approaches are referred to as 'Vector Field Update' (VFU) and 'Energy Source Update' (ESU) respectively. Both VFU and ESU define the thermal and caloric equations of state of the LES. The VFU approach relies on an operator splitting approach, where, at each time iteration, the CMC equations evolution provides an update of the LES vector field in terms of density and sensible energy. The ESU approach is a closure method for which the CMC system provides a model of the energy source term of the LES energy equation, which would be otherwise unclosed.

The first step has been to assess the predictive capabilities of the CMC method by implementing a zero-dimensional stand alone code. The zero-dimensional CMC code has been written in Fortran in a CHEMKIN savvy fashion, and has been employed to inquire the steady state and transients behavior of Methane/Air flames.

The steady state solutions have been obtained for a number of imposed scalar dissipation values, the expected flame sensitivity to scalar dissipation has been recovered, and the typical S-shaped temperature dependence on the scalar dissipation has been recovered. Peak temperature has been found to be a decreasing function of the scalar dissipation up to a limit scalar dissipation value, over which quenching occurs. As expected, the NO production has been found to be an increasing function of temperature, and hence a decreasing function of the scalar dissipation.

The ignition transients test cases have been carried out for various initial temperature fields and scalar dissipation values, showing that the ignition time delay is a decreasing function of the initial temper-

ature and an increasing function of the scalar dissipation. Moreover, the influence on the ignition transient of the presumed scalar dissipation distribution over the mixture fraction space, as well as the impact on the steady state solution of the "constant specific heat" assumption, have been inquired and discussed.

Finally, the predictive capabilities of the zero-dimensional CMC code has been assessed by means of an 'a priori' prediction of the Sandia flame D, finding a satisfactory agreement between the zero-dimensional predictions and the experimental results.

The two LES/CMC coupling have been numerically implemented; in particular, the CMC library relies on a one-dimensional axial formulation, with the convective transport of the CMC equations being modeled only in the axial direction.

The two coupling strategies have been compared one to another with reference to a 2D Hydrogen/Air mixing layer test case, which has been chosen to be laminar so as to isolate the impact of the coupling strategies on the solution accuracy. The comparison between VFU and ESU highlighted a different sensitivity on the solution accuracy of the simplifying assumption employed for the CMC equations implementation.

In particular, the VFU solution is strongly influenced by the one-dimensional nature of the CMC implementation, since the VFU approach implies the direct update of the LES vector field with the solution of the CMC equations at each time step. On the other hand, the ESU solution is less affected by the one-dimensional nature of the CMC implementation, since its effects are confined to the energy source term estimation, while the LES multi-dimensionality is preserved.

An energy conserving 3D version of the LES/CMC code has been implemented, and fully parallelized by means of the MPI libraries. A preliminary consistency and test has been performed for the case of a 3D mixing layer, showing good weak and strong scalability performance up to thousands of cores.

# APPENDIX

# A

# APPENDIX

## A.1 PDF TRANSPORT EQUATION FOR TURBULENT FLOWS

The strongly non linear nature of the Navier-Stokes equations implies that a small difference in the initial conditions can result in a great difference in the space and time evolution of the solution, this is particularly evident for high Reynolds number when the transition from laminar to turbulent flow occurs. This lack of dependence on the initial conditions, results in the stochastic nature of the field, and in the possibility of a statistical approach in modeling turbulent phenomena. Since the field variables are continuous, the term "stochastic" is preferred to the more commonly used "random". In this appendix some useful statistical definitions are recalled and the pdf transport equation is derived.

### A.1.1 *Defining statistical properties*

For a given occurring event implies the evolution of the variable $Y$, calling $Z$ the sample space variable of $Y$, that is one of the possible values of $Y$, the probability of the variable $Y$ to be lower than the sample space variable value $Z$ is called **cumulative probability** $\mathcal{P}(Y < Z)$. The cumulative probability $\mathcal{P}(Y < Z)$ has the following characteristics:

$$\mathcal{P}(Y < Z) \quad : \begin{cases} \mathcal{P}(Y < Z_2) > \mathcal{P}(Y < Z_1) & \text{if} Z_2 > Z_1, \\ \mathcal{P}(Y < Z) \to 0 & \text{if } Z \to 0, \\ \mathcal{P}(Y < Z) \to 1 & \text{if } Z \to \infty. \end{cases} \tag{219}$$

The probability of having $Z_1 < Y < Z_2$ will be $\mathcal{P}(Z_1 < Y < Z_2) = \mathcal{P}(Y < Z_2) - \mathcal{P}(Y < Z_1)$. A **probablity density function** (pdf) can be defined as:

$$P(Z) \equiv \frac{\partial \mathcal{P}(Y < Z)}{\partial Z}. \tag{220}$$

If the derivative in Eq. (220) exists, the probability of $Z < Y < Z + \Delta Z$ will be $P(Z)\Delta Z$. Starting from its definition, the pdf will have the following main properties:

$$P(Z) \quad : \begin{cases} P(Z) \in (-\infty, +\infty) & \\ P(Z) \to 0 & \text{if } Z \to 0 \\ P(Z) \to 0 & \text{if } Z \to \pm\infty \end{cases} \tag{221}$$

For several realizations of the solution, a mean value $\langle Y \rangle$ of $Y$ can be defined as:

$$\langle Y \rangle = \int_0^1 Z d\mathcal{P}(Y < Z) = \int_{-\infty}^{+\infty} Z P(Z) dZ, \tag{222}$$

where the relation in Eq.(220) has been used. The same can be written for the expectation of a generic function of the stochastic variable $Y$, $F(Y)$:

$$\langle F(Y) \rangle = \int_0^1 F(Z) d\mathcal{P}(Y < Z) = \int_{-\infty}^{+\infty} F(Z) P(Z) dZ. \tag{223}$$

These expectations are usually named **ensemble averages**, since they are the mean values of $Y$ and $F(Y)$ over a wide number of identical realisations of the same experiment. In fluid-mechanics, the realisations are the solutions of the same problem, with identical macroscopic initial and boundary conditions, which lead to different solutions because of the non linear nature of the problem.

According to the the pdf definition in (Eq. 220), and once defined the **Heaviside function** $H(Z)$ as:

$$H(Z) = \begin{cases} 0 \text{ if } Z \leq 0, \\ 1 \text{ if } Z > 1, \end{cases} \tag{224}$$

the cumulative probability can be expressed in terms of expectations as follows:

$$\mathcal{P}(Y < Z) = \int_{-\infty}^{Z} P(Z_0)dZ_0 = \int_{-\infty}^{+\infty} H(Z - Z_0)P(Z_0)dZ_0 = \langle H(Z - Y)\rangle \tag{225}$$

Moreover, a pdf $P(Z)$ formulation can be deduced differentiating Eq. (225) with respect to $Z$, leading to:

$$P(Z) = \int_{-\infty}^{+\infty} \delta(Z - Z_0)P(Z_0)dZ_0 = \langle \delta(Z - Y)\rangle \tag{226}$$

The function $\delta(Z - Y)$ is the well known **Dirac delta function**[1]. It has introduced here as the Heaviside derivative $\delta = \partial H/\partial Z$, and is usually called **fine grained pdf**: $\psi = \delta(Y - Z)$. Since the Heaviside function is not continuous, its derivative does not exist as an ordinary derivative, but only as a generalized function. As generalized function, the Dirac delta function can be rigorously defined starting from its properties. If a class of "good" functions $F(Z)$ is defined as a function which is smooth enough and rapidly tending to zero as $Z \to \pm\infty$ [3], for one of this $F(Z)$, the Dirac function affects it such that:

$$\int_{-\infty}^{+\infty} \delta(Z)F(Z)dZ = F(0), \tag{227}$$

from which it is clear that the Dirac function is an even function: $\delta(Z) = \delta(-Z)$. Moreover, starting from the definition in Eq.(227), in the case of a delta function located al $Z = Z_0$, we have:

$$\langle F(Y)\rangle = \langle \int_{-\infty}^{+\infty} \delta(Y - Z)F(Z)dZ\rangle = \int_{-\infty}^{+\infty} F(Z)\langle \delta(Y - Z)\rangle dZ. \tag{228}$$

This equation underlines that the coarse grained pdf $P(Z)$ is the ensemble average of the fine grained pdf $\psi$, which is a Dirac delta function: $P(Z) = \langle \psi \rangle$.

1 The equation (226) should not be considered as a rigorous definition of the Dirac function, this because the function $P(Z)$ is not an arbitrary function and has been used to introduce the delta function, and $\mathcal{P}$ could be discontinuous, so that also its derivative $P$ could be a delta function.

The *single variable problem* shown before can be generalized for a *multi dimensional* problem with $n$ stochastic variable $Y_i$. The **cumulative probability function** $\mathcal{P}(\mathbf{Y} < \mathbf{Z})$ represents the probability that $Y_1 < Z_1, .., Y_n < Z_n$ are jointly valid:

$$\mathcal{P}(\mathbf{Y} < \mathbf{Z}) = \langle H(Z_1 - Y_1)H(Z_2 - Y_2)...H(Z_n - Y_n)\rangle. \tag{229}$$

From this last equations, it can be deduced that also the **fine-grained joint pdf** can be defined, similarly to the one dimensional case, as:

$$\psi \equiv \langle \delta(Z_1 - Y_1)\delta(Z_2 - Y_2)...\delta(Z_n - Y_n)\rangle. \tag{230}$$

So a **joint pdf** can be defined as a generalisation of the one in Eq.(220) before:

$$P(\mathbf{Z}) \equiv \frac{\partial^n \mathcal{P}(\mathbf{Y} < \mathbf{Z})}{\partial Z_1 \partial Z_2 ... \partial Z_n}. \tag{231}$$

It can be deduced that, similarly to the one-dimensional case for a small $\Delta Z$, the probability of $\mathbf{Y}$ being in $\Delta\mathbf{Z}$ is $P(\mathbf{Z})\Delta Z_1 \Delta Z_2 ... \Delta Z_n$. Analogously, the averaged value of a 'good' function of the vector $F(\mathbf{Y})$ can be written as:

$$\langle F(\mathbf{Y})\rangle = \int_\infty F(\mathbf{Z})P(\mathbf{Z})dZ_1 dZ_2 ... dZ_n \tag{232}$$

Moreover, the relation between the joint pdf and the fine grained pdf can be written as:

$$P(\mathbf{Z}) = \langle \psi \rangle \tag{233}$$

Note that the joint pdf $P(\mathbf{Z})$ can be written as the product of the pdfs $P(\mathbf{Z}) = P(Z_1)P(Z_2)...P(Z_n)$ only if $Y_i$ are statistically independent, that is if the statistical behaviour of $Y_i$ is not correlated to the statistical behaviour of the rest of the variable $Y_{j,i\neq j}$. Otherwise, if the statistical behaviour of two given events is correlated, say $\mathcal{A} = (Y_1 < Z_1)$ and $\mathcal{B} = (Y_2 < Z_2)$, according to the Bayes theorem, the cumulative probability of both events to occur is:

$$\mathcal{P}(\mathcal{A}, \mathcal{B}) = \mathcal{P}(\mathcal{A}|\mathcal{B})\mathcal{P}(\mathcal{B}), \tag{234}$$

which means that the probability of the events $\mathcal{A}$ and $\mathcal{B}$ to jointly occur, $\mathcal{P}(\mathcal{A},\mathcal{B})$, is the product of the probability of the event $\mathcal{A}$ to occur in the meanwhile the event $\mathcal{B}$ is occurring $\mathcal{P}(\mathcal{A}|\mathcal{B})$, multiplied by the probability of the event $\mathcal{B}$ to occur $\mathcal{P}(\mathcal{B})$ [2]. Where $\mathcal{P}(\mathcal{A}|\mathcal{B})$ is the **conditional pdf** of the event $\mathcal{A}$ to the event $\mathcal{B}$. In terms of conditional pdfs, for a two-variables problem, we have:

$$P(\mathbf{Z}) = P(Z_1|Y_2 = Z_2)P(Z_2). \tag{235}$$

So that, inverting the previous relations:

$$\langle Y_1|Y_2 = Z_2\rangle = \int_{-\infty}^{+\infty} Z_1 P(Z_1|Y_2 = Z_2)dZ_1 = \frac{\int_{-\infty}^{+\infty} Z_1 P(Z_1, Z_2)dZ_1}{P(Z_2)}. \tag{236}$$

While the unconditional mean value is given by:

$$\langle Y_1\rangle = \int_{-\infty}^{+\infty} \langle Y_1|Y_2 = Z_2\rangle P(Z_2)dZ_2. \tag{237}$$

In the following some properties of the, previously defined, pdf and joint pdfs will be reported [3]; these will be useful for the derivation of the pdf transport equations that will be derived later. The **first property** is the following: *If the generic deterministic function $F(Y_2)$ doesn't depend on $Y_1$, the ensemble average of the product $Y_1F(Y_2)$ is given by*:

$$\langle Y_1F(Y_2)|Y_2 = Z_2\rangle = \langle Y_1|Y_2 = Z_2\rangle F(Y_2) \tag{238}$$

If $Y_1 = F(Y_2)$, where it is important to stress the fact that $F$ is a deterministic function (of random variable), we have that $\langle F(Y_2|Y_2 = Z(2)\rangle = F(Z_2)$. It can be proved that this **second property** is true[3]:

$$\langle Y_1|Y_2 = Z_2\rangle P(Z_2) = \langle Y_1\delta(Z_2 - Y_2)\rangle. \tag{241}$$

2 In the case of the two events are not correlated, $\mathcal{P}(\mathcal{A}|\mathcal{B}) = \mathcal{P}(\mathcal{A})$, this meaning that the occurrence of $\mathcal{B}$ does not affect the probability of $\mathcal{A}$ to occur, hence $\mathcal{P}(\mathcal{A},\mathcal{B}) = \mathcal{P}(\mathcal{A})\mathcal{P}(\mathcal{B})$.

3 This can be proved, multiplying this identity for a good function $F(Z_2)$ and integrating it over $Z_2$:

$$\int_{-\infty}^{+\infty} F(Z_2)\langle Y_1|Z_2\rangle P(Z_2)dZ_2 = \int_{-\infty}^{+\infty} \langle F(Z_2)Y_1|Z_2\rangle P(Z_2)dZ_2 = \langle Y_1F(Y_2)\rangle, \tag{239}$$

Note that for $Y_1 = 1$ we get the relation between fine and coarse grained pdf. The Eq.(241) can be generalized for multiple conditions:

$$\langle Y_0 | \mathbf{Y} = \mathbf{Z} \rangle P(\mathbf{Z}) = \langle Y_0 \psi \rangle. \tag{242}$$

### A.1.2 *Differentiating statistical properties*

Another necessary element to the purpose of deriving the pdf transport equations is to introduce the **generalized derivatives**. As known, regular functions, say $F(Z)$ and $f(Z)$ can be integrated by parts:

$$\int_{-\infty}^{+\infty} F(Z) f'(Z) dZ = (Ff)_{-\infty}^{\infty} - \int_{-\infty}^{+\infty} F'(Z) f(Z) dZ = -\int_{-\infty}^{+\infty} F'(Z) f(Z) dZ \tag{243}$$

This is true only if $F$ is a good function in the sense defined before. For the generalised function, the generalized derivatives are defined on the basis of their properties. Hence the generalized derivatives are defined as those operations that satisfy the integrations by part in Eq.(243). Now, if we suppose $f$ to be the Heaviside function $f(z) = H(Z)$ we have that the Eq.(243) takes the form:

$$\begin{aligned} \int_{-\infty}^{+\infty} F(Z) H'(Z) dZ = -\int_{-\infty}^{+\infty} F'(Z) H(Z) dZ = \\ -\int_{0}^{+\infty} F'(Z) dZ = -F(Z)_0^{+\infty} = F(0), \end{aligned} \tag{244}$$

which is the definition of the Dirac function, and proves that: $\delta(Z) = H'(Z)$. In the same way we can define $\delta'(Z)$ and the **n-th generalised derivatives**:

$$\int_{-\infty}^{+\infty} F(Z) \delta'(Z) dZ = -\int_{-\infty}^{+\infty} F'(Z) \delta(Z) dZ = -F'(0) \tag{245}$$

---

$$\begin{aligned} \int_{-\infty}^{+\infty} F(Z_2) \langle Y_1 \delta(Z_2 - Y_2) \rangle dZ_2 = \\ \langle Y_1 \int_{-\infty}^{+\infty} F(Z_2) \delta(Y_2 - Z_2) P(Z_2) dZ_2 \rangle = \langle Y_1 F(Y_2) \rangle. \end{aligned} \tag{240}$$

This is true for any $F(Z)$, so the relation is proved.

$$\int_{-\infty}^{+\infty} F(Z)\delta^{(n)}(Z)dZ = -\int_{-\infty}^{+\infty} F^{(n)}(Z)\delta(Z)dZ = (-1)^{(n)}F^{(n)}(0) \tag{246}$$

It should be stressed that $f$ is a generalized function, so the Eqns. (244-246) are the definition of a generalized derivative, and not mere integrations by part.

Three more identities involving generalized **time derivatives** including the fine grained pds are introduced in the following. The **first identity** shown here is about the time differentiation of the fine grained pdf:

$$\frac{d}{dt}\delta(Z - Y(t)) = -\frac{\partial}{\partial Z}\left(\frac{dY}{dt}\delta(Z - Y(t))\right) \tag{247}$$

This can be proved, as usually, multiplying both sides by a good function $F(Z)$ and then verifying that the integrals on $Z$ of the two products are the same. In the same way, it can be proved the **second identity**, which is the equivalent relation for the multiple variable problem:

$$\frac{d\psi}{dt} = -\frac{\partial}{\partial Z_i}\left(\frac{dY_i}{dt}\psi\right) \tag{248}$$

Note that to prove this relation the good function will be $F(\mathbf{Z})$ and the integral will be over $\mathbf{Z}$. Moreover, if $Y_i$ depends also on space ($\mathbf{x} = x_1, x_2, x_3$) the ordinary derivative will become $\frac{dY_i}{dt} = \frac{\partial Y_i}{\partial t}$.
The **third identity** is about the differentiation of the product $f_s\psi$, where $f_s = f_s(t)$ is a smooth function, while $\psi$ is the well known fine grained pdf.

$$\frac{d\psi f_s}{dt} = f_s\frac{d\psi}{dt} + \psi\frac{df_s}{dt} \tag{249}$$

Even if this results looks like an ordinary derivative, it needs to be tested as usually, multiplying the LHS and the RHS by $F(\mathbf{Z})$ and verifying that the integrals over $\mathbf{Z}$ are the same [3].

Let now consider some space derivatives of the fine-grained pdf. Assuming that variables $Y_i$ are space dependent on $\mathbf{x} = (x_1, x_2, x_3)$, the **gradient operator** on $\psi$ reads:

$$\nabla\psi = -\frac{\partial}{\partial Z_i}(\psi\nabla Y_i) \tag{250}$$

To check this it's sufficient to treat $\partial/\partial x_i$ analogously to what is done for $\partial/\partial t$ in Eq. (248). For the higher order derivatives it is sufficient to use the relation in Eq.(249), $\nabla\cdot(\mathbf{f_s}\psi) = \psi div(\mathbf{f}_s) + \mathbf{f_s}\nabla(\psi)$. So, using the Eq.(250) twice and noting that $\nabla Y_i$ doesn't depend on $\mathbf{Z}$, we have that the **Laplacian operator** reads:

$$\begin{aligned}\nabla^2\psi = -\nabla\cdot\left(\frac{\partial\psi\nabla Y_i}{\partial Z_i}\right) &= -\frac{\partial\psi\nabla^2 Y_i}{\partial Z_i} - \frac{\partial\nabla\psi\nabla Y_i}{\partial Z_i} = \\ &= -\frac{\partial\psi\nabla^2 Y_i}{\partial Z_i} + \frac{\partial^2\psi(\nabla Y_i\nabla Y_i)}{\partial Z_i\partial Z_j}\end{aligned} \tag{251}$$

Always with the aim of deducing the pdf transport equation, it is useful the following identity, which includes the diffusive coefficient $\rho D$ (supposing that all scalars have similar diffusivities). The values of $\rho$ and $D$ do not depend on $\mathbf{Z}$, and after some manipulation we have [4] the following **divergence relations**:

$$\begin{aligned}\nabla\cdot(\rho D\nabla\psi) &= -\frac{\partial}{\partial Z_i}(\nabla\cdot(\psi\rho D\nabla Y_i)) = \\ &= -\frac{\partial}{\partial Z_i}(\psi\nabla\cdot(\rho D\nabla Y_i)) + \frac{\partial^2}{\partial Z_i\partial Z_j}(\psi\rho D(\nabla Y_i\nabla Y_i)).\end{aligned} \tag{252}$$

If $\rho$ and $D$ are not constant, the left hand side of the Eq.(252), could be rewritten as:

$$\nabla\cdot(\rho D\nabla\psi) = \nabla\cdot(\nabla(\rho D\psi)) - \nabla\cdot(\psi\nabla(\rho D)). \tag{253}$$

Similarly, if we apply the divergence operator to the term $\psi\rho D\nabla Y_i$, we obtain the useful relation:

$$\nabla\cdot(\psi\rho D\nabla Y_i) = \psi\nabla\cdot(\rho D\nabla Y_i) - \frac{\partial}{\partial Z_j}(\psi\rho D(\nabla Y_i\nabla Y_j)). \tag{254}$$

4 The Eq.(252) is a mere identity and do not involve any modeling of the properties of turbulent scalar transport [3]

The best way to get the **differentiation rules for a coarse grained pdf** if to average the fine grained ones. In this way, averaging the Eq.(248), we have:

$$\frac{\partial P(\mathbf{Z})}{\partial t} = -\frac{\partial}{\partial Z_i}\left(\langle \frac{\partial Y_i}{\partial t} | \mathbf{Y} = \mathbf{Z}\rangle P(\mathbf{Z})\right) \tag{255}$$

Combining Eqns.(252,253) and averaging yields to useful result:

$$\begin{aligned} &\nabla \cdot (\langle \rho D \nabla \psi \rangle) = \\ &\quad \nabla^2(\langle \rho D | \mathbf{Y} = \mathbf{Z}\rangle P) - \nabla \cdot (\langle \nabla(\rho D) | \mathbf{Y} = \mathbf{Z}\rangle) = \\ &\quad = -\frac{\partial}{\partial Z_i}(\langle \nabla \cdot (\rho D \nabla Y_i) | \mathbf{Y} = \mathbf{Z}\rangle P) - \\ &\quad - \frac{\partial^2}{\partial Z_i \partial Z_j}(\langle \rho D (\nabla Y_i \nabla Y_i) | \mathbf{Y} = \mathbf{Z}\rangle P), \end{aligned} \tag{256}$$

while averaging Eq.(257) yields:

$$\begin{aligned} &\nabla \cdot (\langle \rho D \nabla Y_i | \mathbf{Y} = \mathbf{Z}\rangle P) = \\ &\quad = (\langle \nabla \cdot (\rho D \nabla Y_i) | \mathbf{Y} = \mathbf{Z}\rangle P) - \frac{\partial}{\partial Z_j}(\langle \psi \rho D (\nabla Y_i \nabla Y_j) | \mathbf{Y} = \mathbf{Z}\rangle P). \end{aligned} \tag{257}$$

All the introduced relations for the joint pdf have been obtained by averaging the relations obtained for the fine grained pdf, so coherently to what said before, these equations are only identities and they are not derived from a transport equation. The utility of these relations will be shown later in the derivation of the pdf transport equation.

This last set of relations, which involve **differentiating conditional expectations**, will be useful in the derivation of the evolution equation of the conditional pdf. As known, for a given random variable $Y$, conventional average and differentiation commute $\langle \partial Y/\partial t \rangle = \partial \langle Y \rangle / \partial t$ since $Y$ does not depend on $t$. Note that it is possible that $\partial \langle Y \rangle / \partial t$ exists while $\partial Y/\partial t$ does not. A conditional expectation depends also on the conditional pdf, this may depend on time, so conditional average and differentiation can not commute. Anyway the product can be differentiated:

$$\frac{\partial}{\partial t}(Y_1 \delta(Z_2 - Y_2)) = \frac{\partial Y_1}{\partial t}\delta(Z_2 - Y_2) - \frac{\partial}{\partial Z_2}\left(Y_1 \frac{\partial Y_2}{\partial t}\delta(Z_2 - Y_2)\right) \tag{258}$$

Once averaged we have:

$$\frac{\partial\langle Y_1|Y_2=Z_2\rangle}{\partial t}P(Z_2)+\langle Y_1|Y_2=Z_2\rangle\frac{\partial P(Z_2)}{\partial t}= \tag{259}$$
$$=\langle\frac{\partial Y_1}{\partial t}|Y_2=Z_2\rangle P(Z_2)-$$
$$-\frac{\partial}{\partial Z_2}\left(\langle Y_1\frac{\partial Y_2}{\partial t}|Y_2=Z_2\rangle P(Z_2)\right)$$

Note that this equation can be easily generalized to more than two dimensions. If $Y_2$ does not depend on $t$ the equation takes the form:

$$\frac{\partial\langle Y_1|Y_2=Z_2\rangle}{\partial t}=\langle\frac{\partial Y_1}{\partial t}|Y_2=Z_2\rangle \tag{260}$$

while for $Y_1=1$ we get Eq.(258).

### A.1.3 *The pdf evolution equations*

We need now to derive the *j*oint pdf equations for a set of scalar fields $Y_i$ whose evolution equations are:

$$\rho\frac{\partial Y_i}{\partial t}+\rho\mathbf{u}\cdot\nabla Y_i-\nabla\cdot(\rho D_i\nabla Y_i)=W_i\quad i=1,...,n \tag{261}$$

This the first time a physical assumption has been introduced, i.e. a Fickian diffusion for the species. The next steps will consist in combining the previously introduced relations, with the species evolution equations and continuity equation, hence each assumption made on the formulation of these physical evolution equations, will affect the derived pdfs transport equations. The first step is deriving an **evolution equation for the fine grained pdf** $\psi$. This is done by combining the species evolution equation (261) and the definition of $\frac{\partial\psi}{\partial t}$ in Eq.(248), and of the gradient $\nabla\psi$ in Eq. (250), and reads:

$$\frac{\partial\psi}{\partial t}=\frac{\partial}{\partial Z_i}(\mathbf{u}\cdot\nabla Y_i-\nabla\cdot(\rho D_i\nabla Y_i)-W_i). \tag{262}$$

If the previous equation is multiplied by the velocity $\mathbf{u}$, the first term on the rhs of the previous equation can be combined with the relation $\mathbf{u}\cdot\nabla\psi=-\frac{\partial\psi(\mathbf{u}\cdot\nabla Y_i)}{\partial Z_i}$. Knowing that the velocity field is independent of the sample space variable $Z_i$, we obtain:

$$\rho\frac{\partial\psi}{\partial t}+\rho\mathbf{u}\cdot\nabla\psi-\frac{\partial}{\partial Z_i}(\nabla\cdot(\rho D_i\nabla Y_i))=-\frac{\partial}{\partial Z_i}(\rho\psi W_i) \tag{263}$$

Just like velocity $\mathbf{u}$, the density $\rho$ is independent of the sample space variable $Z_i$. However $\rho$ is a stochastic function of $t$ and $\mathbf{x}$ and can be stochastically dependent on $Y_i$. A divergence form of the transport equation (263) can be obtained by adding to it the mass transport equation multiplied by the fine-grained pdf $\psi$:

$$\psi\left(\frac{\partial\rho}{\partial t}+\nabla\cdot(\rho\mathbf{u})\right)=0 \tag{264}$$

so as to obtain a conservative form of the evolution equation of the fine grained pdf $\psi$. It incorporates the evolution equation of a scalar $Y_i$ in a turbulent flow, which reads:

$$\frac{\partial\rho\psi}{\partial t}+\nabla(\rho\mathbf{u}\psi)-\frac{\partial}{\partial Z_i}(\nabla\cdot(\rho D_i\nabla Y_i))=-\frac{\partial}{\partial Z_i}(\rho\psi W_i) \tag{265}$$

Here a second assumption can be made, that is all diffusivities are equal $D_i = D$. This allows to use the divergence relation in Eq.(256), the Eq. (265), leading to the pdf transport equation under assumption of Fickian diffusion and equal diffusivities:

$$\begin{aligned}&\frac{\partial\rho\psi}{\partial t}+\nabla(\rho\mathbf{u}\psi)-\nabla\cdot(\rho D\nabla\psi)+ \\ &\quad+\frac{\partial^2}{\partial Z_i\partial Z_i}(\psi\rho D(\nabla Y_i\nabla Y_i))=-\frac{\partial}{\partial Z_i}(\rho\psi W_i)\end{aligned} \tag{266}$$

This equation in the case of $\psi_\eta(\eta = Z_1, \xi = Y_1, W_1 = 0, n = 1)$, yields to:

$$\frac{\partial\rho\psi_\eta}{\partial t}+\nabla\cdot(\rho\mathbf{u}\psi_\eta)=-\frac{\partial^2}{\partial\eta^2}(\rho N\psi_\eta)-\frac{\partial}{\partial\eta}\nabla\cdot(\rho\psi_\eta D_\xi\nabla\xi) \tag{267}$$

If, for the sake of complicity, $\psi \equiv \psi_\eta$ [34], Eq.(267) is identical to Eq. (88), one of the two starting points in sec. 4.2.1. The Eq.(89) in sec. 4.2.1, can be obtained by multiplying by $Y$ Eq. (266), multiplying the species transport equation in Eq. (261) by $\psi_\eta$, and summing these two together, to obtain:

$$\begin{aligned}&\frac{\partial}{\partial t}(\rho Y\psi_\eta)+\nabla\cdot(\rho\mathbf{u}Y\psi_\eta)=\psi W_Y+ \\ &\qquad-\nabla\cdot(\rho D\nabla(Y\psi_\eta))+2\frac{\partial}{\partial\eta}(\psi_\eta\rho D\nabla\xi\nabla Y)-\frac{\partial^2}{\partial\eta^2}(\rho D(\nabla\xi)^2Y\psi_\eta),\end{aligned} \tag{268}$$

In the case of having $\Phi = Y$, is identical to Eq. (90), which is the second starting point of sec. 4.2.1.

## A.2 NON-DIMENSIONAL LES EQUATIONS

For a given dimensional quantity $\phi$ one can alway chose a reference value $\phi^*$ in order to define a non-dimensional quantity $\overline{\phi}$ to have $\phi = \phi^*\overline{\phi}$. So we have:

$$\rho = \overline{\rho}\rho^* \tag{269}$$

$$p = \overline{p}p^* \tag{270}$$

$$u_i = \overline{u_i}u_i^* \tag{271}$$

$$T = \overline{T}T^* \tag{272}$$

$$\mu = \overline{\mu}\mu^* \tag{273}$$

$$k = \overline{k}k^* \tag{274}$$

$$D_\xi = \overline{D_\xi}D_\xi^* \tag{275}$$

$$\mathcal{S} = \overline{\mathcal{S}}\mathcal{S}^* \tag{276}$$

Then some additional reference quality such as time $t^*$, total sensible energy $E^*$, Temperature $T^*$ and speed of sound $a^*$, can be derived from the previous as follows:

$$t^* = \frac{L^*}{u*} \tag{277}$$

$$E^* = \rho^* {u^*}^2 \tag{278}$$

$$T^* = \frac{^L*}{\rho^* R} \tag{279}$$

$$a^* = \sqrt{\gamma P^*/\rho^*} \tag{280}$$

$$D_\xi = \frac{\mu^*}{\rho^*}\frac{1}{Sc} \tag{281}$$

So the Eqns. (162-163) can be rewritten in a non-dimensional form, taking advantage of the Eqns.(269- 281), as follows:

$$\frac{\rho^* {u^*}^2}{L^*}\frac{\partial \overline{\rho u_i}}{\partial t} + \frac{\rho^* {u^*}^2}{L^*}\frac{\partial \overline{\rho}\ \overline{u}_i\overline{u}_j}{\partial x_j} + \frac{p^*}{L^*}\frac{\partial \overline{p}}{\partial x_i} - \frac{\mu^* u^*}{L^*}\frac{\partial \overline{\sigma}_{ij}}{\partial x_j} = 0 \tag{282}$$

$$\frac{\rho^* u^{*3}}{L^*}\frac{\partial \overline{E}}{\partial t} + \frac{\rho^* u^{*3}}{L^*}\frac{\partial (\overline{E}+\overline{p})\overline{u}_j}{\partial x_j} - \frac{\mu^* u^{*2}}{L^{*2}}\frac{\partial \overline{\sigma}_{ij}\overline{u}_i}{\partial x_j} - \frac{k^* T^*}{L^{*2}}\frac{\partial}{\partial x_i}\overline{k}\frac{\partial \overline{T}}{\partial x_i} = \frac{\rho^* u^{*3}}{L^*}\overline{\mathcal{S}} \tag{283}$$

So dividing Eq. (282) by the term $\rho^* {u^*}^2 / L^*$ we have:

$$\frac{\partial \overline{\rho}\,\overline{u_i}}{\partial t} + \frac{\partial \overline{\rho}\;\overline{u}_i\overline{u}_j}{\partial x_j} + \frac{p^*}{\rho^* {u^*}^2}\frac{\partial \overline{p}}{\partial x_i} - \frac{\mu^*}{L^*\rho^* u^*}\frac{\partial \overline{\sigma}_{ij}}{\partial x_j} = 0 \tag{284}$$

The choice of having a unity non-dimensional term multiplying the pressure gradient, leads to the following relation:

$$\frac{p^*}{\rho^* {u^*}^2} = 1 \tag{285}$$

Although the previous relation is satisfied in both the cases of $p^* = \rho^* {u^*}^2$ and $u^* = \sqrt{p^*/\rho^*}$, the latter is preferable in order to ensure the relation $p^* = \rho^* R T^*$. Hence a reference value of the sound speed can be defined as $a^* = \sqrt{\gamma P^*/\rho^*}$. Using these relations the term $\mu^*/\rho^* u^*$ multiplying the last term of the (292) becomes:

$$\frac{\mu^*}{L^*\rho^* u^*} = \frac{\mu^*}{L^*\rho^*\sqrt{\frac{p^*}{\rho^*}}} \tag{286}$$

Using the subscript *in* to indicate the values of the variables at the inlet of the domain of interest, some reference values can be defined as follows:

$$p^* = p_{in} \tag{287}$$

$$T^* = T_{in} \tag{288}$$

$$\mu^* = \mu_{in} \tag{289}$$

$$L^* = L_{in} \tag{290}$$

Where $L_{in}$ is a characteristic length of the problem, such as the diameter in the case of a free jet or pipe flows. Hence the term in Eq. (286) cab rewritten in terms of the Reynolds number $Re = \rho_{in} u_{in} L_{in} / \mu_{in}$

$$\frac{\mu^*}{L^* \rho^* u^*} = \frac{\mu^*}{L^* \rho^* \sqrt{\frac{p^*}{\rho^*}}} \frac{u_{in}}{u_{in}} = \frac{1}{Re} \sqrt{\gamma} M_{in} \tag{291}$$

Where $M_{in} = u_{in}/a^*$ is the inlet of the problem. So the Eq.(292) becomes:

$$\frac{\partial \overline{\rho u_i}}{\partial t} + \frac{\partial \overline{\rho}\ \overline{u}_i \overline{u}_j}{\partial x_j} + \frac{\partial \overline{p}}{\partial x_i} - \frac{1}{Re} \sqrt{\gamma} M_{in} \frac{\partial \overline{\sigma}_{ij}}{\partial x_j} = 0 \tag{292}$$

The same can be done on the Energy equation (283) by dividing it by the term $\rho^* u^{*3} / L^*$, this leading to:

$$\frac{\partial \overline{E}}{\partial t} + \frac{\partial (\overline{E} + \overline{p}) \overline{u}_j}{\partial x_j} - \frac{L^*}{\rho^* u^{*3}} \frac{\mu^* u^{*2}}{L^{*2}} \frac{\partial \overline{\sigma}_{ij} \overline{u}_i}{\partial x_j} - \frac{L^*}{\rho^* u^{*3}} \frac{k^* T^*}{L^{*2}} \frac{\partial}{\partial x_i} \overline{k} \frac{\partial \overline{T}}{\partial x_i} = \overline{\mathcal{S}} \tag{293}$$

Where multiplying factor of the third and fourth terms become respectively:

$$\frac{L^*}{\rho^* u^{*3}} \frac{\mu^* u^{*2}}{L^{*2}} = \frac{\mu^*}{L^* \rho^* u^*} = \frac{\mu_{in}}{L_{in} \rho_{in}} \frac{u_{in}}{u_{in}} \frac{1}{\sqrt{\frac{p^*}{\rho^*}}} = \frac{1}{Re} \sqrt{\gamma} M_{jet} \tag{294}$$

$$\begin{aligned} &\frac{L^*}{\rho^* u^{*3}} \frac{k^* T^*}{L^{*2}} = \frac{k^* T^*}{L^* \rho^* u^{*3}} = \frac{\mu^* C_p^*}{Pr} \frac{T^*}{L^* \rho^* u^{*3}} \frac{u_{in}}{u_{in}} = \\ &= \frac{1}{RePr} C_p \frac{T^*}{\frac{p^*}{\rho^*}} \frac{u_{in}}{\sqrt{\frac{p^*}{\rho^*}}} = \frac{M_{in}}{RePr} \sqrt{\gamma} \frac{C_p}{R} = \\ &= \frac{M_{in}}{RePr} \sqrt{\gamma} \frac{\gamma}{\gamma - 1} \end{aligned} \tag{295}$$

so we have:

$$\frac{\partial \overline{E}}{\partial t} + \frac{\partial (\overline{E} + \overline{p}) \overline{u}_j}{\partial x_j} - \frac{1}{Re} \sqrt{\gamma} M_{jet} \frac{\partial \overline{\sigma}_{ij} \overline{u}_i}{\partial x_j} - \frac{M_{in}}{RePr} \frac{\gamma \sqrt{\gamma}}{\gamma - 1} \frac{\partial}{\partial x_i} \overline{k} \frac{\partial \overline{T}}{\partial x_i} = \overline{\mathcal{S}} \tag{296}$$

The final set of non-dimesional equations is the following:

$$\frac{\partial \overline{\rho}}{\partial t} + \frac{\partial \overline{\rho}\ \overline{u}_i}{\partial x_i} = 0 \tag{297}$$

$$\frac{\partial \overline{\rho}\ \overline{u}_i}{\partial t} + \frac{\partial \overline{\rho}\ \overline{u}_i \overline{u}_j}{\partial x_j} + \frac{\partial \overline{p}}{\partial x_i} - \frac{1}{Re}\sqrt{\gamma} M_{in} \frac{\partial \overline{\sigma}_{ij}}{\partial x_j} = 0 \tag{298}$$

$$\frac{\partial \overline{E}}{\partial t} + \frac{\partial (\overline{E} + \overline{p})\overline{u}_j}{\partial x_j} - \frac{1}{Re}\sqrt{\gamma} M_{jet} \frac{\partial \overline{\sigma}_{ij}\overline{u}_i}{\partial x_j} - \frac{M_{in}}{RePr}\frac{\gamma\sqrt{\gamma}}{\gamma - 1}\frac{\partial}{\partial x_i}\overline{k}\frac{\partial \overline{T}}{\partial x_i} = \overline{\mathcal{S}} \tag{299}$$

$$\frac{\partial \overline{\xi}}{\partial t} + \frac{\partial \overline{\xi}\overline{u}_j}{\partial x_j} - \frac{M_{in}\sqrt{\gamma}}{ReSc}\frac{\partial}{\partial x_i}\overline{\nu}\frac{\partial \overline{\xi}}{\partial x_i} = 0 \tag{300}$$

$$\overline{p} = \overline{\rho}\overline{T}\overline{R} \tag{301}$$

The non-dimensional mixture fraction equation (300) derivation is analogous to the others and has been carried out under the hypothesis of having $D_\xi = \frac{\mu^*}{\rho^*}\frac{1}{Sc}$.

# BIBLIOGRAPHY


[1] N. Peters, *Turbulent Combustion*. Cambridge Monographs on Mechanics, Cambridge University Press, 2000.

[2] M. Valorani, E. Martelli, G. Gargiulo, and P. P. Ciottoli, "CFD Analysis of Laser-Pulse Ignition of GCH4 / GO2 in M3-DLR Test Bench,"

[3] A.Y. Klimenko and R. Bilger, "Conditional moment closure for turbulent combustion," *Progress in Energy and Combustion Science*, vol. 25, pp. 595–687, Dec. 1999.

[4] J. F. R.S. Barlow *Proc. Combust. Inst.*, no. 27, p. 1087–1095, 1998.

[5] N. Peters, "LAminar Flamelet Concepts in Turbulent Combustion," pp. 1231–1250, 1986.

[6] S. Pope, "The PDF Method for turbulent combustion," *CFD Symposium on Aeropropulsion, NASA Lewis, April 1990 (invited talk)*, 1990.

[7] A. Y. Klimenko, "Multicomponent Diffusion of Various Admixtures in Turbulent Flow," no. 3, pp. 3–10, 1990.

[8] R. Bilger, "Conditional moment closure for turbulent reacting flow," *Physics of Fluids*, vol. 5, no. A, pp. 436–444, 1993.

[9] D. Veynante and L. Vervisch, "Turbulent combustion modeling," *Progress in Energy and Combustion Science*, vol. 28, pp. 193–266, Mar. 2002.

[10] H. Pitsch, M. Chen, and N. Peters, "Unsteady Flamelets Modeling of Turbulent Hydrogen-Air Diffusion Flame," pp. 1057–1064, 1998.

[11] H. Pitsch, "Unsteady flamelet modeling of differential diffusion in turbulent jet diffusion flames," *Combustion and Flame*, vol. 123, pp. 358–374, Nov. 2000.

[12] S. B. Pope, "Turbulent premixed Flames," *Annual Review of Fluid Mechanics*, no. Moss 1980, pp. 237–70, 1987.

[13] S. Pope, "PDF Methods for turbulent reactive flows," *Progress in Energy and Combustion Science*, pp. 119–192, 1985.

[14] B. Yang and S. Pope, "An investigation of the accuracy of manifold methods and splitting schemes in the computational implementation of combustion chemistry," *Combustion and Flame*, vol. 112, pp. 16–32, Jan. 1998.

[15] W. K. Bushe, "LES of non-premixed turbulent reacting flows with Conditional Source term Estimation," *Center for Turbulence Research Annual Research Briefs 1998*, 1998.

[16] W. K. Bushe and H. Steiner, "Conditional moment closure for large eddy simulation of nonpremixed turbulent reacting flows," *Physics of Fluids*, vol. 11, no. 7, p. 1896, 1999.

[17] B. Jin, R. Grout, and W. K. Bushe, "Conditional Source-Term Estimation as a Method for Chemical Closure in Premixed Turbulent Reacting Flow," *Flow, Turbulence and Combustion*, vol. 81, pp. 563–582, Apr. 2008.

[18] W. E. Mell, V. Nilsen, G. KosaÃÅly, and J. J. Riley, "Investigation of closure models for nonpremixed turbulent reacting flows," *Physics of Fluids*, vol. 6, p. 1331, Mar. 1994.

[19] E. Mastorakos and R. W. Bilger, "Second-order conditional moment closure for the autoignition of turbulent flows," *Physics of Fluids*, vol. 10, no. 6, p. 1246, 1998.

[20] N. Swaminathan and B. B. Dally, "Cross stream dependence of conditional averages in elliptic region of flows behind a bluff-

body of flows behind a bluff-body," *Physics of fluids*, vol. 10, no. 9, pp. 2424–2426, 1998.

[21] S. H. Kim, K. Y. Huh, and L. Tao, "Application of the elliptic conditional moment closure model to a two-dimensional nonpremixed methanol bluff-body flame," *Combustion and Flame*, vol. 120, pp. 75–90, Jan. 2000.

[22] M. Roomina, "Conditional moment closure (CMC) predictions of a turbulent methane-air jet flame," *Combustion and Flame*, vol. 125, pp. 1176–1195, May 2001.

[23] M. Fairweather and R. Woolley, "First-order conditional moment closure modeling of turbulent, nonpremixed hydrogen flames," *Combustion and Flame*, vol. 133, pp. 393–405, June 2003.

[24] C. B. Devaud and K. N. C. Bray, "Assessment of the applicability of conditional moment closure to a lifted turbulent flame : first order model," vol. 132, pp. 102–114, 2003.

[25] Y. Wright, G. Depaola, K. Boulouchos, and E. Mastorakos, "Simulations of spray autoignition and flame establishment with two-dimensional CMC," *Combustion and Flame*, vol. 143, pp. 402–419, Dec. 2005.

[26] I. Kim and E. Mastorakos, "Simulations of turbulent lifted jet flames with two-dimensional conditional moment closure," *Proceedings of the Combustion Institute*, vol. 30, pp. 911–918, Jan. 2005.

[27] I. S. Kim and E. Mastorakos, "Simulations of Turbulent Non-Premixed Counterflow Flames with First-Order Conditional Moment Closure," *Flow, Turbulence and Combustion formerly: Applied Scientific Research*, vol. 76, pp. 133–162, Apr. 2006.

[28] M. Fairweather and R. Woolley, "Conditional moment closure calculations of a swirl-stabilized, turbulent nonpremixed methane flame," *Combustion and Flame*, vol. 151, pp. 397–411, Nov. 2007.

[29] C. Markides, G. De Paola, and E. Mastorakos, "Measurements and simulations of mixing and autoignition of an n-heptane plume in a turbulent flow of heated air," *Experimental Thermal and Fluid Science*, vol. 31, pp. 393–401, Apr. 2007.

[30] E. Richardson, N. Chakraborty, and E. Mastorakos, "Analysis of direct numerical simulations of ignition fronts in turbulent non-premixed flames in the context of conditional moment closure," *Proceedings of the Combustion Institute*, vol. 31, pp. 1683–1690, Jan. 2007.

[31] G. De Paola, E. Mastorakos, Y. M. Wright, and K. Boulouchos, "Diesel Engine Simulations with Multi-Dimensional Conditional Moment Closure," *Combustion Science and Technology*, vol. 180, pp. 883–899, Apr. 2008.

[32] M. Bolla, Y. M. Wright, K. Boulouchos, G. Borghesi, and E. Mastorakos, "Soot Formation Modeling of n -Heptane Sprays Under Diesel Engine Conditions Using the Conditional Moment Closure Approach," *Combustion Science and Technology*, vol. 185, pp. 766–793, May 2013.

[33] S. H. Kim and H. Pitsch, "Conditional filtering method for large-eddy simulation of turbulent nonpremixed combustion," *Physics of Fluids*, vol. 17, no. 10, p. 105103, 2005.

[34] S. Navarro-Martinez, A. Kronenburg, and F. D. Mare, "Conditional Moment Closure for Large Eddy Simulations," *Flow, Turbulence and Combustion*, vol. 75, pp. 245–274, Dec. 2005.

[35] S. Navarro-Martinez and a. Kronenburg, "LES-CMC simulations of a turbulent bluff-body flame," *Proceedings of the Combustion Institute*, vol. 31, pp. 1721–1728, Jan. 2007.

[36] S. Navarro-Martinez and A. Kronenburg, "LES CMC simulations of a lifted methane flame," *Proceedings of the Combustion Institute*, vol. 32, no. 1, pp. 1509–1516, 2009.

[37] J. Floyd, a. M. Kempf, a. Kronenburg, and R. H. Ram, "A simple model for the filtered density function for passive scalar combustion LES," *Combustion Theory and Modelling*, vol. 13, pp. 559–588, Aug. 2009.

[38] S. Navarro-Martinez and S. Rigopoulos, "Differential Diffusion Modelling in LES with RCCE-Reduced Chemistry," *Flow, Turbulence and Combustion*, vol. 89, pp. 311–328, Oct. 2011.

[39] A. Triantafyllidis, E. Mastorakos, and R. Eggels, "Large Eddy Simulations of forced ignition of a non-premixed bluff-body methane flame with Conditional Moment Closure," *Combustion and Flame*, vol. 156, pp. 2328–2345, Dec. 2009.

[40] A. Triantafyllidis and E. Mastorakos, "Implementation Issues of the Conditional Moment Closure Model in Large Eddy Simulations," *Flow, Turbulence and Combustion*, vol. 84, pp. 481–512, May 2009.

[41] I. Stanković, A. Triantafyllidis, E. Mastorakos, C. Lacor, and B. Merci, "Simulation of Hydrogen Auto-Ignition in a Turbulent Co-flow of Heated Air with LES and CMC Approach," *Flow, Turbulence and Combustion*, vol. 86, pp. 689–710, Aug. 2010.

[42] B. Thornber, R. Bilger, a.R. Masri, and E. Hawkes, "An algorithm for LES of premixed compressible flows using the Conditional Moment Closure model," *Journal of Computational Physics*, vol. 230, pp. 7687–7705, July 2011.

[43] A. Garmory and E. Mastorakos, "Capturing localised extinction in Sandia Flame F with LES-CMC," *Proceedings of the Combustion Institute*, vol. 33, no. 1, pp. 1673–1680, 2011.-

[44] S. Ayache and E. Mastorakos, "Conditional Moment Closure/Large Eddy Simulation of the Delft-III Natural Gas Non-premixed Jet Flame," *Flow, Turbulence and Combustion*, vol. 88, pp. 207–231, Sept. 2011.

[45] G. Borghesi, E. Mastorakos, C. B. Devaud, and R. W. Bilger, "Modeling evaporation effects in conditional moment closure for spray autoignition," *Combustion Theory and Modelling*, vol. 15, pp. 725–752, Oct. 2011.

[46] A. Garmory and E. Mastorakos, "Sensitivity analysis of LES-CMC predictions of piloted jet flames," *International Journal of Heat and Fluid Flow*, vol. 39, pp. 53–63, Feb. 2013.

[47] I. Stanković, E. Mastorakos, and B. Merci, "LES-CMC Simulations of Different Auto-ignition Regimes of Hydrogen in a Hot Turbulent Air Co-flow," *Flow, Turbulence and Combustion*, vol. 90, pp. 583–604, Feb. 2013.

[48] J. Smagorisky, "General circulation experiments with the primitive equations," *Mon. Weather Rev.*, vol. 91, pp. 99 – 164, 1963.

[49] N. Chakraborty and E. Mastorakos, "Numerical investigation of edge flame propagation characteristics in turbulent mixing layers Numerical investigation of edge flame propagation characteristics," vol. 105103, no. 2006, 2013.

[50] R. F. M. J. Kee, R.J., "Chemkin-ii: A fortran chemical kinetics package for the analysis of gas-phase chemical kinetics," *Technical Report, Sandia National Labs., Livermore, CA (USA)*, no. SAND-89-8009, 1989.

[51] C. a. Kennedy and A. Gruber, "Reduced aliasing formulations of the convective terms within the Navier Stokes equations for a compressible fluid," *Journal of Computational Physics*, vol. 227, pp. 1676–1700, Jan. 2008.

[52] S. Pirozzoli, "Generalized conservative approximations of split convective derivative operators," *Journal of Computational Physics*, vol. 229, pp. 7180–7190, Sept. 2010.

[53] S. Pirozzoli and M. Bernardini, "Probing high-Reynolds-number effects in numerical boundary layers," *Physics of Fluids*, vol. 25, no. 2, p. 021704, 2013.

[54] F. Salvadore, M. Bernardini, and M. Botti, "GPU accelerated flow solver for direct numerical simulation of turbulent flows," *Journal of Computational Physics*, vol. 235, pp. 129–142, Feb. 2013.

[55] S. Pirozzoli and M. Bernardini, "Wall pressure fluctuations in transonic shock/boundary layer interaction," *Procedia Engineering*, vol. 6, pp. 303–311, Jan. 2010.

[56] C.-W. Shu and S. Osher, "Efficient implementation of essentially non-oscillatory shock-capturing schemes," *Journal of Computational Physics*, vol. 77, no. 2, pp. 439 – 471, 1988.

[57] S. Pirozzoli and T. Colonius, "Generalized characteristic relaxation boundary conditions for unsteady compressible flow simulations," *Journal of Computational Physics*, vol. 248, pp. 109–126, Sept. 2013.

[58] K. W. Thomson, "Time Dependent Boundary Conditions for Hyperbolic Systems," *Journal of Computational Physics*, vol. 68, no. 1, pp. 1–24, 1987.

[59] T. Poinsot and S. K. Lele, "Boundary Conditions for Direct Simulations of Compressible Viscous Flows," 1992.

[60] G. Lodato, P. Domingo, and L. Vervisch, "Three-dimensional boundary conditions for direct and large-eddy simulation of compressible viscous flows," *Journal of Computational Physics*, vol. 227, pp. 5105–5143, May 2008.

[61] D. H. Rudy and J. C. Strikwerda, "A nonreflecting outflow boundary condition for subsonic navier-stokes calculations," *Journal of Computational Physics*, vol. 36, no. 1, pp. 55 – 70, 1980.

[62] M. Israeli and S. A. Orszag, "Approximation of radiation boundary conditions," *Journal of Computational Physics*, vol. 41, no. 1, pp. 115 – 135, 1981.

[63] G. D. B. Peter N. Brown and A. C. Hindmarsh, "Vode: A variable-coefficient ode solver," *SIAM Journal on Scientific and Statistical Computing*, vol. 10, no. 5, p. 1038–1051, 1989.

[64] D. D. Bowman C.T, Hanson R.K., "Gri-mech 2.11, available from: Web page," *available at web site*, 1995.

[65] J. Buckmaster, "Edge-flames," *Progress in Energy and Combustion Science*, vol. 28, pp. 435–475, Jan. 2002.

[66] R. Yetter, R A, Dryer, F.L and H, "A Comprehensive Reaction Mechanism For Carbon Monoxide / Hydrogen / Oxygen Kinetics," *Combustion Science and Technology*, vol. 79, pp. 97–128, 1991.